Coumarinyl-Caged Ceramides, a New Tool for Assessing the Biological Effects of Ceramide in Cells

By

Jenna Day

Thesis submitted to the Faculty of Graduate and Postdoctoral Studies

University of Ottawa

In partial fulfillment of the requirements for the

M.Sc. Degree in the

Ottawa Carleton Chemistry Institute

University of Ottawa

Candidate	**Supervisor**
Jenna Day	**Dr. Linda J. Johnston**

Abstract

Ceramide, a sphingolipid, is an important lipid second messenger that is involved in regulating a number of cellular processes, including programmed cell death, cell growth and differentiation, as well as cellular responses to stress stimuli. Many of the biological effects of ceramide are linked to its ability to modulate the biophysical properties of membranes and cause clustering of signalling molecules in ceramide-rich domains, which allows for more efficient signal transmission in the cell. However, the specific roles of different ceramide species in these signaling pathways have yet to be clearly established. Assessing the effects of long N-acyl chain ceramides in cells involves some limitations due to their poor solubility and their low membrane permeability. Caging these molecules with photolabile protecting groups allows for their delivery into cells where photochemical uncaging of the biologically active compound can be achieved with spatial and temporal control.

A series of coumarinyl-caged ceramides has been prepared in order to probe the biological effects of ceramide in cells. This unique series of compounds was used to investigate the dependence of these cellular effects on N-acyl chain length. Hereafter, I describe the photophysical and photochemical characterization of these novel caged ceramides, assess their uptake and measure the biological effects of the different ceramides which are generated photochemically in HeLa cells. The caged ceramides were shown to be taken up by the cells and to cause a decrease in viability, with UV irradiation, that can be detected after 24 hours of treatment. An investigation of the mechanism of cell death induced by coumarinyl-caged

ceramides in HeLa cells revealed that cell death proceeds in a caspase-independent manner and involves the mitochondria. The role of the mitochondria in this cell death pathway, however, remains to be studied further. RIP1 kinase activity, which was also probed in the cells, was determined to not be implicated in cell death caused by photochemically generated ceramide. Intracellular ROS generation, however, was shown to occur in this system, but results primarily from UV irradiation of the free coumarin. Overall, the results from this study have provided insight into the signalling pathways triggered by treatment of HeLa cells with the bioactive lipid ceramide using coumarin photocages.

Acknowledgements

I would first and foremost like to thank my supervisor, Dr. Linda Johnston, for her constant guidance and support throughout the completion of this research project. Linda, your patience and kindness have been phenomenal. It has certainly been interesting and I have learned a great deal – not only about chemistry, but about thinking critically.

I would also like to extend a very special thank you to Dr. Will Costain of the NRC for his invaluable input and contributions to this project. In addition, I would like to thank the members of my research group, who I truly consider my friends after our time spent together at NRC-Sussex. An added thank you goes out to Maohui, Zhengfang and Zygmunt for technical assistance and to Daniel for useful chats when I first took on this project. To my friends, inside and outside of the Chemistry department, I also thank you for being a part of these years.

The constant encouragement and praise from my family has helped me immensely in achieving this accomplishment. Mom and Dad, you have taught me to aim high, to follow my dreams and to pursue what makes me happy, which is what I have done and continue to do every day. Krista and Steven, thank you simply for being there and for listening to the stories about my “grad student life” – I really appreciate it. It is now time for all of the hard work to pay off and I look forward to the journey ahead.

Table of Contents

Abstract.....ii

Acknowledgements.....iv

Table of Contents.....v

List of Abbreviations.....viii

List of Figures.....xi

List of Tables.....xvii

List of Schemes.....xvii

Chapter 1: Introduction to Cellular Membranes and the Bioactive Lipid Ceramide.....1

1.1 - Structure and Function of Biological Membranes.....1
1.2 - Ceramide Generation in Biological Systems.....5
1.3 - The Biological Activity of Ceramide.....10
1.4 - Photocages for Biological Applications.....18
1.5 - Coumarinyl-caged Ceramides.....25
1.6 - References.....27

Chapter 2: Synthesis, Photophysical Characterization and Cellular Uptake of Coumarinyl-Caged Ceramides.....31

2.1 - Introduction: Photolabile Protecting Groups for Ceramide.....31
2.2 - Results.....32

2.2.1 - Synthesis of Bhc-Caged Ceramides.....32
2.2.2 - Synthesis of Tcmoc- and Btcmoc-Caged Ceramides.....34
2.2.3 - Photophysical Characterization of Coumarinyl-Caged Ceramides.....35
2.2.4 - Photochemical Characterization of Coumarinyl-Caged Ceramides.....41
2.2.5 - Uptake of Coumarinyl-Caged Ceramides in HeLa Cells.....48

2.3 - Discussion and Conclusions.....51
2.4 - References.....56

Chapter 3: Effects of Photochemically Generated Ceramide on the Morphology and Viability of HeLa cells……...58

3.1 - Introduction: Ceramide and Cell Death……..58
3.2 - Results……63

3.2.1 - Morphology of HeLa Cells Subjected to Ceramide Treatments……...63
3.2.2 - Measuring the Viability of HeLa Cells Exposed to Bhc-Caged Cer….67
3.2.3 - Measuring the Effects of Btcmoc-Caged Cers on Viability……...78

3.3 - Discussion and Conclusions……81
3.4 - References……..88

Chapter 4: Investigation of the Mechanism of Cell Death Involved with the Photochemical Generation of Ceramide *in Vitro*……90

4.1 - Introduction: The Role of Ceramide in Cell Death……...90
4.2 - Results……98

4.2.1 - Probes for Assessing Mitochondrial Membrane Potential……98
4.2.2 - Probing Caspase Activation……105
4.2.3 - Probing the Involvement of the RIP1 Kinase……111
4.2.4 - ROS Detection and Use of Scavengers……113

4.3 - Discussion and Conclusions……..119
4.4 - References……...124

Chapter 5: Experimental Procedures.....127

5.1 - Chemicals……127
5.2 - Absorbance and Fluorescence Spectroscopy……...129
5.3 - Photolysis and Photoproduct Analysis……129
5.4 - Cell Culture of the HeLa Cell Line……..130
5.5 - Bright Field and Fluorescence Microscopy……131
5.6 - Cell Viability Assays……..132
5.7 - Mitochondrial Staining Experiments with JC-1 and TMRM…….135
5.8 - Caspase 3/7 Activity Assays……...136
5.9 - Necrosis Inhibitor Experiment……137
5.10 - Carboxy-H_2DCFDA Reactive Oxygen Species (ROS) Detection……..138
5.11 - References……139

Chapter 6: Concluding Remarks and Future Directions……..140

6.1 - Concluding Remarks…….140
6.2 - Future Directions……142
6.3 - Claims to Original Research……144
6.4 - References……...145

List of Abbreviations

Apaf-1	apoptosis protease activating factor-1
aSMase	acid sphingomyelinase
ATP	adenosine triphosphate
Bhc	6-bromo-7-hydroxycoumarin
BHNB	4-bromo-5-hydroxy-2-nitrobenzhydryl
Bnz	benzoin
Btcmoc	6-bromo-7-methoxytriethylene glycol-conjugated coumarin
Bn	benzyl
Carboxy-H_2DCFDA	5-(and-6)-carboxy-2',7'-dichlorodihydro-fluorescein diacetate
Cer	ceramide
CerS	ceramide synthase
CERT	ceramide transport protein
Cer-1P	ceramide-1-phosphate
Chol	cholesterol
CNB	α-carboxy-2-nitrobenzyl
Cou	coumaryl
DCF	dichlorofluorescein
DECM	7-(diethylamino)coumarin
DISC	death-inducing signaling complex
DMNB	4,5-dimethoxy-2-nitrobenzyl
DMNPE	4,5-dimethoxy-1-(2-nitrophenyl)ethyl
DNA	deoxyribonucleic acid
DOPC	1,2-dioleoyl-s*n*-glycero-3-phosphocholine

ER	endoplasmic reticulum
ESM	egg sphingomyelin
FCCP	carbonyl cyanide-4-(trifluoromethoxy)phenylhydrazone
Hcm	7-hydroxy-4-hydroxymethylcoumarin
HPLC	high performance liquid chromatography
IDO	indoleamine 2,3-dioxygenase
JC-1	5,5',6,6'-tetrachloro-1,1',3,3'-tetraethylbenzimidazolylcarbocyanine iodide
L_d	liquid-disordered phase
L_o	liquid-ordered phase
LDH	lactate dehydrogenase
MCRM	mitochondrial ceramide-rich macrodomains
MNI	methoxynitroindoline
MOMP	mitochondrial outer membrane permeabilization
mTEG	methoxytriethylene glycol
MTT	3-(4,5-dimethylthiazol-2-yl)-2,5-diphenyl tetrazolium bromide
NAD(P)H	nicotinamide adenine dinucleotide (phosphate)
NB	2-nitrobenzyl
Nec-1	necrostatin-1
NIR	near-infrared
NPE	1-(2-nitrophenyl)ethyl
PC	phosphatidylcholine
PCD	programmed cell death
PE	phosphatidylethanolamine
pHP	para-hydroxyphenylacyl
PI	propidium iodide

PI(3)P	phosphatidylinositol-3-phosphate
PI(3,4,5)P_3	phosphatidylinositol-3,4,5-trisphosphate
POPC	1-palmitoyl-2-oleoyl-*sn*-glycero-3-phosphocholine
PS	phosphatidylserine
RIP1	receptor interacting protein-1
RIP3	receptor interacting protein-3
RNA	ribonucleic acid
ROS	reactive oxygen species
SMase	sphingomyelinase
SPT	serine palmitoyl transferase
S1P	sphingosine-1-phosphate
TBHP	tert-butyl hydroperoxide
Tcmoc	7-methoxytriethylene glycol-conjugated coumarin
TMRM	tetramethylrhodamine methyl ester
TNF	tumour necrosis factor
UV	ultraviolet
WST-1	4-[3-(4-iodophenyl)-2-(4-nitrophenyl)-2H-5-tetrazolio]-1,3-benzene disulfonate, sodium salt
z-VAD-fmk	carbobenzoxy-valyl-alanyl-aspartyl-[O-methyl]-fluoromethylketone

List of Figures

Figure 2-1. Absorbance spectra (A) and fluorescence emission spectra with 374 nm excitation (B) of the Bhc-coumarin (**4**) and of the Bhc-caged C16 Dihydro-Cer (**9a**) in KMops pH 7.4 (solvent A) and in KMops (pH 7.4) containing 50% ethanol (solvent B).

38

Figure 2-2. Absorbance spectra of A) Btcmoc-caged (**21**-**24**) and B) Tcmoc-caged (**19**-**20**) ceramides and parent coumarins (**17**-**18**), as well as fluorescence emission spectra (C) of select compounds in KMops (pH 7.4) (Solvent A) or in KMops (pH 7.4) containing 10% ethanol (Solvent C).

40

Figure 2-3. Representative reversed-phase HPLC chromatograms showing the separation and detection by fluorescence of the Btcmoc-caged ceramides **21** and **23** and of the free coumarin (**18**) photo-product, which are used for monitoring the time course of photolysis. Fluorescence detection at 440 nm was performed with 325 nm excitation. Eluent: 75% EtOH (increasing to 95% over the time period of 0 to 3 min), 25% H_2O; flow rate = 0.5 mL/min.

43

Figure 2-4. Time course of photolysis of the Bhc-caged C16 Dihydro-Cer (**9a**) in KMops (pH 7.4) containing 50% EtOH (A) and time course of photolysis of the Btcmoc- and Tcmoc-caged Cers (**23**, **19** and **20**) in KMops containing 10% EtOH (B) with irradiation in a Rayonet photochemical reactor with 4 lamps (350 nm). Samples were placed in a 4 mL quartz cuvette. Photolysis of the caged ceramides was quantified by HPLC analysis using Coumarin 480 as an internal standard.

44

Figure 2-5. Fluorescence spectroscopic analysis of the time course of photolysis of the Bhc-caged C16 Cer (**9b**) in KMops (pH 7.4) containing ≤ 1% EtOH (A) and in serum-free medium containing ≤ 1% EtOH (B) with irradiation in a Rayonet photochemical reactor with 4 lamps (350 nm). Samples were placed in a 4 mL quartz cuvette. Fluorescence emission spectra were collected at different time points throughout the UV irradiation and fluorescence intensity was quantified as the area under the curve.

46

Figure 2-6. Time course of photolysis, in a micro-well plate, of the Bhc-caged C16 Cer (**9b**), the Btcmoc-caged Cers (**21**, **23**) and the Tcmoc-caged C16 Cer (**20**) in KMops (pH 7.4) containing 10% EtOH with irradiation in a Rayonet photochemical reactor with 4 lamps (350 nm). Photolysis was quantified by HPLC analysis using Coumarin 480 as an internal standard.

47

Figure 2-7. The Bhc-caged C16 Cer (**9b**) is taken up by HeLa cells with 2 hours of incubation, as assessed from the localized coumarin fluorescence in the cells. Bright field (A,C) and fluorescence images (B,D) of HeLa cells incubated with (top) and without (bottom) the **9b** in serum-free medium (20 µM) for 2 hours in the dark and irradiated in a UV reactor (350 nm) for 6 min. The medium was then removed and the cells were washed once with PBS buffer (1X) which was used as the imaging medium. The images were acquired using a 100X oil immersion objective. Fluorescence images were acquired in the DAPI channel and are scaled at 200-1200 counts. The inset in image D is to illustrate the morphology of the control sample (Display: 200-350 counts).

49

Figure 2-8. The Btcmoc-caged C22 Cer (**23**) is taken up by HeLa cells with 2.5 hours of incubation, as assessed from localized fluorescence emission in the cells. Bright field (A, C and E) and fluorescence images (B, D and F) of HeLa cells incubated with and without **23** in serum-free medium (20 µM) for up to 2.5 hours in the dark. Samples were washed and imaging was performed in PBS buffer (1X). The images were acquired using a 100X oil immersion objective. Fluorescence images were acquired in the DAPI channel and are scaled at 500-1500 counts.

51

Figure 3-1. HeLa cells treated with C2 Cer exhibit morphological features that are consistent with apoptosis. Bright field images of HeLa cells incubated for 24 hours in the presence of C2 Cer (B) or C16 Cer (C), at a concentration of 20 µM, in serum-free medium. An untreated control sample (A) was included for comparison. The images were acquired using a 40X objective.

64

Figure 3-2. Treatment of HeLa cells with the Bhc-caged C16 Cer (**9b**) causes morphological changes that are different than those observed with C2 Cer treatment. Bright field images of HeLa cells treated with ceramide species in serum-free medium (20 µM) for 24 hrs (along with untreated vehicle controls). For UV-irradiated samples (A-D), the culture plate was removed from the incubator after 7.5 hrs and irradiated for 4 min (350 nm). The images were acquired using a 20X objective.

66

Figure 3-3. Effects of exogenously added C2 and C16 ceramides (20 μM in serum-free medium) on cell viability, as assessed by MTT assay after 24 hours of treatment in the dark (no UV). Data is from a single representative experiment (n=2) and error bars indicate the standard deviation within each treatment group (n = 12-18 values).

68

Figure 3-4. Effects of exogenously added C2 and C16 ceramides (20 μM in serum-free medium) on cell viability, as assessed by WST-1 assay after 24 hours of treatment in the dark (no UV). Data is from a single representative experiment and error bars indicate the standard deviation for each treatment group (n = 10 values).

69

Figure 3-5. Dose-response profiles of exogenously added C2 and C16 ceramides and of the Bhc-caged C16 Cer (**9b**), as assessed by WST-1 assay after 24 hours of treatment in the dark (no UV). Data is from a single experiment and error bars indicate the standard deviation (n = 4-6 values).

73

Figure 3-6. Effects of the Bhc-caged C16 Cer (**9b**) on cell viability when different lengths of UV irradiation were used for uncaging, after 4 hours of incubation. Viability was assessed by WST-1 assay after 24 hours of treatment. Data is from a single experiment and error bars indicate the standard deviation for each treatment group (n = 12 values).

75

Figure 3-7. UV irradiation of the Bhc-caged C16 Cer (**9b**) in HeLa cells causes a decrease in viability that is not observed in the absence of UV. Relative viability (%) of cells treated with the caged ceramide **9b** or with the control compounds C2 Cer, C16 Cer and Bhc (20 μM) in serum-free medium, as assessed by WST-1 assay after 24 hours of treatment. Data is from several experiments (n=3-10) and error bars indicate the standard error mean. * Indicates statistical significance ($p < 0.05$) of the difference in the relative viability, with reference to the respective (0 and 6 min UV) untreated controls.

77

Figure 3-8. Effects of the Btcmoc-caged C22 Cer (**23**) on cell viability when different lengths of UV irradiation were used, after 2 hours of incubation. Viability was assessed by WST-1 assay after 24 hours of treatment. Data is from a single experiment and error bars indicate the standard deviation for each treatment group (n = 10-12 values).

79

Figure 3-9. UV irradiation of the Btcmoc-caged ceramides (**21**-**24**) and of the free Btcmoc-coumarin (**18**) causes similar effects on the viability of HeLa cells. Relative

viability (%) of cells treated with the Btcmoc-caged ceramides or with the control compounds C2 Cer and the free coumarin **18** (20 µM), as assessed by WST-1 assay after 24 hours of treatment. Data is from 1-3 experiments and error bars indicate the standard error mean (for n=1 experiment, SEM is from 6-12 values for a given treatment group).

81

Figure 4-1. Treatment of HeLa cells with FCCP causes a decrease in the red to green JC-1 fluorescence ratio. Fluorescence images of HeLa cells stained with JC-1 (5 µg/mL) in serum-free medium and treated with FCCP (7 µM) on the microscope stage (B,D) or left untreated (A,C). Samples were washed before imaging in PBS buffer (1X). Fluorescence images were acquired using a 100X oil immersion objective in the red channel (100 ms exposure) and in the green channel (200 ms exposure) and are scaled appropriately (red: 100-2500 counts; green: 100-1200 counts). Quantification of red and green fluorescence intensity, as well as of the red/green ratio, was performed within individual cells. Fluorescence intensity was quantified as the blank-corrected mean intensity.

99

Figure 4-2. The Bhc-caged C16 Cer (**9b**) causes a decrease in the mitochondrial membrane potential, as assessed using JC-1 staining. Two-colour (red/green) composite fluorescence images of HeLa cells incubated with (E-H) and without (A-D) **9b** in serum-free medium (20 µM) for 4 hours in the dark and then stained with JC-1 (5 µg/mL). Samples were washed and imaging was done in PBS buffer (1X). UV irradiation was performed on the microscope with an appropriate filter. Images were acquired in the red and green channels using a 100X oil immersion objective. The images have been scaled with matched display ranges (Untreated – red: 100-2400 counts, green: 100-2800 counts; **9b** – red: 100-900 counts, green: 100-800 counts). Note: display range for “Before UV” images was adjusted due to photobleaching (for both samples - red: 100-3600 counts, green: 100-1400 counts).

101

Figure 4-3. The mitochondrial dye JC-1 is significantly photobleached in HeLa cells exposed to UV irradiation. A) Fluorescence images (Before and After UV) of HeLa cells stained with JC-1 (5 µg/mL) in serum-free medium and exposed to UV irradiation. Samples were washed and imaging was performed in PBS buffer (1X). Fluorescence images were acquired with a 100X oil immersion objective, in the red and green channels and are scaled appropriately (red: 100-1000 counts; green: 200-800 counts). B) Quantification of the relative fluorescence intensity as a function of UV exposure for an irradiated sample (Exposed) and an unirradiated sample (Control). Fluorescence images were acquired in the red and green channels with a series of sequential exposures and the fluorescence intensity was quantified in each channel as the blank-corrected mean intensity. The fluorescence intensity measured from the initial image was set to 100%, in each case, for quantification.

104

Figure 4-4. Caspase 3/7 activity assay results for HeLa cells treated with C2 Cer, C16 Cer or Bhc-caged C16 Cer (**9b**), at a concentration of 20 µM, in serum-free medium. Samples were incubated in the dark for 2 hours, irradiated in a UV reactor (350 nm) for 9 min (or left unirradiated) and an assay was performed after 18 hours. Data shown are mean values from a single experiment and error bars indicate the standard deviation (n=5 values per treatment group).

106

Figure 4-5. Caspase 3/7 activity assay results for HeLa cells treated with C2 Cer or with the Bhc-caged C16 Cer (**9b**), at a concentration of 20 µM, in serum-free medium. Samples were incubated in the dark for 2 hours, irradiated in a UV reactor (350 nm) for 0, 9, 12 or 15 min and an assay was performed after 24 hours. Data shown are mean values from a single experiment and error bars indicate the standard deviation (n=4 values per treatment group).

108

Figure 4-6. C2 Ceramide causes caspase 3/7 activation in HeLa cells which can be blocked by the caspase inhibitor Z-DEVD-fmk, whereas cell death with the Bhc-caged C16 Cer (**9b**) occurs independently of caspase 3/7 activation. Caspase 3/7 activity assay results (A) and WST-1 cell viability assay results (B) for HeLa cells treated with C2 Cer or with the caged ceramide **9b**, at a concentration of 20 µM, in serum-free medium. Samples were pre-treated with Z-DEVD-fmk (100 µM) for 1 hour, incubated in the dark for 2 hours with the compounds, irradiated in a UV reactor (350 nm) for 9 min (caspase assay) / 6 min (viability assay) and an assay was performed after 24 hours. Data shown are average values for the fold increase in caspase 3/7 activity and for the relative cell viability, which were obtained from 2 independent experiments and error bars indicate the standard deviation.

110

Figure 4-7. Caspase 3/7 activity assay results for HeLa cells treated with C2 Cer or with the Btcmoc-caged ceramides (**22** and **23**), at a concentration of 20 µM, in serum-free medium. Samples were incubated in the dark for 2 hours, irradiated in a UV reactor (350 nm) for 9 min and an assay was performed after 24 hours. Data shown are mean values from a single experiment and error bars indicate the standard deviation (n=6 values per treatment group).

111

Figure 4-8. The Bhc-caged C16 Cer (**9b**) exhibits a form of cell death that is not blocked by the necrosis inhibitor Nec-1s. WST-1 cell viability assay results for HeLa cells treated with C2 Cer or the caged ceramide **9b**, at a concentration of 20 µM, in serum-free medium. The samples were pre-treated with the inhibitors Z-DEVD-fmk and Nec-1s (100 µM each) for 1 hour, incubated in the dark for 2 hours, irradiated in a UV reactor (350 nm) for 6 min and an assay was performed after 24 hours. Data shown are mean values for relative cell viability from a single experiment and error bars indicate the standard deviation (n= 6-12 values per treatment group).

113

Figure 4-9. UV irradiation of the free coumarins Bhc (**4**) and Btcmoc (**18**) causes ROS generation in HeLa cells. Carboxy-H_2DCFDA fluorescence assay results for ROS detection in HeLa cells treated with the control species TBHP (100 µM), with the free coumarin **4** (20 µM), or with the free coumarin **18** (20 µM) in HBSS buffer. The cells were stained with carboxy-H_2DCFDA (10 µM) for 45 min in the dark and washed once with buffer. The samples were then incubated in the dark for 2 hours, irradiated in a UV reactor (350 nm) for 6 min (or left unirradiated) and the fluorescence emission at 520 nm (with 485 nm excitation) was measured. Data is normalized to the untreated control for each set of conditions (0 and 6 min UV irradiation). Data shown are mean values for the fold increase in fluorescence intensity from a single experiment and error bars indicate the standard deviation (n= 12 values per treatment group).

115

Figure 4-10. ROS generation upon UV irradiation of the Bhc-coumarin (**4**) in HeLa cells can be blocked by the scavengers ascorbic acid and Trolox. Carboxy-H_2DCFDA fluorescence assay results for ROS detection in HeLa cells treated with the free coumarin **4** (20 µM) in HBSS buffer. The cells were stained with carboxy-H_2DCFDA (10 µM) for 45 min in the dark and washed once with buffer. The samples were then pre-treated for 1 hour with different scavengers, incubated in the dark for 2 hours with the free coumarin **4** and irradiated in a UV reactor (350 nm) for 6 min (or left unirradiated). The fluorescence emission at 520 nm (with 485 nm excitation) was measured. Data shown are mean values for the fluorescence intensity from a single experiment and error bars indicate the standard deviation (n= 6-12 values per treatment group).

116

Figure 4-11. A) Carboxy-H_2DCFDA fluorescence assay results for ROS detection in HeLa cells treated with the Bhc-coumarin (**4**) or with the Bhc-caged C16 Cer (**9b**) (20 µM) in HBSS buffer. The cells were stained with carboxy-H_2DCFDA (10 µM) for 45 min in the dark and washed once with buffer. The samples were then pre-treated for 1 hour with Trolox, incubated in the dark for 2 hours with the compounds and irradiated in a UV reactor (350 nm) for 6 min (or left unirradiated). The fluorescence emission at 520 nm (with 485 nm excitation) was measured. Data is normalized to the untreated control for each set of conditions. Data shown are mean values for the fold increase in fluorescence intensity from a single experiment and error bars indicate the standard deviation (n= 6-12 values per treatment group). B) WST-1 cell viability assay results for HeLa cells treated with the free coumarin **4** and with the caged ceramide **9b** (20 µM) in serum-free medium. The samples were then pre-treated for 1 hour with Trolox, incubated in the dark for 2 hours with the compounds and irradiated in a UV reactor (350 nm) for 6 min (or left unirradiated). The assay was performed after 24 hours. Data shown are average values for relative cell viability from two experiments and error bars indicate the standard deviation.

118

List of Tables

Table 1-1. Chain length specific properties of ceramides in biological systems. From references 39, 40 and 55.

16

Table 2-1. Photophysical properties of the Bhc-caged C16 Dihydro-Cer (**9a**), the Btcmoc-caged Cers (**21**-**24**), the Tcmoc-caged Cers (**19**-**20**) and the parent coumarins (**4**, **17**-**18**).

41

List of Schemes

Scheme 1-1. Structure of the plasma membrane. From reference 3.

2

Scheme 1-2. Structure of some common membrane lipids. A) Phosphatidylcholine (PC); B) Phosphatidylethanolamine (PE); C) Phosphatidylserine (PS); D) Phosphatidylinositol (PI). R_1,R_2= fatty acids.

3

Scheme 1-3. Structure of representative raft components: sphingolipids and cholesterol. A) Ceramide (Cer); B) Sphingomyelin (SM); C) Cholesterol. R= long-chain (C16 or greater) saturated fatty acid.

5

Scheme 1-4. The aSMase hydrolyzes sphingomyelin (SM) to give ceramide (Cer). A) Breakdown of SM to give Cer and phosphorylcholine. Adapted from reference 11. B) Coalescence of small raft domains to form large signaling platforms through the action of the aSMase. Adapted from reference 14.

6

Scheme 1-5. *De novo* biosynthesis of ceramide. Adapted from reference 16.

8

Scheme 1-6. Overview of ceramide metabolism. Adapted from reference 16.

9

Scheme 1-7. Extrinsic and intrinsic pathways of apoptotic signaling in biological systems. Reproduced from reference 41 with approval.

13

Scheme 1-8. Cell signaling during necrosis in biological systems. Reproduced from reference 41 with approval.

14

Scheme 1-9. Structure of common photo-removable protecting groups. Adapted from reference 83.

20

Scheme 1-10. Generalized reaction scheme for the photolysis of nitrobenzyl-caged compounds. From reference 82.

20

Scheme 1-11. Generalized photolysis of a (coumarin-4-yl)methyl-caged alcohol. Adapted from reference 84.

21

Scheme 1-12. Mechanism of photocleavage of (coumarin-4-yl)methyl esters. Reproduced from reference 85 with approval.

22

Scheme 1-13. Structures of (coumarin-4-yl)methyl phototriggers. From reference 84.

23

Scheme 2-1. Synthesis of the Bhc-caged C16 Dihydro-Cer (**9a**) and of the Bhc-caged C16 Cer (**9b**). (a) CH_3SO_3H, rt, 2 h, 95%; (b) H_2O, reflux, 2 d, 99%; (c) MOMCl, DIPEA, CH_2Cl_2, 0^oC, 2 h, 89%; (d) phosgene, THF/toluene, 3 h, 0^oC, 94%; (e) DIPEA, DMAP, THF/CH_2Cl_2 (2:1), rt, 36 h, 25%; (f) $NaHSO_4 \cdot SiO_2$, CH_2Cl_2, 2 h, rt, 70%.

33

Scheme 2-2. Synthesis of the pegylated Tcmoc- (**19**-**20**) and Btcmoc-caged ceramides (**21**-**24**) with short, long or very long N-acyl chains. (a) CH_3SO_3H, rt, 2 h; (b) KF, AcOH, DMF, rt, 36 h; (c) PBu_3, DIAD, THF, *MW*, 60 ^oC, 30 min; (d) K_2CO_3, THF/MeOH (1:1), 0 ^oC, 1 h.

35

Scheme 3-1. Representation of the morphological features of apoptosis and necrosis. Reproduced from reference 15 with approval.

60

Scheme 3-2. Cellular conversion of the MTT tetrazolium salt to the MTT formazan product. Adapted from reference 19.

61

Scheme 3-3. Conversion of the WST-1 tetrazolium salt to the respective formazan product. Adapted from reference 23.

62

Scheme 4-1. Structure of the mitochondrial membrane potential probe JC-1 (A) and of the uncoupling agent FCCP (B).

92

Scheme 4-2. Biochemical reactivity of the probe used for the caspase 3/7 luminescence assay. From reference 25.

95

Scheme 4-3. Structure of the RIP1 inhibitor Nec-1s. From reference 31.

96

Scheme 4-4. Intracellular conversion of carboxy-H_2DCFDA to the fluorescent product. From reference 34.

97

Chapter 1: Introduction to Cellular Membranes and the Bioactive Lipid Ceramide

1.1– Structure and Function of Biological Membranes

Biological membranes are essential for the life of most living organisms. They are primarily responsible for isolating cellular contents from the extracellular environment, as well as delimiting sub-cellular compartments and organelles from one another, which makes them key components of the cell. Membranes are heavily involved in the homeostasis of cells by allowing the exchange of nutrients and metabolites from one compartment to another. Moreover, the compartmentalization resulting from the presence of different biological membranes throughout the cell allows for effective localization of key catabolic, metabolic and signalling events. Biomembranes are implicated in processes such as the synthesis of ATP, as well as cell-to-cell communication by maintaining concentration gradients of different solutes between the different environments. Proteins, which are also found in the membrane, are responsible for sensing external signals allowing the cell to adapt to different environmental stresses.[1]

The fluid mosaic model introduced by Singer and Nicolson in 1972 depicted the biological membrane as a homogeneously fluid phase in which lipid molecules and other components, such as proteins, could diffuse laterally.[2] Since the introduction of this model, there has been ongoing work towards a more accurate representation of the biological membrane. The general structure of these membranes consists of a bilayer of lipid molecules held together mainly by non-

covalent interactions. The lipid molecules adopt a bilayer arrangement due to their amphiphilic nature allowing for the hydrophobic lipid tails to be shielded from the aqueous environment while the hydrophilic headgroups are exposed to the intra- and extracellular fluids. Given that the hydrophobic chains of the lipids are not able to form hydrogen bonds with water molecules, it is energetically favourable for them to pack closely together in order to minimize the surface area of contact with water. This phenomenon, which is known as the hydrophobic effect, is the physical basis of lipid bilayer formation. Some biomembranes also contain large amounts of cholesterol, which plays a structural role within the membrane. The sterol molecules are oriented within the bilayer, having their hydroxyl groups close to the polar headgroups of the lipid molecules. The many different proteins that are embedded in the membrane are responsible for various functions in the cell. Scheme 1-1 depicts the plasma membrane and its components.[3]

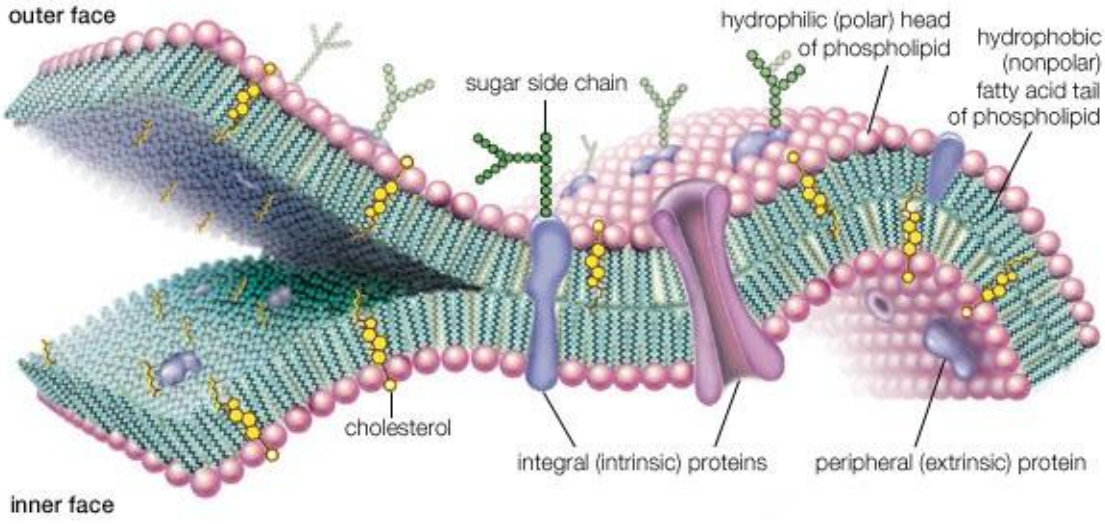

Scheme 1-1. Structure of the plasma membrane. From reference 3.

The plasma membrane is largely made up of glycerophospholipids, also known as phospholipids. These lipid molecules are comprised of a glycerol-based

skeleton, a polar or charged headgroup that is variable in nature and two hydrocarbon tails which are typically long chain fatty acids with a length between 14 and 24 carbon atoms. In the structure of glycerophospholipids, positions 1 and 2 of the glycerol backbone are esterified with long chain fatty acids and position 3 serves as the site of attachment of the headgroup.[4] It is the nature of the headgroup moiety that defines the particular type of phospholipid.

The four types of phospholipids that predominate in the plasma membrane are phosphatidylcholine (PC) lipids, phosphatidylethanolamine (PE) lipids, phosphatidylserine (PS) lipids and sphingolipids. Other phospholipids, such as phosphatidylinositol (PI) lipids, are present in smaller quantities but are functionally very important, for cell signalling for instance.[1] The generalized structures of PC, PE, PS and PI lipids are shown in Scheme 1-2. As seen below, most of these lipids are electrostatically neutral at physiological pH. However, in PS lipids, the headgroup contains a net negative charge, which has an impact on the extent of electrostatic interactions between these molecules and ions, other lipids, as well as proteins in the environment.

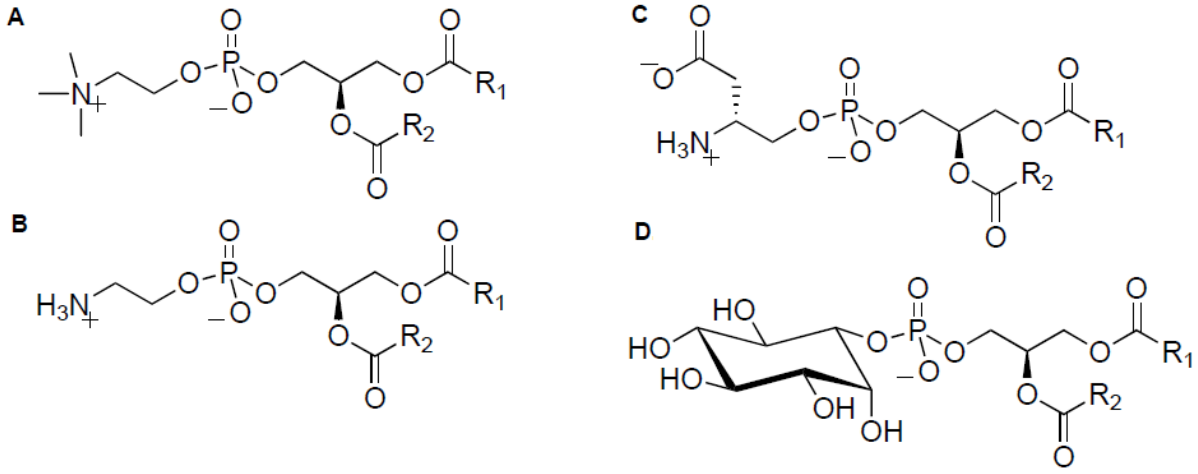

Scheme 1-2. Structure of some common membrane lipids. A) Phosphatidylcholine (PC); B) Phosphatidylethanolamine (PE); C) Phosphatidylserine (PS); D) Phosphatidylinositol (PI). R_1,R_2= fatty acids.

The fluidity of biological membranes, which is related to the degree of packing of the lipids forming the bilayer, is important for different cellular processes, such as membrane transport and enzyme activity. The packing of the lipids is influenced by the level of unsaturation of the hydrocarbon chains. Glycerophospholipids most often have a saturated fatty acid at position 1 and an unsaturated fatty acid at position 2 (see Scheme 1-2). Naturally occurring unsaturated fatty acids are typically in the *cis* configuration, which introduces a bend in the fatty acid chain. One or more of these bends in the hydrocarbon chain disfavours tight packing of the lipid molecules, which induces fluidity and increased lateral mobility in the membrane. Although the bulk of membrane lipids are fluid, there is increasing evidence for the importance of ordered membrane domains. Much recent work has focused on determining the importance of lateral organization in the bilayer for the execution of various biological functions by membrane proteins.[5] One form of lateral segregation in biological membranes is the formation of dynamic nanoscale domains called lipid rafts. These membrane domains are rich in cholesterol and in sphingolipids. As shown in Scheme 1-3, sphingolipids are made up of a long acyl chain moiety that is variable in length, which is linked to a sphingoid base by an amide bond.

In contrast to most biological phospholipids, the acyl chains of sphingolipids exhibit a low degree of unsaturation, which allows them to pack tightly together. It is the differential packing ability of sphingolipids and phospholipids making up the membrane that gives rise to phase separation and formation of liquid-ordered lipid rafts.[5] Sphingomyelin, a sphingolipid, is one of the main constituents of lipid rafts.[6]

This sphingolipid contains a phosphocholine group, which, once removed, gives rise to ceramide (see Scheme 1-3). Ceramide can also be generated by other biochemical pathways, which will be described in the next section of this chapter. Apart from its structural role in the membrane, ceramide plays a role in signal transduction in the cell.[7] Cholesterol, which is also present in the membrane, can promote the formation of rafts due to favourable packing interactions between saturated lipids and this sterol.[8] Lipid rafts are believed to function as platforms for the clustering of proteins that are involved in cell signalling.[9]

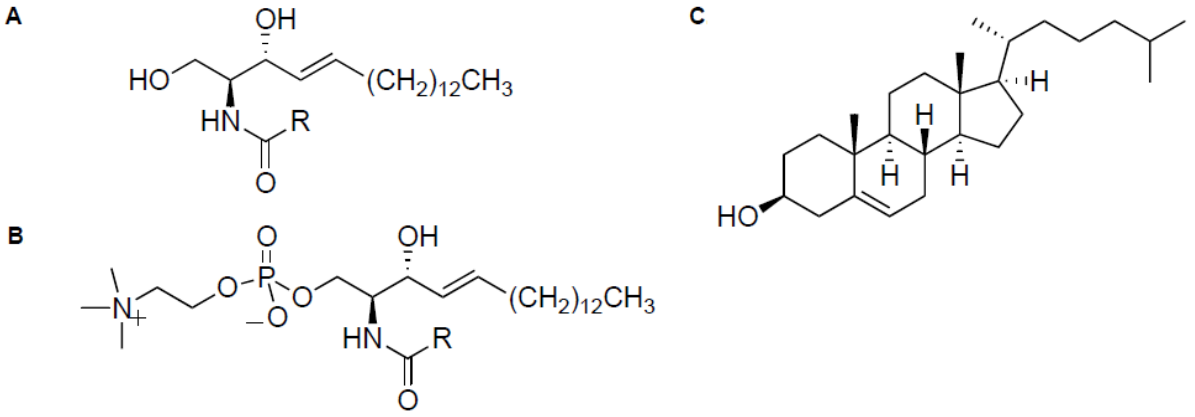

Scheme 1-3. Structure of representative raft components: sphingolipids and cholesterol. A) Ceramide (Cer); B) Sphingomyelin (SM); C) Cholesterol. R= long-chain (C14 or greater) saturated fatty acid.

1.2 – Ceramide Generation in Biological Systems

There are a number of routes for generating ceramide in the cell. One route involves the hydrolysis of sphingomyelin by sphingomyelinase (SMase) enzymes in the membrane. The production of ceramide from the breakdown of complex sphingolipids, such as sphingomyelin, is known as the salvage pathway for ceramide generation.[10] The family of SMase enzymes includes the acid sphingomyelinase (aSMase), the alkaline SMase and neutral SMases. The aSMase

is primarily found in the outer leaflet of the plasma membrane, as well as in the endolysosomal cellular compartments. This enzyme is a phosphodiesterase that hydrolyzes sphingomyelin to produce ceramide and phosphorylcholine, as shown in Scheme 1-4 (A).[11] Ceramide generation from sphingomyelin in the membrane is believed to cause the coalescence of small rafts to give larger membrane platforms, as depicted in Scheme 1-4 (B).[12-14] Ceramide-enriched plasma membrane domains are implicated in different cell signalling processes. These domains mediate membrane receptor clustering, which allows for more efficient signal transmission in the cell.[15]

A

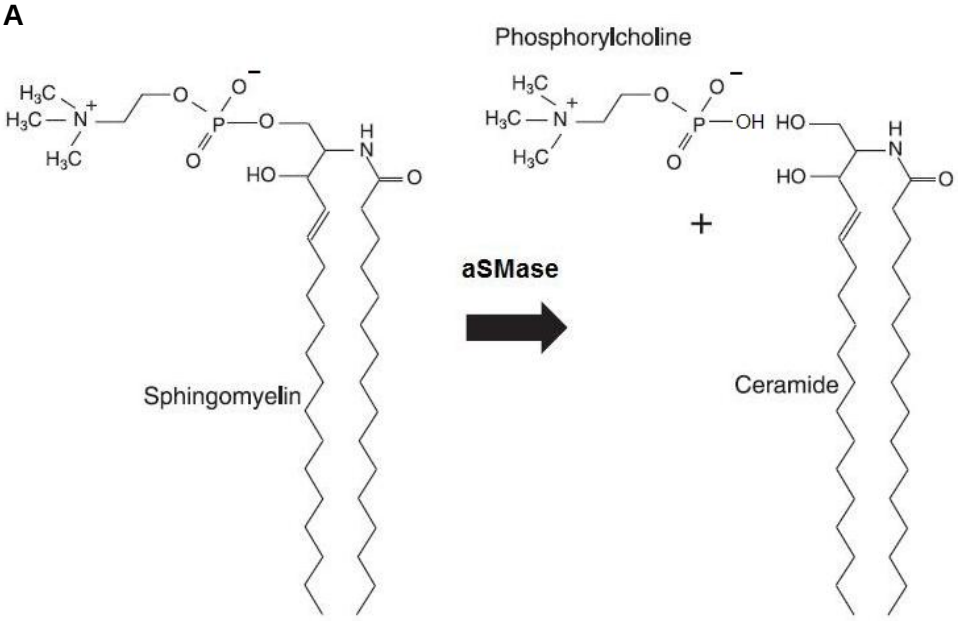

B

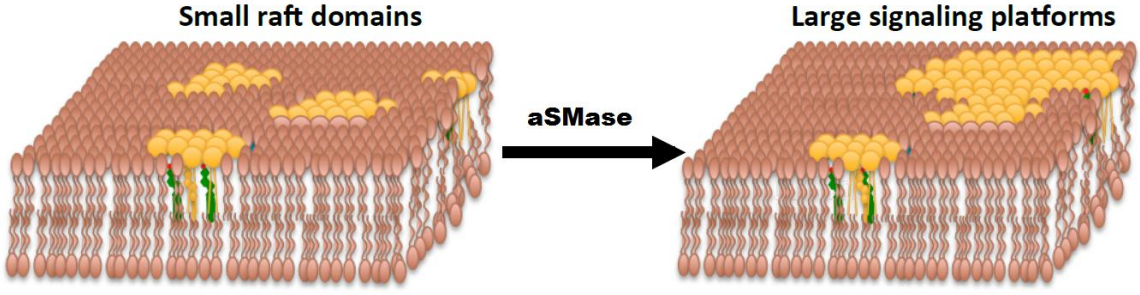

Scheme 1-4. The aSMase hydrolyzes sphingomyelin (SM) to give ceramide (Cer). A) Breakdown of SM to give Cer and phosphorylcholine. Adapted from reference 11. B) Coalescence of small raft domains to form large signaling platforms through the action of the aSMase. Adapted from reference 14.

Ceramide can also be synthesized biochemically at the level of the endoplasmic reticulum (ER) via a pathway termed *de novo* ceramide generation, as outlined in Scheme 1-5.[16] *De novo* ceramide synthesis involves the condensation of serine and palmitate by serine palmitoyltransferase (SPT), as well as a reduction step in order to yield sphinganine. Ceramide is then obtained from acylation of the amine moiety of sphinganine with an acyl-CoA of variable chain length by an enzyme of the ceramide synthase (CerS) family.[17] CerS enzymes can also be referred to as (dihydro)ceramide synthases since they generate dihydroceramide and not ceramide directly. Dihydroceramide, which lacks the unsaturation in its long acyl-chain, can yield ceramide by the action of desaturases.[7] The CerS family of enzymes is comprised of six distinct isoforms.[18] These enzymes exhibit substrate specificity for different acyl-CoA moieties allowing them to generate unique ceramides with distinct N-acyl chain lengths.[19] For example, long-chain C16 ceramide is known to be generated by CerS5 and CerS6, whereas very long-chain C24 ceramide is produced by CerS2.[18,20]

In addition to the two main biosynthetic pathways described above, the activity of some metabolic enzymes can contribute to ceramide production in biological systems. For instance, ceramide can be generated as a result of reverse activity of the acid ceramidase, hydrolysis of complex glycosylated lipids or hydrolysis of Cer-1-P.[21-23] Ceramide can also be metabolized to other sphingolipids by different enzymes, as shown in Scheme 1-6.[16] Namely, it can be phosphorylated by ceramide kinase, glycosylated by glucosylceramide synthase or used by sphingomyelin synthases in the biosynthesis of sphingomyelin. Alternatively,

ceramide can be broken down by one of the many ceramidases, leading to the formation of sphingosine.[24] Sphingosine can in turn be phosphorylated by a sphingosine kinase enzyme in order to produce sphingosine-1-phosphate (S1P).[7]

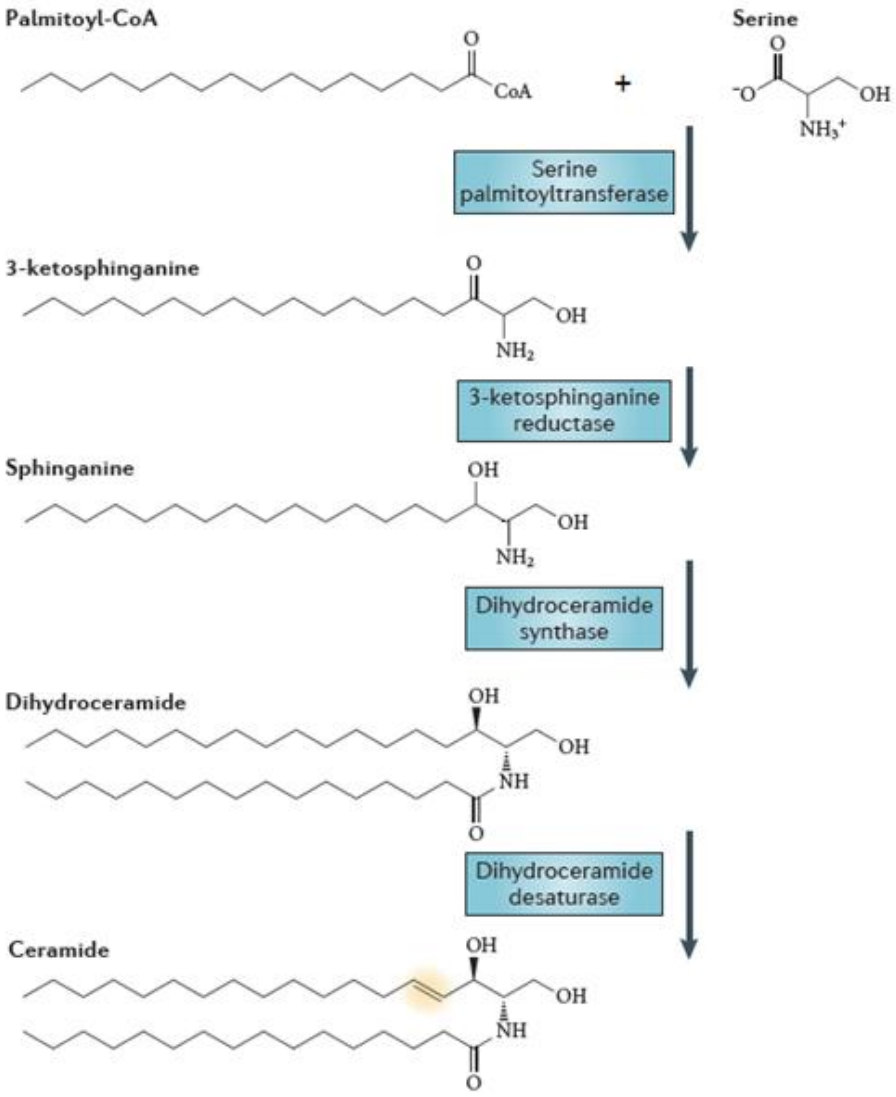

Scheme 1-5. *De novo* biosynthesis of ceramide. Adapted from reference 16.

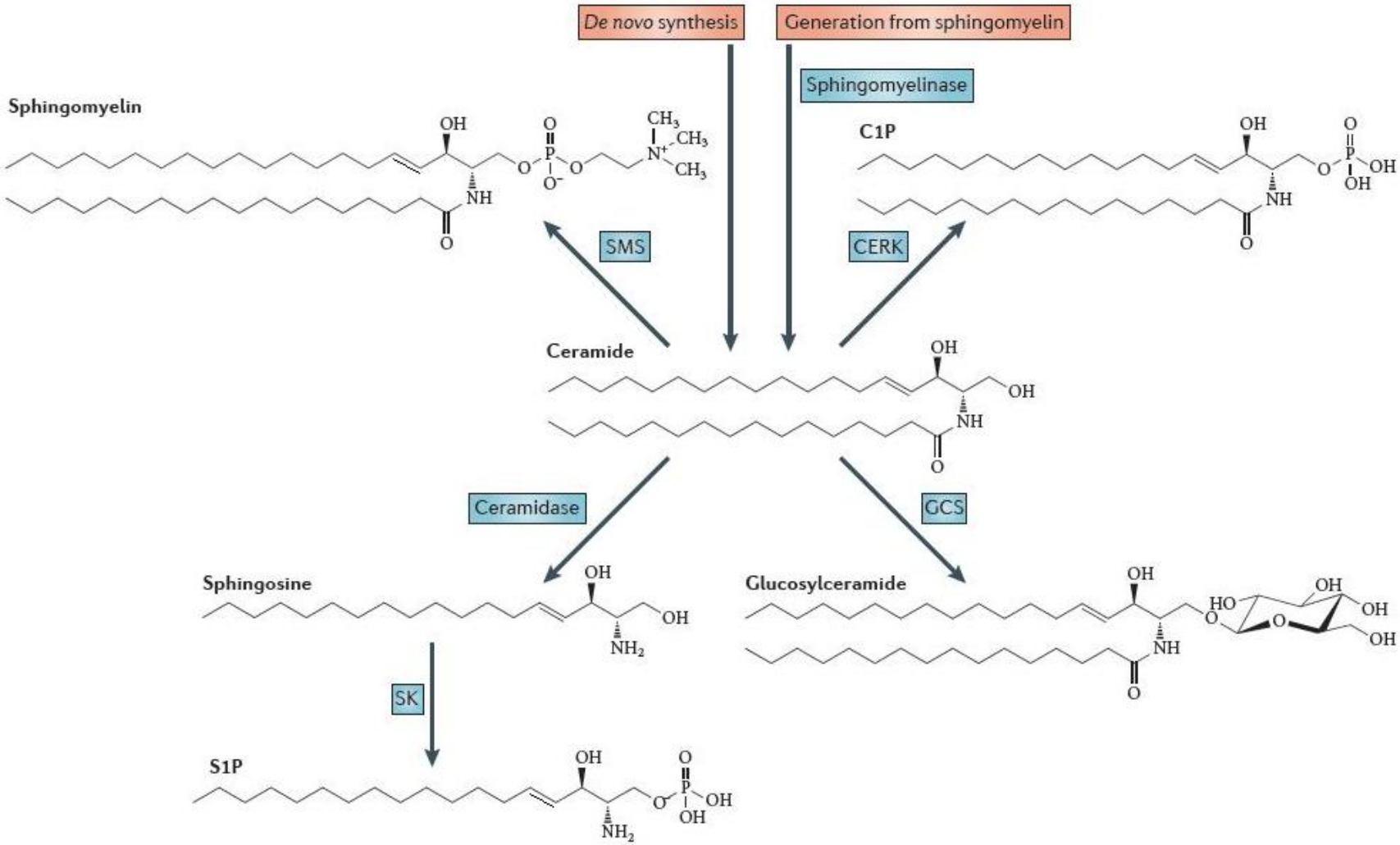

Scheme 1-6. Overview of ceramide metabolism. Adapted from reference 16.

As mentioned above, ceramides are produced in the ER and are transferred to the Golgi apparatus or to other biological membranes by vesicular transport or by the action of ceramide-binding proteins, such as the ceramide transport protein (CERT). CERT is involved in the intermembrane transfer of ceramides, but not of other sphingolipids. Also, this protein can effectively transfer long-chain ceramides (C14-C20), but not very long-chain ceramides.[25] Inhibition of CERT, which causes cellular accumulation of long-chain ceramides, is associated with apoptosis. Overall, cellular ceramide levels are controlled by these various enzymes of lipid metabolism and, as a result, the biological activity of ceramide is regulated within the cell.[16]

1.3 – The Biological Activity of Ceramide

Apart from its structural role in the membrane, ceramide is a lipid second messenger involved in mediating a wide variety of cellular processes, such as growth, differentiation, senescence, cell-cycle arrest and programmed cell death.[7,16] In some cases, ceramide exerts its effects by promoting the coalescence of small raft domains into large signalling platforms, as mentioned above. Defects in ceramide generation and metabolism are known to be involved in the pathogenesis of diseases, such as cancer, by contributing to tumour cell survival and resistance to chemotherapy.[26] Other diseases, such as cystic fibrosis, chronic obstructive pulmonary disorder, as well as Alzheimer's disease have also been linked to increased concentrations of ceramide.[27-29] In the biological membranes of resting cells, ceramide is present at low concentrations. However, in response to various

stress stimuli, the concentration of ceramide increases rapidly, reaching levels as high as 10% of the total membrane lipids in apoptotic cells.[30] A number of different extracellular agents and insults, such as chemotherapeutic drugs and UV irradiation, activate sphingomyelinases, which cleave sphingomyelin in the membrane, in order to generate ceramide.[30] In addition, treating cells with micromolar concentrations of exogenous ceramides allows for reaching intracellular ceramide levels that resemble those observed as a result of applying external stresses.[31,32]

Despite the numerous studies pertaining to ceramide that have been conducted over the last several decades, the role of this bioactive lipid in cell death is still poorly understood. Many studies have shown, however, that cell death in response to ceramide treatment occurs in a programmed fashion and is controlled by specific biochemical pathways. Programmed cell death (PCD), which was first described in the mid-1960s, allows for the elimination of unwanted cells in biological systems.[33] PCD involves three stages, which are the initiation phase, the commitment phase and the execution phase.[34] The initiation step typically takes place in the cellular compartment where the stress was induced, whereas the commitment step (or the “point of no return”) often occurs at the level of the mitochondria.[35] “Type I PCD”, which is also known as apoptosis, is undergone by the cell for the purpose of development, homeostasis, defence or aging.[36] Apoptosis is characterized by several biochemical features, such as a decrease in the mitochondrial membrane potential, the activation of selective proteases, the cleavage of chromosomal DNA and of certain cellular proteins, as well as the externalization of phosphatidylserine in the plasma membrane.[37] Ceramide has

been shown to cause apoptosis in a variety of cell lines.[38-40] Apoptosis can occur through the execution of an extrinsic or intrinsic pathway, as outlined in Scheme 1-7.[41]

The extrinsic pathway of apoptosis is initiated by extracellular stress signals that promote the recruitment of specific transmembrane receptors.[42] The binding of extracellular death receptor ligands, such as the tumour necrosis factor (TNF), to these transmembrane receptors leads to receptor aggregation and formation of a "death-inducing signalling complex" (DISC). Downstream in the signalling cascade, a family of cysteine proteases, which are called caspases, are activated.[43] These enzymes are responsible for cleaving various substrates during apoptotic cell death. Initiator caspases 8 and 10 are recruited by the DISC and, in turn, effector caspases 3 and 7 are activated.[41] This is a key event in the commitment of the cell to apoptosis.

Alternatively, the intrinsic pathway of apoptosis is triggered from within the cell by mitochondrial outer membrane permeabilization (MOMP) in response to various apoptotic stimuli.[42] Many studies have shown that the mitochondria play a central role in apoptosis.[44,45] In a particular study, up to 20% of exogenously added ceramides taken up by HL-60 cells were recovered in the mitochondria. In the presence of apoptotic stimuli, MOMP causes dissipation of the mitochondrial membrane potential ($\Delta\psi_m$) and promotes the release of apoptogenic proteins, such as cytochrome *c*, from the mitochondrial intramembrane space into the cytosol.[45] Cytochrome *c* then associates with the "apoptosis protease activating factor-1" (Apaf-1) in order to form the apoptosome complex. This complex is responsible for

mediating the activation of caspase 9, which in turn activates the executioner caspases 3 and 7.[41]

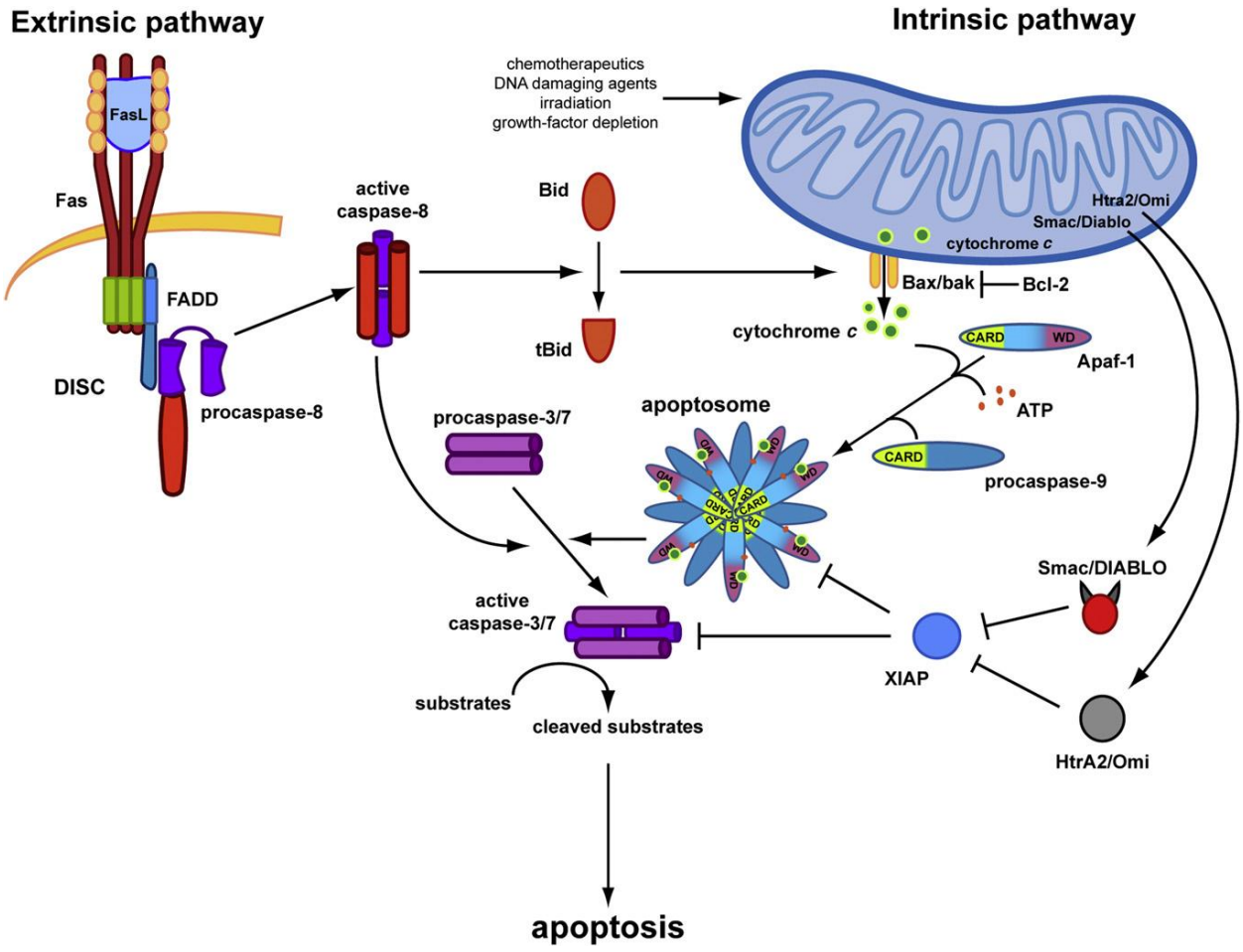

Scheme 1-7. Extrinsic and intrinsic pathways of apoptotic signaling in biological systems. Reproduced from reference 41 with approval.

"Type II PCD", which is also known as necrosis, is a form of cell death resulting from exposure to conditions of intense physico-chemical stress.[46] Necrotic cell death, which was long viewed as a mode of cell death that takes place in an uncontrolled manner, is now recognized as a form of regulated cell death implicating specific molecular targets.[47] Necrosis is undergone by the cell in the absence of the

biochemical markers of apoptosis and typically occurs in a caspase-independent manner.[46] The biochemical features of necrotic cell death are an increase in cell volume, the loss of plasma membrane integrity and the spilling of intracellular contents into the extracellular space.[48] Caspase-independent cell death with ceramide has been shown to occur in different cell lines.[49,50] As shown in scheme 1-8, some key mediators of necrotic cell death are the receptor interacting protein-1 (RIP1) and the receptor interacting protein-3 (RIP3).[41,51] The RIP1/RIP3 signalling cascade is known to involve increased intracellular reactive oxygen species (ROS) production.[52,53] In summary, ceramide can exhibit different biological activity based on the cellular context.

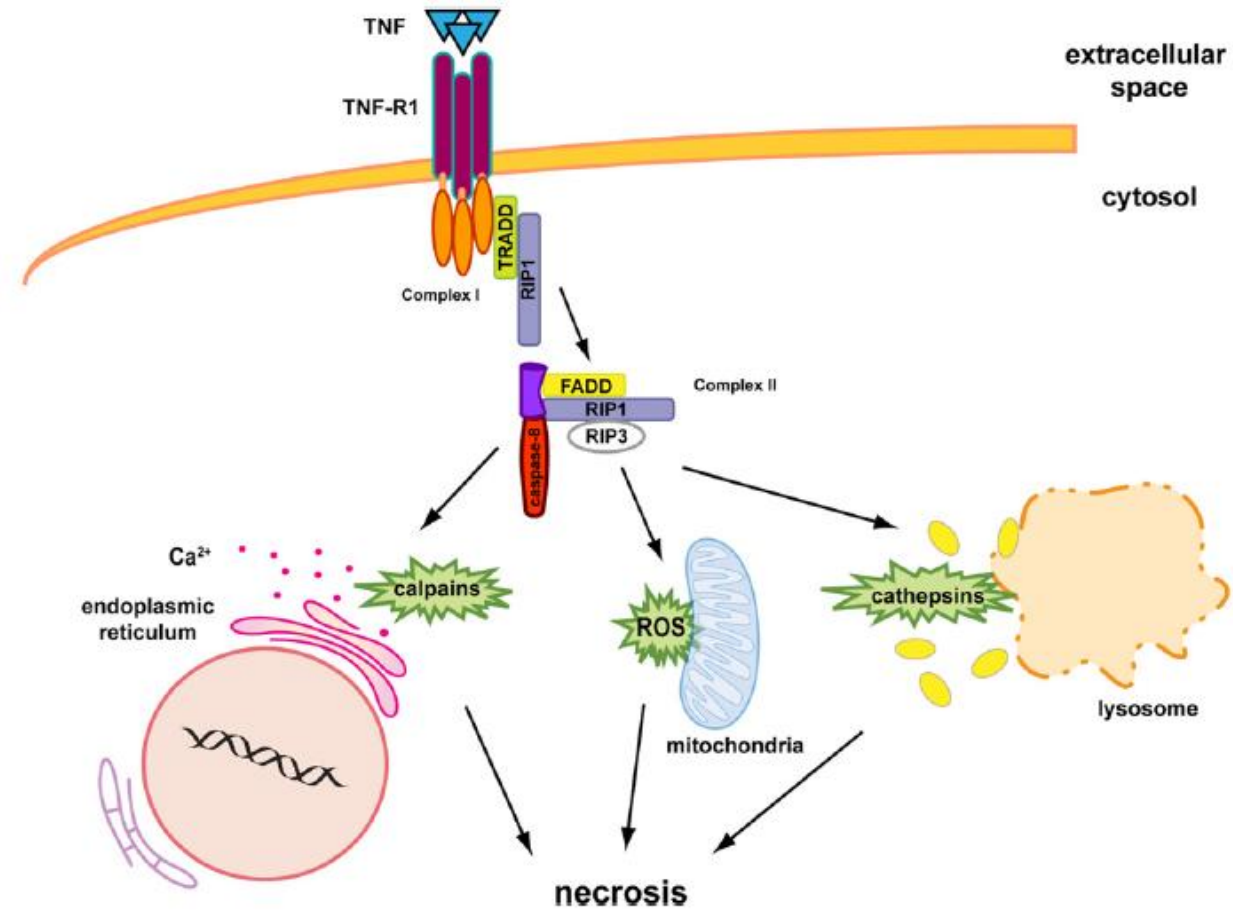

Scheme 1-8. Cell signaling events during necrosis in biological systems. Reproduced from reference 41 with approval.

Given the complexity of ceramide metabolism and structure, an abundance of individual molecular species of ceramide are present in the cell and they are found in different subcellular compartments.[54] Specific ceramides have been shown to cause distinct biological effects that are dependent on their N-acyl chain length.[19] The biological effects of some short-, long- and very long-chain ceramides are reported in Table 1-1.[39,40,55] Long-chain C16 Cer is known to be an important mediator of apoptosis.[20] In fact, several reports have shown that, under pro-apoptotic conditions, there is an increase in the endogenous levels of this long-chain ceramide in cells. For example, increased levels of C16 Cer, as well as C24 Cer have been detected in HeLa cells subjected to ionizing radiation.[56] The increase in the cellular levels of C16 Cer was attributed to enhanced activity of the CerS5 enzyme, which is responsible for *de novo* generation of this ceramide. In fact, the overexpression of CerS5 significantly promoted apoptosis in the irradiated cells. However, overexpression of CerS2, which is involved in the biosynthesis of very long-chain C24 Cer, reduced apoptosis by nearly half. These findings suggest that C24 Cer has a protective effect in HeLa cells and that the balance between C16 and C24 ceramides is important in regulating apoptosis in these cells.[56] Due to its very long N-acyl chain, C24 Cer interacts less with cholesterol, which could impair the functionality of lipid rafts and apoptotic signalling. This might explain the pro-proliferative effects that have been reported with C24 Cer.[19] The biological activity of the very long-chain C22 Cer has not been extensively studied to date. Therefore, the effects of this particular ceramide on cell viability are not well known. However, it has been observed that, in Huh7 cells undergoing apoptosis, the levels of C16 Cer were increased by 2-fold while the levels of C22 Cer remained unchanged.[57] In

addition, exogenous C22 Cer was shown to cause a decrease in the viability of HCT116 cells.[58] Based on these findings, one could hypothesize that C22 Cer has some anti-proliferative properties in cells, without exhibiting high apoptotic activity.[19]

The differential effects of long- and very long-chain ceramides have been investigated previously. Apoptosis induced by UV-C irradiation was shown to be associated with increases in the levels of long-chain C16, C18 and C20 ceramides, but not very long-chain ceramides.[19] Moreover, it was determined that Bak and Bax, which are mitochondrial proteins of the Bcl-2 family, are essential for the accumulation of long-chain ceramides in response to UV-C irradiation.[59] Furthermore, the formation of mitochondrial ceramide-rich macrodomains (MCRM) is thought to promote the activation and translocation of Bak and Bax, which facilitates mitochondrial outer membrane permeabilization (MOMP) leading to apoptosis.[45] Overall, the role of specific ceramides in the pathogenesis of different diseases is dependent on factors such as their chemical structures, the cellular compartments in which they are located or generated, as well as the biochemical pathway involved in their generation.

Table 1-1. Chain length specific properties of ceramides in biological systems.

Ceramide Species	Biological Effect
C16 Cer	Pro-apoptotic
C22 Cer	Anti-proliferative
C24 Cer	Pro-proliferative
C2 Cer*	Pro-apoptotic

***** C2 Cer is a short-chain ceramide commonly used as a water-soluble analogue to mimic endogenous ceramides. From references 39, 40 and 55.

Due to the physical properties of ceramides, studying the biological effects of these lipids in cells is challenging. Ceramide, with its two aliphatic chains and neutral headgroup is a hydrophobic molecule that exhibits very low aqueous solubility and poor membrane permeability.[31] Short-chain (C2-C8) analogues of natural ceramides are routinely employed for studying ceramide bioactivity in cells. However, because the short-chain analogues may localize within cellular compartments in a non-physiological manner, the relevance of the results obtained from these studies must be questioned.[60] Due to their enhanced solubility, short-chain ceramides are not restricted to specific membrane compartments in the cell, whereas natural long-chain ceramides are confined to the subcellular location in which they are generated biochemically.[31,61] It has, however, been shown by radiolabelling studies in A549 cells that a deacylation/reacylation process, which implicates the recycling of the sphingosine backbone, takes place in order to metabolize short-chain C6 Cer to endogenous long- and very long-chain C16 and C24 ceramides.[62,63] Briefly, short-chain ceramides can be employed as derivatives of natural ceramides for studying the activity of this family of bioactive sphingolipids in cells, but caution must be used in interpreting the findings obtained from such work.

Another approach for studying the biological effects of ceramide in cells has consisted in using cationic ceramide analogues, such as LCL124. Due to the positive charge contained in the structure of LCL124, it readily accumulates in the mitochondria and initiates apoptosis by causing mitochondrial membrane depolarization.[38] Alternatively, a solvent mixture of ethanol and dodecane (98:2)

can be used to disperse long-chain ceramides in aqueous solution. This method was shown to be effective in delivering long-chain ceramides to U937 cells and HCT116 cells.[58,64] However, experimental techniques for manipulating the concentration and intracellular localization of signalling lipids, such as natural long-chain ceramides, in an acute and minimally invasive manner are limited.[65] Photo-release technology is an alternative approach for studying the biological effects of ceramide in cells. This method relies on the use of a caging moiety to mask the bioactivity of the lipid. After uptake of the caged compound, photo-release can be used to generate ceramide with spatial and temporal control. This technology can be applied to different ceramides in order to study the N-acyl chain length dependence of ceramide bioactivity in cells.

1.4 – Photocages for Biological Applications

The caging of complex biomolecules is gaining interest as a strategy for delivering these molecules into cells. Photocages are light-sensitive probes that are designed to deliver a compound of interest, in its inactive form, to a desired location within the cell. The biologically active form of the molecule is then released by the means of UV irradiation.[66] Photo-removable protecting groups offer spatial and temporal control due to the fact that light can be precisely manipulated during the photo-release process.[67] For these reasons, photocaging technology is an attractive approach that can be applied towards understanding biological problems. Caged compounds were first used in living cells in the 1970s, when caged cAMP and caged ATP were prepared and studied.[68,69] Since then, photocages have been used to

release calcium[70-72], neurotransmitters[73,74], inositols[75,76], peptides[77,78], mRNA[79], DNA[80], as well as other important biomolecules.

Photo-removable protecting groups that are used for caging applications are required to possess certain properties. In order to minimize damage to cells, these chromophores should absorb light strongly at visible or near infrared (NIR) wavelengths and they should exhibit efficient and fast photo-release. In addition, the cage, as well as the by-products of photolysis should be biologically inert. Furthermore, the by-products should absorb light at shorter wavelengths than the cage. In order to measure the usefulness of a photocage for biological applications, the efficiency and rate of photolysis should be considered. These properties can be determined by laser flash photolysis.[81] The efficiency of photo-conversion, which is the percentage of caged compound that is converted to the uncaged material, is influenced by the extinction coefficient (ε) at the irradiation wavelength and by the quantum yield (Φ) of photo-release. The extinction coefficient refers to the proportion of incident light absorbed by the compound and the quantum yield is defined as the proportion of molecules that undergo photolysis to form the desired product after absorbing a photon.[82]

As shown in Scheme 1-9, there are four major classes of photo-removable protecting groups that are reported in the literature, which are the 2-nitrobenzyl (NB) groups, the benzoin groups (Bnz), the para-hydroxyphenacyl (pHP) groups and the benzyl (Bn) groups.[83] The last category comprises coumaryl (Cou) groups, for which the general structure is shown below (see Scheme 1-9). The most widely used photo-removable protecting groups are the NB groups. The photo-cleavage of

NB photocages occurs by the mechanism outlined in Scheme 1-10.[82] Although NB groups have been commonly employed for photocage applications, there are several drawbacks associated with these phototriggers. Some of these drawbacks are slow rates of substrate release, short wavelength absorption maxima (< 350 nm), small two-photon cross-sections, as well as the generation of reactive nitroso side products upon photolysis.[67] These shortcomings limit the use of NB photocages for biological applications. Much work has been done to address some of the limitations of NB photocages, but this will not be discussed any further here.

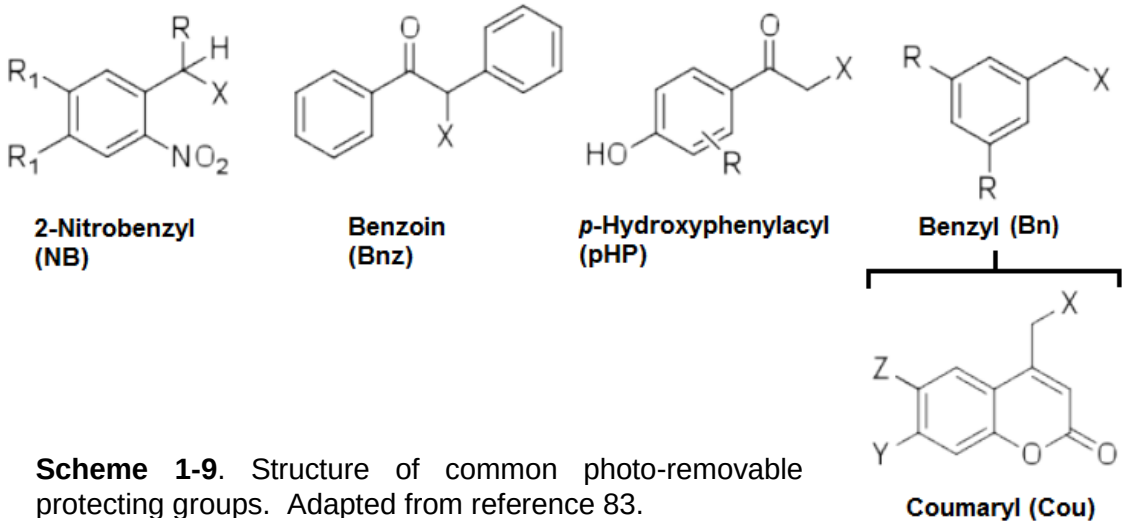

Scheme 1-9. Structure of common photo-removable protecting groups. Adapted from reference 83.

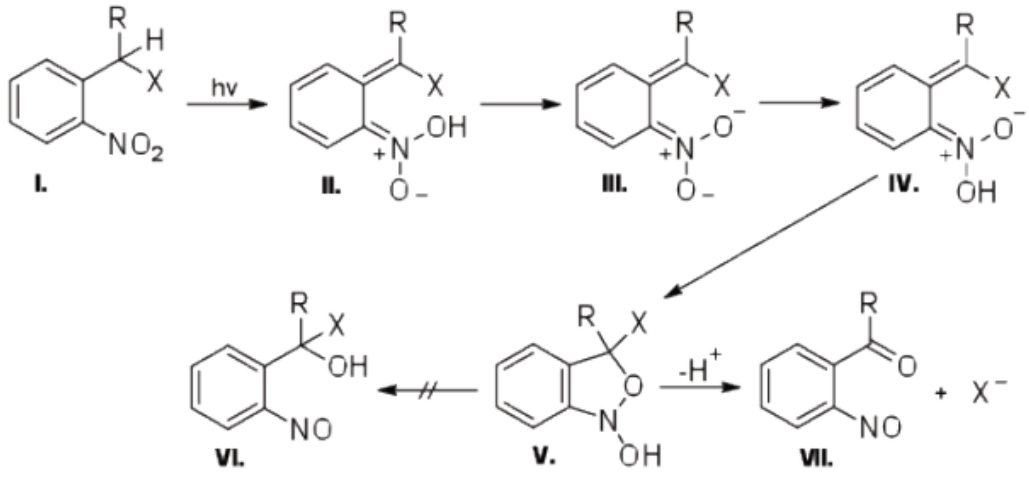

Scheme 1-10. Generalized reaction scheme for the photolysis of nitrobenzyl-caged compounds. From reference 82.

(Coumarin-4-yl)methyl phototriggers are a more recently developed class of caging groups that have been used to release phosphates, carboxylates, amines, alcohols, phenols and carbonyls.[84] The general structure of (coumarin-4-yl)methyl caging groups is a benzo-α-pyrone called coumarin with a methylene group at position 4 allowing for attachment to the leaving group (see Scheme 1-9 above). The photochemical reactivity exhibited by these compounds, which is shown in Scheme 1-11, is typical of arylalkyl-type photo-removable protecting groups.[84] Upon photolysis, the bond between the carbon of the methylene group and the heteroatom (oxygen, in the example shown below) is cleaved to give an anion of the leaving group (A^-), as well as a coumarin cation (CM^+) as a by-product. The coumarin cation is then trapped by the solvent (CM-OH) and the anion of the leaving group is protonated (H-A) and undergoes decarboxylation (slow step) in order to yield the free alcohol as well as carbon dioxide.

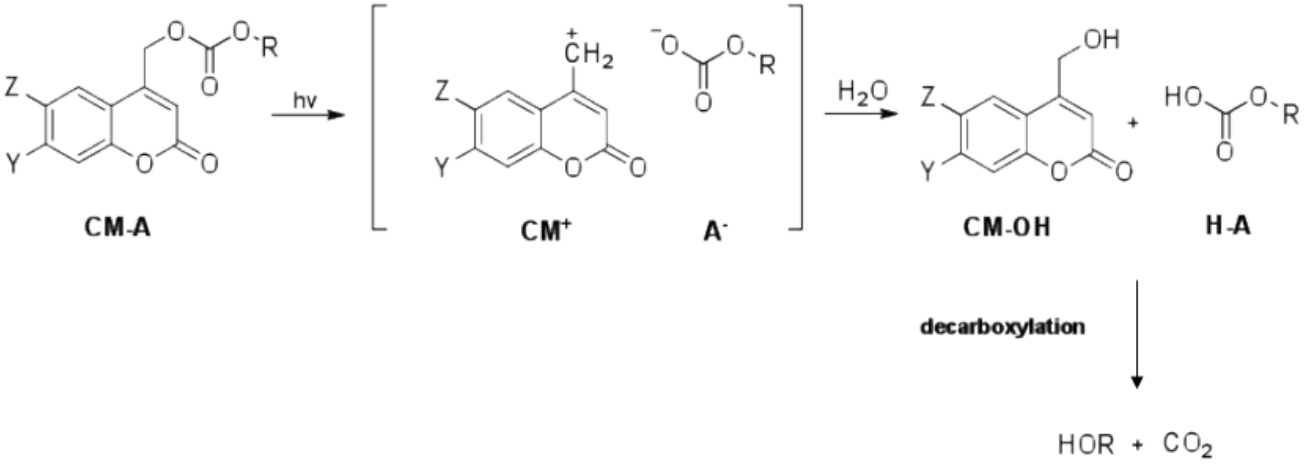

Scheme 1-11. Generalized photolysis of a (coumarin-4-yl)methyl-caged alcohol. Adapted from reference 84.

As outlined in Scheme 1-12, the following major processes are involved in the release of the substrate from a π,π* excited singlet state (^{1}[CM-A]*): 1) a bond breaking step affording the singlet ion pair (^{1}[CM^+A^-]) via a heterolytic pathway (rate constant= k_1) and 2) hydrolysis of the singlet ion pair to CM-OH and HA (rate constant= k_2) or recombination to ground state CM-A (rate constant= k_{rec}). It is also noteworthy that the use of electron-donating substituents can stabilize CM^+ and increasing acid strength can delocalize the negative charge in A^- in order to enhance k_1 over k_{rec}.[85]

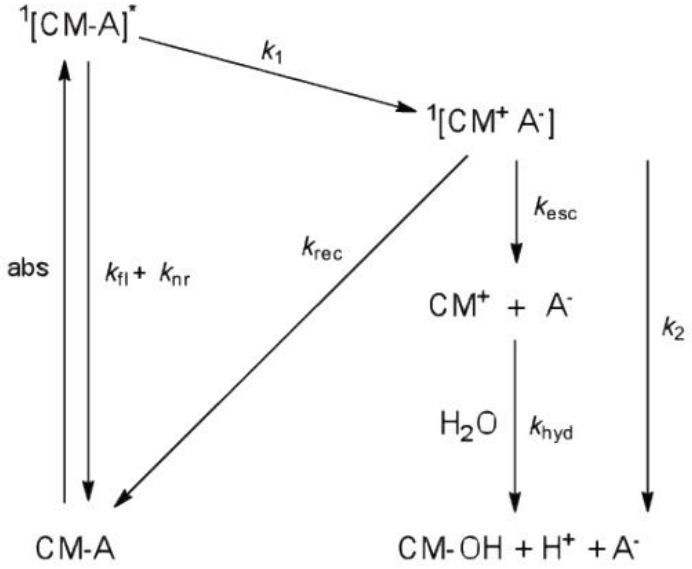

Scheme 1-12. Mechanism of photocleavage of (coumarin-4-yl)methyl esters. Reproduced from reference 85 with approval.

(Coumarin-4-yl)methyl phototriggers offer several advantages over conventional photo-removable protecting groups. For instance, they have large extinction coefficients at wavelengths greater than 300 nm, high photolysis efficiency (high Φ) at longer UV wavelengths (> 350 nm), fast photolysis kinetics (for the initial photocleavage step), large two-photon excitation cross-sections, as well as improved stability in the dark (i.e. resistance to hydrolysis). As shown in Scheme 1-

13, there are four subtypes of (coumarin-4-yl)methyl phototriggers that have been reported to date, which are the 7-alkoxy groups, the 6,7-dialkoxy groups, the 6-bromo-7-alkoxy groups and the 7-dialkylamino groups.[84] The photophysical and photochemical properties of coumarinyl cages depends strongly on the nature of the substituents on the coumarin ring. Namely, an electron-donating substitution at the C6 or C7 position shifts the absorption maximum to longer wavelengths. Particularly, 7-dialkylamino groups exhibit an absorption maximum that is red-shifted by more than 80 nm.[84] Also, the presence of the bromine atom in the 6-bromo-7-hydroxy-4-hydroxymethylcoumarin (Bhc) group (6-bromo-7-alkoxy subtype) lowers the pKa of the C7 hydroxyl group, which causes it to be deprotonated at pH 7. This causes a red-shift of the absorption maximum by 60 nm.[84] Overall, the spectral properties of some of these caging groups are advantageous when using coumarinyl-caged compounds for biological applications.

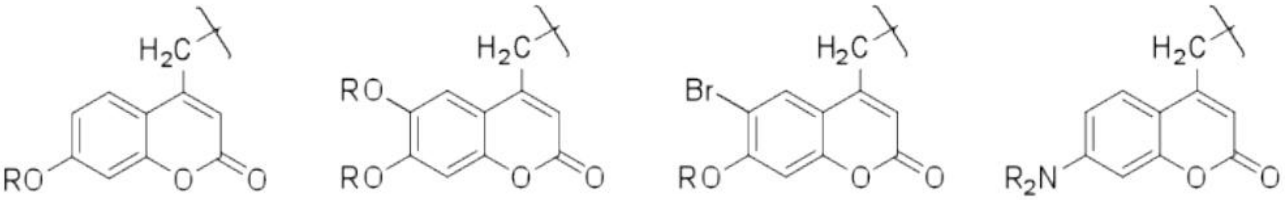

Scheme 1-13. Structures of (coumarin-4-yl)methyl phototriggers. From reference 84.

Although caged compounds have been widely used to generate a variety of biomolecules, there are relatively few examples where photocaging technology has been applied to lipids. The photo-removable protecting groups that have most often

been used for caging lipids are the NB and coumarinyl groups.[65] The 7-diethylamino-(coumarin-4-yl)methyl group was used to cage the lipid second messengers phosphatidylinositol-3-phosphate (PI(3)P) and phosphatidylinositol-3,4,5-trisphosphate (PI(3,4,5)P_3) and these compounds were used in cells.[86,87] The caging of sphingolipids, such as sphingosine and dihydrosphingosine, with the 2-nitrobenzyl group has also been reported in the literature.[88] These photocages were administered to cells and whole-cell patch clamp experiments were conducted in order to measure the effects of the photochemical generation of the sphingolipids on calcium-activated currents in neurons. S1P, a phosphorylated metabolite of sphingosine, has been caged with 1-(2-nitrophenyl)diazoethane and used to measure effects on DNA synthesis.[89] In addition, the caging technology has been used for ceramide-1-phosphate (Cer-1P), a phosphorylated metabolite of ceramide. Caged Cer-1P analogues bearing the fluorescent caging moieties 7-(diethylamino)coumarin (DECM) and 4-bromo-5-hydroxy-2-nitrobenzhydryl (BHNB) were prepared and delivered to cells in order to measure the effects of photochemically generated Cer-1P on cell growth.[90] Moreover, a caged ceramide has been reported in the literature, where the release of the active form of the lipid requires two steps, photo-cleavage and lactonization.[91] However, this caged ceramide was not administered to cells. Further development of tailored caged lipid molecules is required in order to gain a better understanding of the cellular signalling pathways involving lipid second messengers.[65]

1.5 - Coumarinyl-caged Ceramides

In earlier work by our group, which was done in collaboration with the group of Dr. R. Bittman, Bhc-caged ceramides were prepared for the purpose of investigating the effects of ceramides in biological systems. The coumarinyl caging moiety, which has been used to prepare other caged lipids that are reported in the literature, was chosen based its advantages over other types of photo-removable protecting groups (e.g. NB group). For instance, coumarinyl groups absorb light at longer wavelengths, possess higher quantum yields of photolysis and exhibit higher extinction coefficients.[65] These properties allow for reduced phototoxicity upon uncaging in biological systems. Furthermore, the presence of bromine in the Bhc group causes the phenolate form of the compound to predominate at physiological pH, which allows for uncaging at longer wavelengths.[84]

Bhc-caged C16 Dihydro-Cer (**9a**) was synthesized by our collaborators and was shown to undergo efficient photorelease in solution. Also, its uptake into cells was successfully demonstrated.[92] In another report by our group, it was demonstrated that UV irradiation and photolysis of the Bhc-caged C16 Cer (**9b**) in supported lipid bilayers prepared from POPC causes the formation of small ordered ceramide domains that phase separate from the bulk fluid membrane.[93] Moreover, the generation of ceramide from Bhc-caged ceramides, such as Bhc-caged C16 Cer (**9b**), in phase-separated (L_d/L_o) supported lipid bilayers prepared from DOPC/ESM/Chol was shown to promote the reorganization of liquid-ordered (L_o) domains in the model membrane system.[94]

For the purpose of studying the N-acyl chain length dependence of the biological effects of ceramide in cells, a series of methoxytriethylene glycol-conjugated, also referred to as (mTEG)ylated or “pegylated”, caged ceramides were synthesized and are reported here. (7-mTEGylated-coumarin-4-yl)methoxycarbonyl- (Tcmoc-) and 6-bromo-7-mTEGylated-coumarin-4-yl)methoxycarbonyl- (Btcmoc-)caged ceramides were prepared in a manner similar to the Bhc-caged ceramides, which will be described in the next chapter. It was anticipated that the presence of the mTEG group on the coumarinyl moiety of the caged ceramides would increase the aqueous solubility and membrane permeability of the compounds.

In the work presented here, the goals were to evaluate the effectiveness of using coumarinyl-caged ceramides for delivering specific ceramides to cells and to determine the biological effects of generating ceramide photochemically in cells through UV irradiation of the caged ceramides. These questions were addressed by initially measuring the photophysical and photochemical properties of the caged ceramides and assessing their uptake in cells (Chapter 2). The effects of the photochemical generation of ceramide on cell viability were also assessed and the N-acyl chain length dependence of these effects was evaluated using a series of mTEGylated caged ceramides (Chapter 3). Furthermore, in order to elucidate the mechanism by which the photochemical generation of ceramide in cells causes changes in viability, different cell signalling pathways were probed by performing various bioassays (Chapter 4). Overall, a novel approach was utilized for studying

the biological effects of specific ceramides in cells and the findings obtained from this work are presented and discussed in the chapters that follow.

1.6 - References

(1) Alberts, B.; Bray, D.; Lewis, J.; Raff, M.; Roberts, K.; Watson, J. D. In *Molecular Biology of the Cell, Third Edition*; Garland Publishing, Inc.: 1994, p 477.
(2) Singer, S. J.; Nicolson, G. L. *Science* **1972**, *175*.
(3) In *Encyclopædia Britannica Online*.
(4) Hauser, H.; Poupart, G. In *The Structure of Biological Membranes*; Yeagle, P. L., Ed.; CRC Press: 2005, p 1.
(5) Brown, D. A.; London, E. *Journal of Biological Chemistry* **2000**, *275*, 17221.
(6) Pike, L. J. *Journal of Lipid Research* **2006**, *47*, 1597.
(7) Hannun, Y. A.; Obeid, L. M. *Nat Rev Mol Cell Biol* **2008**, *9*, 139.
(8) Ahmed, S. N.; Brown, D. A.; London, E. *Biochemistry* **1997**, *36*, 10944.
(9) Simons, K.; Ikonen, E. *Nature* **1997**, *387*, 569.
(10) Kitatani, K.; Idkowiak-Baldys, J.; Hannun, Y. A. *Cellular Signalling* **2008**, *20*, 1010.
(11) Smith, E. L.; Schuchman, E. H. *The FASEB Journal* **2008**, *22*.
(12) Bollinger, C. R.; Teichgräber, V.; Gulbins, E. *Biochimica et Biophysica Acta (BBA) - Molecular Cell Research* **2005**, *1746*, 284.
(13) Cremesti, A. E.; Goni, F. M.; Kolesnick, R. *FEBS Letters* **2002**, *531*, 47.
(14) Carter Ramirez, D. M., University of Ottawa, 2013.
(15) Carpinteiro, A.; Dumitru, C.; Schenck, M.; Gulbins, E. *Cancer Letters* **2008**, *264*, 1.
(16) Morad, S. A. F.; Cabot, M. C. *Nat Rev Cancer* **2013**, *13*, 51.
(17) Linn, S. C.; Kim, H. S.; Keane, E. M.; Andras, L. M.; Wang, E.; Merrill Jr, A. H. *Biochemical Society Transactions* **2001**, *29*, 831.
(18) Mullen, T. D.; Obeid, L. M. *Anti-Cancer Agents in Medicinal Chemistry- Anti-Cancer Agents)* **2012**, *12*, 340.
(19) Grösch, S.; Schiffmann, S.; Geisslinger, G. *Progress in Lipid Research* **2012**, *51*, 50.
(20) Mullen, T. D.; Jenkins, R. W.; Clarke, C. J.; Bielawski, J.; Hannun, Y. A.; Obeid, L. M. *Journal of Biological Chemistry* **2011**, *286*, 15929.
(21) Ishibashi, Y.; Nakasone, T.; Kiyohara, M.; Horibata, Y.; Sakaguchi, K.; Hijikata, A.; Ichinose, S.; Omori, A.; Yasui, Y.; Ishida, H.; Kiso, M.; Okino, N.; Ito, M. *Journal of Biological Chemistry* **2007**, *282*, 11386.
(22) Mitra, P.; Maceyka, M.; Payne, S. G.; Lamour, N.; Milstien, S.; Chalfant, C. E.; Spiegel, S. *FEBS Letters* **2007**, *581*, 735.
(23) Okino, N.; He, X.; Gatt, S.; Sandhoff, K.; Ito, M.; Schuchman, E. H. *Journal of Biological Chemistry* **2003**, *278*, 29948.
(24) Xu, R.; Jin, J.; Hu, W.; Sun, W.; Bielawski, J.; Szulc, Z.; Taha, T.; Obeid, L. M.; Mao, C. *The FASEB Journal* **2006**, *20*, 1813.
(25) Kumagai, K.; Yasuda, S.; Okemoto, K.; Nishijima, M.; Kobayashi, S.; Hanada, K. *Journal of Biological Chemistry* **2005**, *280*, 6488.
(26) Reynolds, C. P.; Maurer, B. J.; Kolesnick, R. N. *Cancer Letters* **2004**, *206*, 169.
(27) He, X.; Huang, Y.; Li, B.; Gong, C.-X.; Schuchman, E. H. *Neurobiology of Aging* **2010**, *31*, 398.

(28) Petrache, I.; Natarajan, V.; Zhen, L.; Medler, T. R.; Richter, A. T.; Cho, C.; Hubbard, W. C.; Berdyshev, E. V.; Tuder, R. M. *Nat Med* **2005**, *11*, 491.
(29) Teichgraber, V.; Ulrich, M.; Endlich, N.; Riethmuller, J.; Wilker, B.; De Oliveira-Munding, C. C.; van Heeckeren, A. M.; Barr, M. L.; von Kurthy, G.; Schmid, K. W.; Weller, M.; Tummler, B.; Lang, F.; Grassme, H.; Doring, G.; Gulbins, E. *Nat Med* **2008**, *14*, 382.
(30) Hannun, Y. A. *Science* **1996**, *274*.
(31) Hannun, Y. A.; Luberto, C. *Trends in Cell Biology* **2000**, *10*, 73.
(32) Huang, W.-C.; Chen, C.-L.; Lin, Y.-S.; Lin, C.-F. *Journal of Lipids* **2011**, *2011*, 15.
(33) Lockshin Ra Fau - Williams, C. M.; Williams, C. M. *Journal of Insect Physiology* **1965**, *11*, 123.
(34) Taha, T. A.; Mullen, T. D.; Obeid, L. M. *Biochimica et Biophysica Acta (BBA) - Biomembranes* **2006**, *1758*, 2027.
(35) Ferri, K. F.; Kroemer, G. *Nat Cell Biol* **2001**, *3*, E255.
(36) Vaux, D. L.; Strasser, A. *Proceedings of the National Academy of Sciences* **1996**, *93*, 2239.
(37) Strasser, A.; O'Connor, L.; Dixit, V. M. *Annual Review of Biochemistry* **2000**, *69*, 217.
(38) Beckham, T. H.; Lu, P.; Jones, E. E.; Marrison, T.; Lewis, C. S.; Cheng, J. C.; Ramshesh, V. K.; Beeson, G.; Beeson, C. C.; Drake, R. R.; Bielawska, A.; Bielawski, J.; Szulc, Z. M.; Ogretmen, B.; Norris, J. S.; Liu, X. *Journal of Pharmacology and Experimental Therapeutics* **2013**, *344*, 167.
(39) Fillet, M.; Bentires-Alj, M.; Deregowski, V.; Greimers, R.; Gielen, J.; Piette, J.; Bours, V.; Merville, M.-P. *Biochemical Pharmacology* **2003**, *65*, 1633.
(40) Hartfield, P. J.; Mayne, G. C.; Murray, A. W. *FEBS Letters* **1997**, *401*, 148.
(41) Lamkanfi, M.; Dixit, V. M. *Cell Host & Microbe* **2010**, *8*, 44.
(42) Galluzzi, L.; Vitale, I.; Abrams, J. M.; Alnemri, E. S.; Baehrecke, E. H.; Blagosklonny, M. V.; Dawson, T. M.; Dawson, V. L.; El-Deiry, W. S.; Fulda, S.; Gottlieb, E.; Green, D. R.; Hengartner, M. O.; Kepp, O.; Knight, R. A.; Kumar, S.; Lipton, S. A.; Lu, X.; Madeo, F.; Malorni, W.; Mehlen, P.; Nunez, G.; Peter, M. E.; Piacentini, M.; Rubinsztein, D. C.; Shi, Y.; Simon, H. U.; Vandenabeele, P.; White, E.; Yuan, J.; Zhivotovsky, B.; Melino, G.; Kroemer, G. *Cell Death Differ* **2012**, *19*, 107.
(43) Thornberry, N. A.; Lazebnik, Y. *Science* **1998**, *281*, 1312.
(44) Babiychuk, E. B.; Atanassoff, A. P.; Monastyrskaya, K.; Brandenberger, C.; Studer, D.; Allemann, C.; Draeger, A. *PLoS One* **2011**, *6*, e23706.
(45) Lee, H.; Rotolo, J. A.; Mesicek, J.; Penate-Medina, T.; Rimner, A.; Liao, W.-C.; Yin, X.; Ragupathi, G.; Ehleiter, D.; Gulbins, E. *PLoS One* **2011**, *6*, e19783.
(46) Festjens, N.; Vanden Berghe, T.; Vandenabeele, P. *Biochimica et Biophysica Acta (BBA) - Bioenergetics* **2006**, *1757*, 1371.
(47) Fulda, S. *Cancer Biol Ther* **2013**, *14*, 999.
(48) Berghe, T. V.; Vanlangenakker, N.; Parthoens, E.; Deckers, W.; Devos, M.; Festjens, N.; Guerin, C. J.; Brunk, U. T.; Declercq, W.; Vandenabeele, P. *Cell Death Differ* **2010**, *17*, 922.
(49) Thon, L.; Möhlig, H.; Mathieu, S.; Lange, A.; Bulanova, E.; Winoto-Morbach, S.; Schütze, S.; Bulfone-Paus, S.; Adam, D. *The FASEB Journal* **2005**, *19*, 1945.
(50) Zhao, S.; Yang, Y.-N.; Song, J.-G. *Journal of Cellular Physiology* **2004**, *199*, 47.
(51) Degterev, A.; Hitomi, J.; Germscheid, M.; Ch'en, I. L.; Korkina, O.; Teng, X.; Abbott, D.; Cuny, G. D.; Yuan, C.; Wagner, G.; Hedrick, S. M.; Gerber, S. A.; Lugovskoy, A.; Yuan, J. *Nat Chem Biol* **2008**, *4*, 313.

(52) Lin, Y.; Choksi, S.; Shen, H.-M.; Yang, Q.-F.; Hur, G. M.; Kim, Y. S.; Tran, J. H.; Nedospasov, S. A.; Liu, Z.-g. *Journal of Biological Chemistry* **2004**, *279*, 10822.
(53) Vanlangenakker, N.; Vanden Berghe, T.; Krysko, D. V.; Festjens, N.; Vandenabeele, P. *Current Molecular Medicine* **2008**, *8*.
(54) Hannun, Y. A.; Obeid, L. M. *Journal of Biological Chemistry* **2011**, *286*, 27855.
(55) Hartmann, D.; Lucks, J.; Fuchs, S.; Schiffmann, S.; Schreiber, Y.; Ferreirós, N.; Merkens, J.; Marschalek, R.; Geisslinger, G.; Grösch, S. *The International Journal of Biochemistry & Cell Biology* **2012**, *44*, 620.
(56) Mesicek, J.; Lee, H.; Feldman, T.; Jiang, X.; Skobeleva, A.; Berdyshev, E. V.; Haimovitz-Friedman, A.; Fuks, Z.; Kolesnick, R. *Cellular Signalling* **2010**, *22*, 1300.
(57) Chatzakos, V.; Rundlöf, A. K.; Ahmed, D.; de Verdier, P. J.; Flygare, J. *Biochemical Pharmacology* **2012**, *84*, 712.
(58) Rénert, A.-F.; Leprince, P.; Dieu, M.; Renaut, J.; Raes, M.; Bours, V.; Chapelle, J.-P.; Piette, J.; Merville, M.-P.; Fillet, M. *Journal of Proteome Research* **2009**, *8*, 4810.
(59) Siskind, L. J.; Mullen, T. D.; Romero Rosales, K.; Clarke, C. J.; Hernandez-Corbacho, M. J.; Edinger, A. L.; Obeid, L. M. *Journal of Biological Chemistry* **2010**, *285*, 11818.
(60) Sot, J.; Goñi, F. M.; Alonso, A. *Biochimica et Biophysica Acta (BBA) - Biomembranes* **2005**, *1711*, 12.
(61) Venkataraman, K.; Futerman, A. H. *Trends in Cell Biology* **2000**, *10*, 408.
(62) Chapman, J. V.; Gouazé-Andersson, V.; Messner, M. C.; Flowers, M.; Karimi, R.; Kester, M.; Barth, B. M.; Liu, X.; Liu, Y.-Y.; Giuliano, A. E.; Cabot, M. C. *Biochemical Pharmacology* **2010**, *80*, 308.
(63) Ogretmen, B.; Pettus, B. J.; Rossi, M. J.; Wood, R.; Usta, J.; Szulc, Z.; Bielawska, A.; Obeid, L. M.; Hannun, Y. A. *Journal of Biological Chemistry* **2002**, *277*, 12960.
(64) Ji, L.; Zhang, G.; Uematsu, S.; Akahori, Y.; Hirabayashi, Y. *FEBS Letters* **1995**, *358*, 211.
(65) Höglinger, D.; Nadler, A.; Schultz, C. *Biochimica et Biophysica Acta (BBA) - Molecular and Cell Biology of Lipids* **2014**, *1841*, 1085.
(66) Ellis-Davies, G. C. R. *Nat Meth* **2007**, *4*, 619.
(67) Mayer, G.; Heckel, A. *Angewandte Chemie International Edition* **2006**, *45*, 4900.
(68) Engels, J.; Schlaeger, E. J. *Journal of Medicinal Chemistry* **1977**, *20*, 907.
(69) Kaplan, J. H.; Forbush, B.; Hoffman, J. F. *Biochemistry* **1978**, *17*, 1929.
(70) Adams, S. R.; Kao, J. P. Y.; Grynkiewicz, G.; Minta, A.; Tsien, R. Y. *Journal of the American Chemical Society* **1988**, *110*, 3212.
(71) Ellis-Davies, G. C.; Kaplan, J. H. *Proceedings of the National Academy of Sciences* **1994**, *91*, 187.
(72) Ellis-Davies, G. C. R.; Kaplan, J. H. *The Journal of Organic Chemistry* **1988**, *53*, 1966.
(73) Milburn, T.; Matsubara, N.; Billington, A. P.; Udgaonkar, J. B.; Walker, J. W.; Carpenter, B. K.; Webb, W. W.; Marque, J.; Denk, W. *Biochemistry* **1989**, *28*, 49.
(74) Wieboldt, R.; Gee, K. R.; Niu, L.; Ramesh, D.; Carpenter, B. K.; Hess, G. P. *Proceedings of the National Academy of Sciences* **1994**, *91*, 8752.
(75) Walker, J. W.; Feeney, J.; Trentham, D. R. *Biochemistry* **1989**, *28*, 3272.
(76) Walker, J. W.; Somlyo, A. V.; Goldman, Y. E.; Somlyo, A. P.; Trentham, D. R. *Nature* **1987**, *327*, 249.
(77) Rothman, D. M.; Petersson, E. J.; Vázquez, M. E.; Brandt, G. S.; Dougherty, D. A.; Imperiali, B. *Journal of the American Chemical Society* **2004**, *127*, 846.

(78) Walker, J. W.; Gilbert, S. H.; Drummond, R. M.; Yamada, M.; Sreekumar, R.; Carraway, R. E.; Ikebe, M.; Fay, F. S. *Proceedings of the National Academy of Sciences* **1998**, *95*, 1568.
(79) Ando, H.; Furuta, T.; Tsien, R. Y.; Okamoto, H. *Nat Genet* **2001**, *28*, 317.
(80) Monroe, W. T.; McQuain, M. M.; Chang, M. S.; Alexander, J. S.; Haselton, F. R. *Journal of Biological Chemistry* **1999**, *274*, 20895.
(81) Klan, P.; Solomek, T.; Bochet, C. G.; Blanc, A.; Givens, R.; Rubina, M.; Popik, V.; Kostikov, A.; Wirz, J. *Chemical Reviews* **2013**, *113*, 119.
(82) Corrie, J. E. T. In *Dynamic Studies in Biology: Phototriggers, Photoswitches and Caged Biomolecules*; Givens, R., Goeldner, M., Eds.; Wiley-VCH: 2005, p 1.
(83) Givens, R.; Kotala, M. B.; Lee, J.-I. In *Dynamic Studies in Biology: Phototriggers, Photoswitches and Caged Biomolecules*; Givens, R., Goeldner, M., Eds.; Wiley-VCH: 2005, p 96.
(84) Furuta, T. In *Dynamic Studies in Biology: Phototriggers, Photoswitches and Caged Biomolecules*; Givens, R., Goeldner, M., Eds.; Wiley-VCH: 2005, p 29.
(85) Schmidt, R.; Geissler, D.; Hagen, V.; Bendig, J. *The Journal of Physical Chemistry A* **2007**, *111*, 5768.
(86) Subramanian, D.; Laketa, V.; Müller, R.; Tischer, C.; Zarbakhsh, S.; Pepperkok, R.; Schultz, C. *Nat Chem Biol* **2010**, *6*, 324.
(87) Mentel, M.; Laketa, V.; Subramanian, D.; Gillandt, H.; Schultz, C. *Angewandte Chemie International Edition* **2011**, *50*, 3811.
(88) Scott, R. H.; Pollock, J.; Ayar, A.; Thatcher, N. M.; Zehavi, U. In *Methods in Enzymology*; Alfred H. Merrill, J. Y. A. H., Ed.; Academic Press: 2000; Vol. Volume 312, p 387.
(89) Qiao, L.; Kozikowski, A. P.; Olivera, A.; Spiegel, S. *Bioorganic & Medicinal Chemistry Letters* **1998**, *8*, 711.
(90) Lankalapalli, R. S.; Ouro, A.; Arana, L.; Gómez-Muñoz, A.; Bittman, R. *The Journal of Organic Chemistry* **2009**, *74*, 8844.
(91) Shigenaga, A.; Morishita, K.; Yamaguchi, K.; Ding, H.; Ebisuno, K.; Sato, K.; Yamamoto, J.; Akaji, K.; Otaka, A. *Tetrahedron* **2011**, *67*, 8879.
(92) Kim, Y. A.; Ramirez, D. M. C.; Costain, W. J.; Johnston, L. J.; Bittman, R. *Chemical Communications* **2011**, *47*, 9236.
(93) Carter Ramirez, D. M.; Kim, Y. A.; Bittman, R.; Johnston, L. J. *Soft Matter* **2013**, *9*, 4890.
(94) Carter Ramirez, D. M.; Pitre, S. P.; Kim, Y. A.; Bittman, R.; Johnston, L. J. *Langmuir* **2013**, *29*, 3380.

Chapter 2: Synthesis, Photophysical Characterization and Cellular Uptake of Coumarinyl-Caged Ceramides

This chapter contains material adapted from the following manuscripts: Kim, Y. A.; Carter Ramirez, D. M.; Costain, W. J.; Johnston, L. J.; Bittman, R. *Chemical Communications* **2011**, *47*, 9236.

Kim, Y. A.; Day, J.; Lirette, C. A.; Costain, W. J.; Johnston, L. J.; Bittman, R. Synthesis and properties of short PEGylated coumarin-caged ceramides. *Submitted.*

Contributions: The synthesis of all coumarinyl-caged ceramides was done by Y. A. Kim from the group of Dr. R. Bittman at Queens College of CUNY. The uptake experiment for the PEGylated coumarin-caged ceramide was performed by C. A. Lirette from the University of Ottawa.

2.1 - Introduction: Photolabile Protecting Groups for Ceramide

The use of photolabile protecting groups has gained interest over the last several decades as a strategy for studying complex molecular processes that occur in the cell. Many of these molecular processes implicate specific biomolecules that act on very precise intracellular targets. Lipids, which are involved in many different cell signalling pathways, are highly hydrophobic molecules that are mostly impermeable to the cell membrane. Incorporating a caging moiety in these molecules can allow for their delivery into cells. Moreover, caging bioactive lipids with a photolabile protecting group temporarily renders them biologically inert, allowing them to reach a particular intracellular location before they exert a desired effect. The bioactive species can then be released in the cell with spatial and temporal control by the means of a photolysis reaction using light.[1,2]

As described in the previous chapter, ceramide is a bioactive sphingolipid that is implicated in various cellular processes. Namely, ceramide plays a role in

apoptosis[3,4] and necrosis[5-7], which are forms of programmed cell death. In order to study the bioactivity of specific ceramides in cells, we have developed a series of caged compounds incorporating ceramide molecules with variable N-acyl chain lengths and different coumarinyl caging moieties. These compounds will be referred to hereafter as coumarinyl-caged ceramides (or caged ceramides). The synthesis, which was performed by the group of Dr. R. Bittman[8], is described briefly in the next sections of this chapter. In addition, the photophysical and photochemical properties of the compounds were characterized and these results are presented in subsequent sections of this chapter. Lastly, since the compounds were designed to be used in cell studies, this chapter includes the results from experiments assessing uptake of the caged ceramides in cells.

2.2 - Results

2.2.1 - Synthesis of Bhc-Caged Ceramides

The 6-bromo-7-hydroxy-4-hydroxymethylcoumarin- (Bhc-) caged C16 Dihydro-Cer (**9a**) and the Bhc-caged C16 Cer (**9b**) were prepared as described previously.[8] The synthesis of these caged ceramides is shown in Scheme 2-1. Briefly, 4-bromoresorcinol and methyl 4-chloroacetoacetate were reacted in a Pechmann condensation[9] with methanesulfonic acid (CH_3SO_3H) as a catalyst to yield 4-(chloromethyl)coumarin, which was then hydrolyzed in water under reflux to give the Bhc-coumarin (**4**). This diol was chemoselectively protected at the phenolic position using methoxymethyl chloride (MOMCl) in the presence of DIPEA (*N*,*N*-diisopropylamine) to afford the MOM ether. The primary alcohol was then activated

by treatment with a phosgene solution to generate the chloroformate species, which would be used in a coupling reaction with the commercially available lipids, C16 Dihydro-ceramide (**7a**) and C16 ceramide (**7b**). The coupling was performed by reacting the activated species with the lipid in the presence of DIPEA and DMAP (4-dimethylaminopyridine) in a 2:1 mixture of tetrahydrofuran (THF) and dichloromethane (CH_2Cl_2) at room temperature for 36 hours. It is noteworthy that selective coupling to the primary hydroxyl group was achieved without protecting the allylic hydroxyl group in the long-chain ceramides. The lack of reactivity at this position could be attributed to steric hindrance from the two long hydrocarbon chains in the lipid. Lastly, the MOM groups were removed with silica-supported sodium hydrogen sulfate ($NaHSO_4 \cdot SiO_2$) as a heterogeneous catalyst[10] in order to yield the caged ceramides **9a** and **9b**.

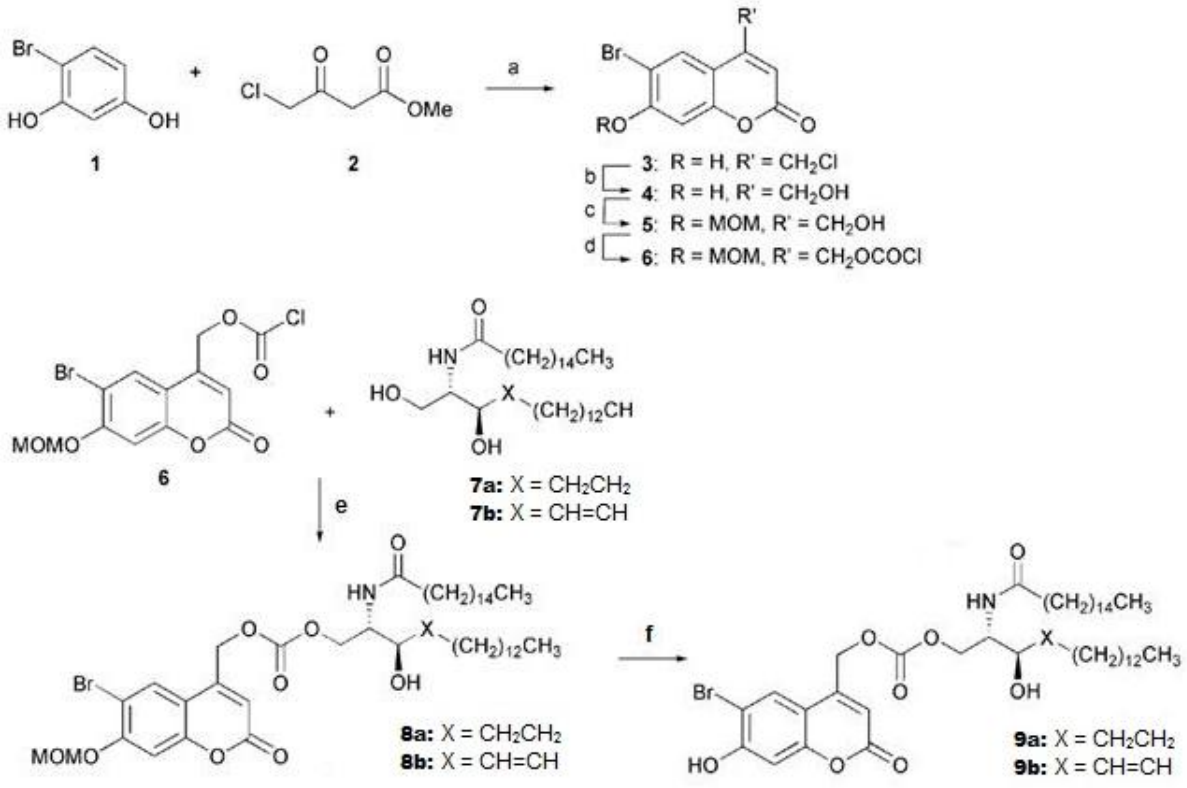

Scheme 2-1. Synthesis of the Bhc-caged C16 Dihydro-Cer (**9a**) and of the Bhc-caged C16 Cer (**9b**). (a) CH_3SO_3H, rt, 2 h, 95%; (b) H_2O, reflux, 2 d, 99%; (c) MOMCl, DIPEA, CH_2Cl_2, 0^oC, 2 h, 89%; (d) phosgene, THF/toluene, 3 h, 0^oC, 94%; (e) DIPEA, DMAP, THF/CH_2Cl_2 (2:1), rt, 36 h, 25%; (f) $NaHSO_4 \cdot SiO_2$, CH_2Cl_2, 2 h, rt, 70%.

2.2.2 - Synthesis of Tcmoc- and Btcmoc-Caged Ceramides

Photo-responsive compounds bearing the methoxytriethylene glycol-conjugated (mTEG-conjugated) coumarin caging moiety were synthesized by the Bittman group using similar methods to those described above for the Bhc-caged compounds. The synthesis of Tcmoc- and Btcmoc-caged compounds is shown in Scheme 2-2. An initial Pechmann condensation reaction of resorcinol or 4-bromoresorcinol with methyl 4-chloroacetate, catalyzed by methanesulfonic acid, was performed in order to generate two different 4-(chloromethyl)coumarin species. Acetic acid was then reacted with the alkyl halide moiety of the coumarins in the presence of potassium fluoride at room temperature with DMF (dimethylformamide) as a solvent, which allowed for an acetate protecting group to be incorporated. In order to install the methoxytriethylene glycol (mTEG) moiety onto the coumarins, etherification of the phenolic hydroxyl group with triethyleneglycol monomethyl ether was performed using a microwave-assisted Mitsunobu reaction[11] in the presence of DIAD (diisopropyl azodicarboxylate) and Bu_3P (tributylphosphine) in THF. Hydrolysis of the acetate group with potassium carbonate in a 1:1 mixture of THF and methanol gave the alcohol, affording each of the free coumarin species (7-mTEGylated-coumarin-4-yl)methoxycarbonyl (Tcmoc) **17** and (6-bromo-7-mTEGylated-coumarin-4-yl)methoxycarbonyl (Btcmoc) **18**. The Tcmoc and Btcmoc coumarins were converted to the corresponding chloroformates and coupling reactions with different ceramides (C6, C16, C18, C22 and C24 ceramides) were performed under conditions similar to those described above in order to yield a series of pegylated caged ceramides (**19**-**24**).

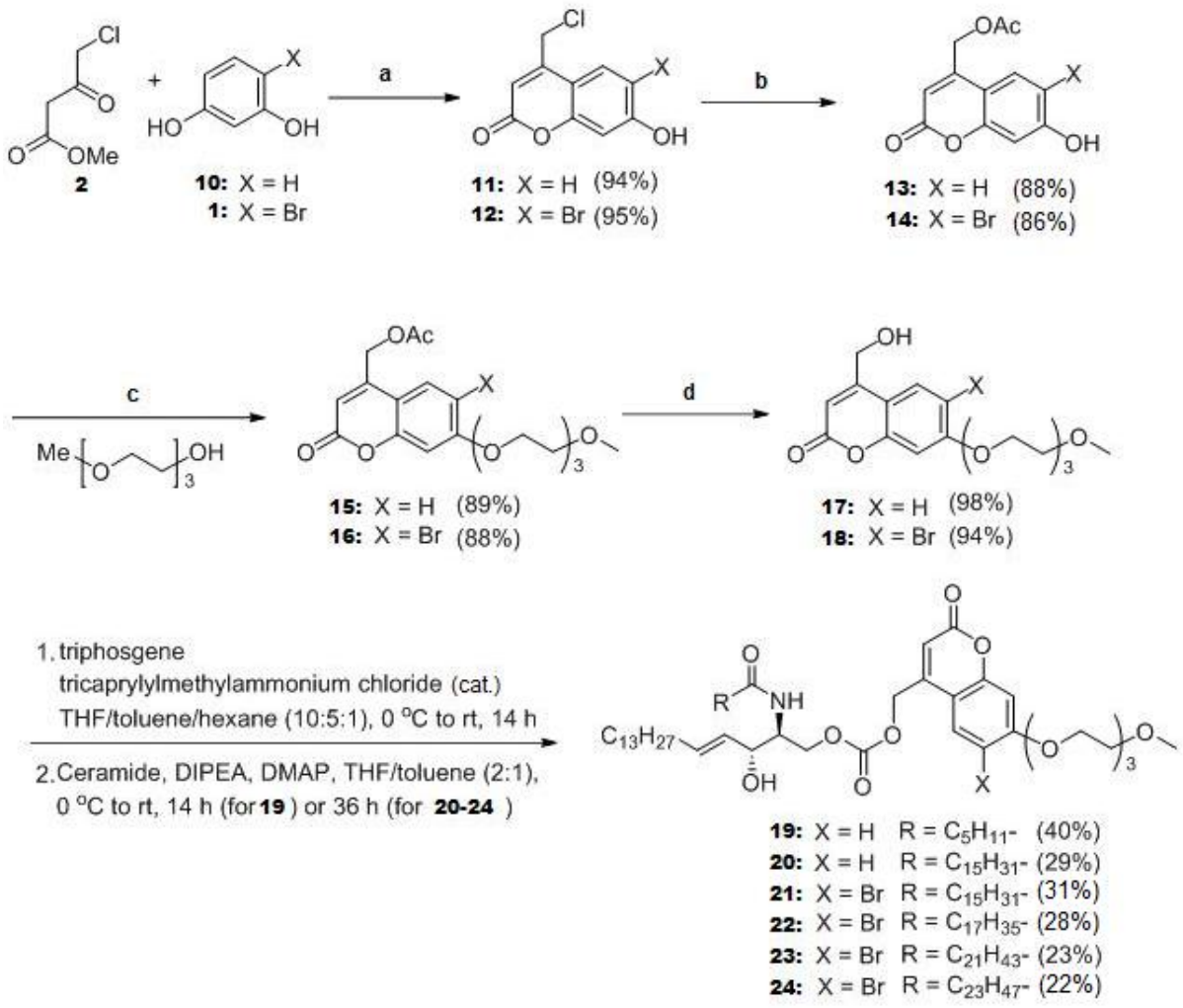

Scheme 2-2. Synthesis of the pegylated Tcmoc- (**19**-**20**) and Btcmoc-caged ceramides (**21**-**24**) with short, long or very long N-acyl chains. (a) CH_3SO_3H, rt, 2 h; (b) KF, AcOH, DMF, rt, 36 h; (c) PBu_3, DIAD, THF, *MW*, 60 ^oC, 30 min; (d) K_2CO_3, THF/MeOH (1:1), 0 ^oC, 1 h.

2.2.3 - Photophysical Characterization of Coumarinyl-Caged Ceramides

Prior to conducting cell studies with caged ceramides, photophysical characterization of the compounds was required in order to determine the appropriate conditions to be used for achieving efficient photolytic cleavage. The characterization was done by first recording the absorbance and fluorescence spectra of the caged ceramides in solution. Determination of the quantum yield of

fluorescence (Φ_{fl}) for each of the caged ceramides was also performed by absorbance and fluorescence spectroscopy.

The photophysical properties of the Bhc-coumarin (**4**) and of the Bhc-caged C16 Dihydro-Cer (**9a**), were reported previously by our group.[8] Dihydroceramides, such as the caged compound **9a**, are structurally similar to ceramides, but lack the unsaturation in their fatty acid chain. Since we do not expect this structural difference to influence the photophysics of the compound, the photophysical properties of the Bhc-caged C16 Cer (**9b**) are assumed here to be consistent with those measured earlier for the related caged dihydroceramide. The results from this earlier photophysical characterization work for the caged dihydroceramide **9a** and the parent coumarin **4** are presented here for comparative purposes. In performing these measurements, KMops buffer with a pH of 7.4 was used as a solvent in order to simulate a physiological environment for the compounds, which were to further be used in cell studies. In some cases, particularly with the caged ceramides, ethanol was incorporated in the aqueous medium in order to ensure complete solubilization of the compounds.

The absorbance and emission spectra of the Bhc-related compounds are displayed in Figure 2-1 and the spectral characteristics, as well as the fluorescence quantum yields are presented in Table 2-1. As seen in Figure 2-1 (A), the free Bhc-coumarin (**4**) displayed an absorbance spectrum with a single maximum at 366 nm in KMops buffer (pH 7.4; solvent A). However, in KMops buffer containing 50% ethanol (solvent B), the absorbance spectrum had two distinct peaks, one at 343 and one at 374 nm. With its phenolic hydroxyl group (pKa ~6.2), the Bhc-coumarin

exists as a mixture of two different forms under these conditions, the phenol and the phenolate anion, which are responsible for the peaks at the shorter and longer wavelengths, respectively. In the same solvent system (solvent B), the Bhc-caged Dihydro-C16 Cer (**9a**) exhibited peak absorbance at 338 nm with a shoulder at 380 nm, which suggests that the coumarinyl moiety of the compound is found primarily in the protonated state under these conditions. When we consider the structures of the free coumarin **4** and of the caged lipid **9a**, the differences in the spectral characteristics of the two compounds could be indicative of hydrogen bonding interactions within the structure of the caged ceramide, which are not present with the free coumarin. In the event that there is some aggregation of the caged lipid molecules, these interactions could be occurring between the phenolic group of the coumarin and amide or ester moieties in the lipid backbone, at an intra- or intermolecular level.[12]

Fluorescence emission spectra for the Bhc-coumarin (**4**), the Bhc-caged C16 Dihydro-Cer (**9a**), as well as for Coumarin 460 (Φ_{fl} = 0.59 in ethanol)[13], which was selected as a reference standard for fluorescence quantum yield (Φ_{fl}) determination based on good spectral overlap, are displayed in Figure 2-1 (B). The fluorescence emission maximum of the free coumarin **4** with excitation at 374 nm (in solvent mixture B) was determined to be 467 nm and the quantum yield of fluorescence was determined to be 0.50 with reference to Coumarin 460, a relatively high value. As for the caged dihydroceramide **9a**, the fluorescence emission maximum was almost identical to that of the free coumarin (466 nm), but the quantum yield of fluorescence that was measured for this compound with reference to the standard was 0.02 (in

solvent mixture B), which is 100-fold lower than that of the free coumarin. Based on the expected photochemical reactivity of the photocage, the very low fluorescence quantum yield of the caged ceramide in comparison to the free coumarin chromophore is reasonable since the competing photochemical reaction reduces the fluorescence quantum yield of the caged compound.

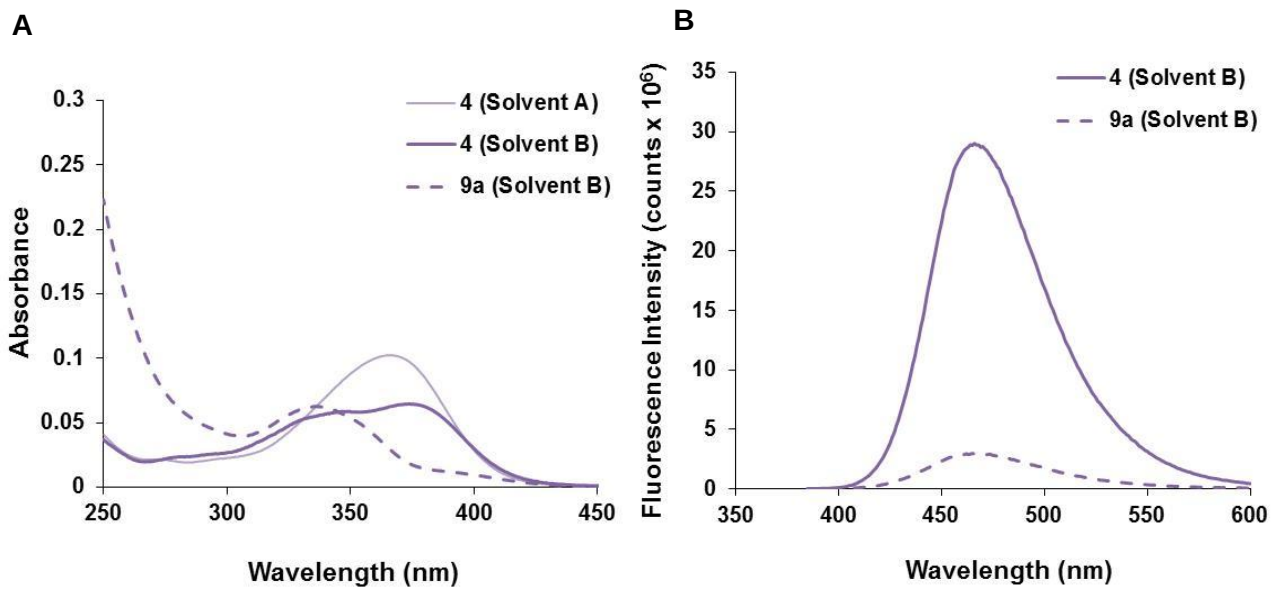

Figure 2-1. Absorbance spectra (A) and fluorescence emission spectra with 374 nm excitation (B) of the Bhc-coumarin (**4**) and of the Bhc-caged C16 Dihydro-Cer (**9a**) in KMops pH 7.4 (solvent A) and in KMops (pH 7.4) containing 50% ethanol (solvent B). Spectra are from reference 8.

The photophysical properties of the more recently synthesized Tcmoc- and Btcmoc-caged ceramides were characterized by similar methods. In the structure of these compounds, the phenolic hydroxyl group was replaced with a mTEG moiety in order to yield a series of "pegylated" caged ceramides. The fluorescence quantum yields were determined using Coumarin 440 (Φ_{fl} = 0.56 in ethanol)[14] as a reference standard, which was selected based on its good spectral overlap with the mTEGylated compounds. Absorbance spectra and fluorescence emission spectra

for the Btcmoc-caged ceramides (**21**-**24**), as well as for the parent coumarin **18** were recorded and are displayed in Figure 2-2 (panels A and C). The photophysical properties for these compounds are presented in Table 2-1. The brominated free Btcmoc-coumarin, which was characterized in KMops buffer (solvent A), exhibited an absorption maximum at 327 nm and a fluorescence emission maximum at 398 nm. A very low quantum yield of fluorescence of 0.01 was measured for the free Btcmoc-coumarin, which differs substantially from the larger value obtained for the Bhc-coumarin (**4**). As for the caged ceramides incorporating the Btcmoc coumarinyl moiety (**21**-**24**), they all showed similar spectral characteristics as the parent coumarin **18** (λ_{abs}**=** ~330 nm and λ_{em}= ~408 nm) in KMops buffer (pH 7.4) containing 10% ethanol (solvent C), but a slight shift to longer wavelengths (~10 nm) was observed for the fluorescence emission maximum. Very low fluorescence quantum yields, on the order of 0.01, were measured for the Btcmoc-caged ceramides, which is consistent with the value obtained for the Bhc-caged C16 Dihydro-Cer (**9a**).

For the Tcmoc-related compounds, which lack the bromine atom at position 6 in the coumarinyl moiety, the absorbance spectra were recorded and are shown in Figure 2-2 (B). The photophysical properties of the Tcmoc-related compounds are presented in Table 2-1. The Tcmoc-related compounds exhibited absorption maxima that were shifted to slightly shorter wavelengths (~6-10 nm) in comparison to the Btcmoc-related compounds. The free Tcmoc-coumarin (**17**) exhibited peak absorbance at 321 nm and maximum fluorescence emission at 398 nm (with excitation at 330 nm) when the spectra were acquired in KMops buffer (solvent A). The fluorescence quantum yield measured for this compound was 0.30, under these

conditions. The Tcmoc-caged C6 Cer (**19**) and the Tcmoc-caged C16 Cer (**20**), in solvent mixture C, showed similar spectral characteristics (λ_{abs}= ~320 nm and λ_{em}= ~408 nm) as the parent coumarin **17**. The fluorescence quantum yields measured for these caged compounds were significantly reduced in comparison to that of the free Tcmoc-coumarin, which is consistent with what was observed for the Bhc-related compounds. The values obtained were 0.06 for the caged ceramide **19** and 0.05 for the caged ceramide **20**, which, although relatively low, are slightly higher than those measured for the Btcmoc-caged ceramides (**21**-**24**).

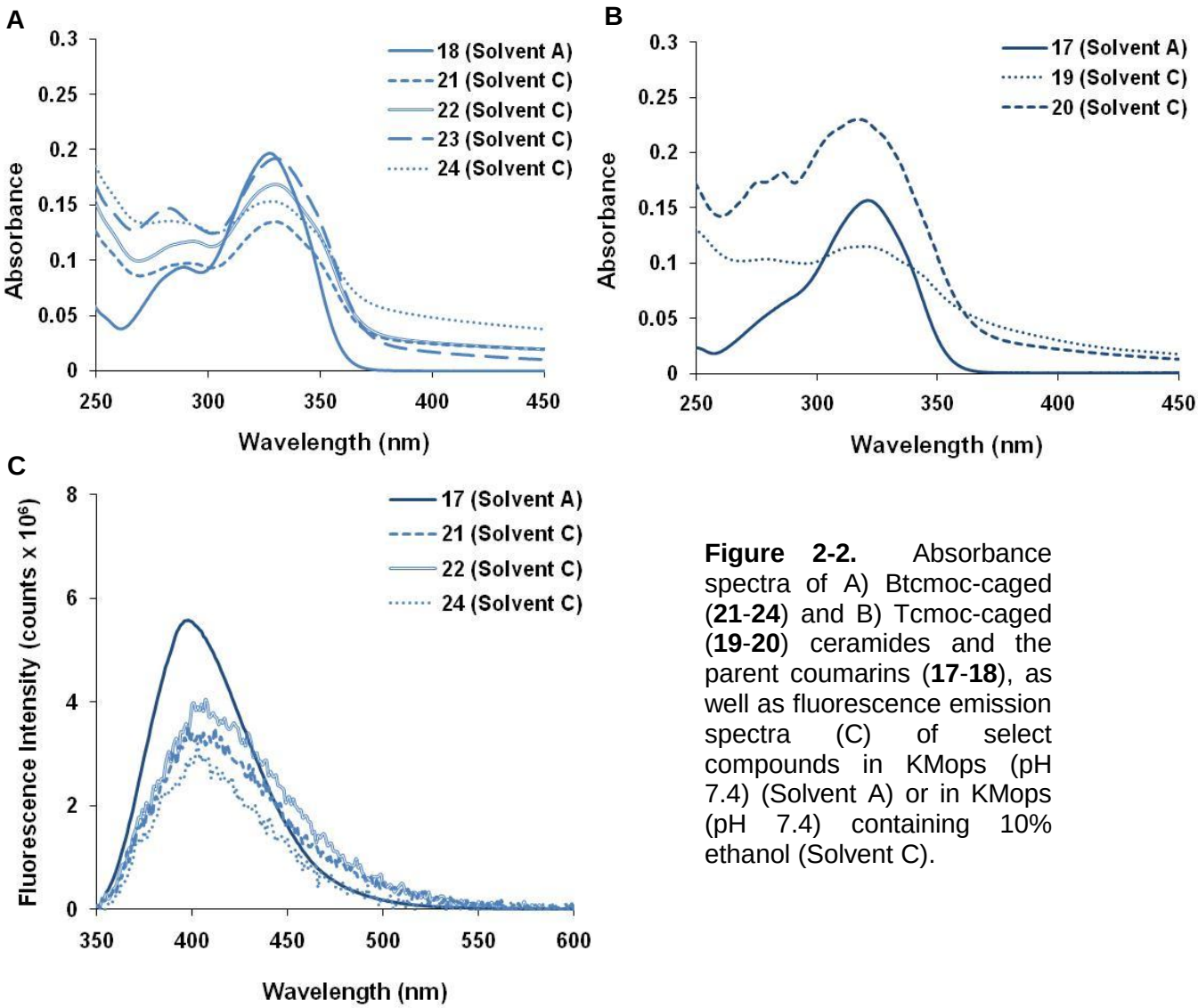

Figure 2-2. Absorbance spectra of A) Btcmoc-caged (**21**-**24**) and B) Tcmoc-caged (**19**-**20**) ceramides and the parent coumarins (**17**-**18**), as well as fluorescence emission spectra (C) of select compounds in KMops (pH 7.4) (Solvent A) or in KMops (pH 7.4) containing 10% ethanol (Solvent C).

Table 2-1. Photophysical properties of the Bhc-caged C16 Dihydro-Cer (**9a**), the Btcmoc-caged Cers (**21**-**24**), the Tcmoc-caged Cers (**19**-**20**) and the parent coumarins (**4**, **17**-**18**).

	λ_{abs}	λ_{em}	Φ_{fl}	Solvent
4[a]	366	466	0.47[c]	A[e]
	343, 374[b]	467	0.50[c]	B[f]
9a[a]	338, > 380 (sh)	466	0.02[c]	B[f]
18	327	398	0.01[d]	A[e]
21	329	408	0.01[d]	C[g]
22	330	407	0.01[d]	C[g]
23	331	408	0.01[d]	C[g]
24	328	408	0.01[d]	C[g]
17	321	398	0.30[d]	A[e]
19	320	408	0.06[d]	C[g]
20	318	408	0.05[d]	C[g]

[a] All values for **4** and **9a** are from published work from our group.[8] [b] Coexistence of the protonated (343 nm) and deprotonated (374 nm) forms of the Bhc-coumarin (**4**). [c] Quantum yields of fluorescence for excitation at 374 nm with reference to Coumarin 460 (Φ_{fl} = 0.59). [d] Quantum yields of fluorescence for excitation at 330 nm with reference to Coumarin 440 (Φ_{fl} = 0.56). [e] Solvent A: KMops (pH 7.4). [f] Solvent B: KMops (pH 7.4) containing 50% ethanol (v/v). [g] Solvent C: KMops (pH 7.4) containing 10% ethanol (v/v).

2.2.4 - Photochemical Characterization of Coumarinyl-Caged Ceramides

The time course of photolysis of the different coumarinyl caged ceramides was investigated as a qualitative indication of the amount of UV exposure required to generate ceramide photochemically using these compounds. A reversed-phase high performance liquid chromatography (HPLC) method was developed based on a published protocol.[8] The method allowed for separation and quantification of the relative amounts of caged ceramide and free coumarin photo-product found in sample aliquots that were obtained at different time points throughout the photolysis

reaction. A reversed-phase octadecyl- (C18)-silica column was chosen based on the affinity of the hydrophobic lipid moiety of the caged ceramides for the hydrophobic surface of this column. The quantification was performed by fluorescence detection of the coumarinyl compounds (caged ceramide and free coumarin) upon their elution from the column. The absorbance at 325 and 375 nm was also monitored, but this data was not used for the purpose of quantifying the compounds due to a large “solvent spike” that was present in these traces at the beginning of each run. The samples were prepared in aqueous KMops buffer (pH 7.4) and were injected into the column which contained primarily ethanol as the mobile phase. This created a solvent peak in the short retention time range that could not easily be resolved from the free coumarin peak.

For preparatory photolysis experiments, UV irradiation at 350 nm was performed and sample aliquots were removed at different time points and added to a fixed amount of Coumarin 480. This dye was chosen as an internal standard for HPLC analysis based on its appropriate retention time under the optimized solvent and flow rate conditions. Evidently, it was required that the standard be eluted from the column with a retention time that was different than that of the free coumarin photo-product. Coumarin 480, with the relatively large alkyl groups present in its structure, displayed a retention time of about 3.5 minutes under the conditions used, which was a distinctly longer retention time than that of each of the free coumarins being studied. The separation by HPLC of the caged compound and the free coumarin is based on the fact that the caged ceramide, with its long acyl chains in the lipid moiety, interacts more strongly with the stationary phase and is eluted from

the column at a longer retention time. Figure 2-3 shows representative HPLC traces for caged ceramides with long (C14–C18) and very long (C20–C24) N-acyl chains.

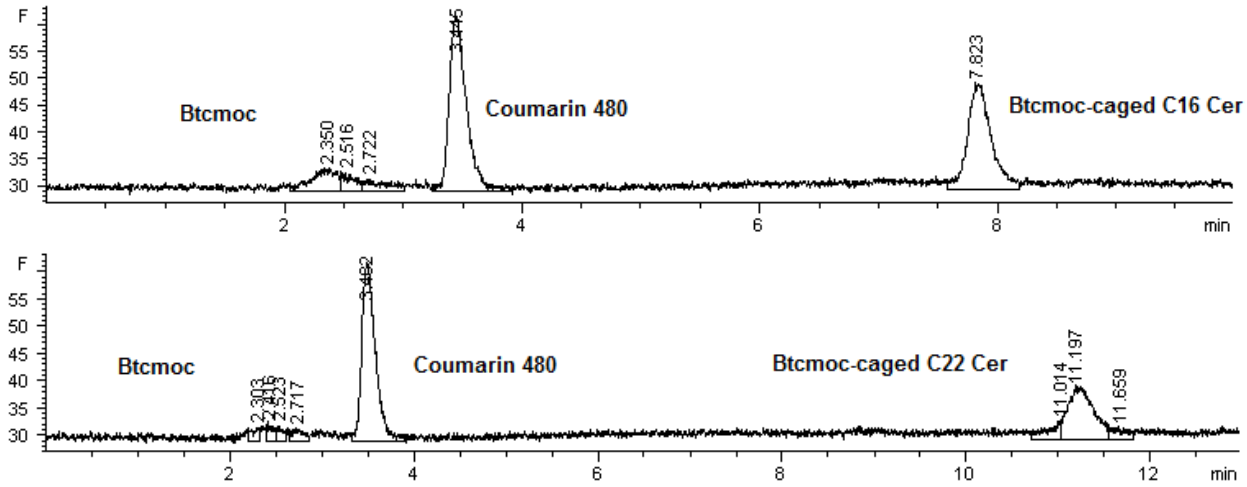

Figure 2-3. Representative reversed-phase HPLC chromatograms showing the separation and detection by fluorescence of the Btcmoc-caged C16 and C22 ceramides (**21** and **23**) and of the free coumarin (**18**) photo-product, which are used for monitoring the time course of photolysis. Fluorescence detection at 440 nm was performed with 325 nm excitation. Eluent: 75% EtOH (increasing to 95% over the time period of 0 to 3 min), 25% H_2O; flow rate = 0.5 mL/min.

Initial preparatory photolysis experiments were performed for caged ceramide samples that were prepared in KMops buffer containing ethanol (50 or 10%) and placed in a 4 mL quartz cuvette. In studying the time course of photolysis of the Bhc-caged C16 Dihydro-Cer (**9a**) by HPLC, fluorescence detection at 480 nm was performed with excitation at 325 nm. Previous studies showed that the caged dihydroceramide **9a** undergoes almost complete photolysis (> 90%) with 4 minutes of UV irradiation (Figure 2-4 (A)).[8] For the Btcmoc- and Tcmoc-caged ceramides, fluorescence detection was performed at 440 nm with 325 nm excitation. As seen in Figure 2-4 (B), photolysis of the Btcmoc-caged C22 Cer (**23**) required, qualitatively, about 2.5 times the amount of UV exposure time (10 minutes) as did the caged

dihydroceramide **9a** in order to achieve ~90% photolysis. Although these preparatory photolysis experiments were conducted under roughly the same conditions, it's important to keep in mind that they were performed at different times. As a result of this, small variations in the lamp intensity between experiments could have occurred, but we do not believe that this accounts entirely for the differences observed in the time required for uncaging of the different caged ceramides. As for the time course of photolysis of the Tcmoc-caged compounds (**19**-**20**), the results shown in Figure 2-4 (B) suggest that the photolytic cleavage of these compounds, under the same conditions, is not as efficient as that of the compounds containing the bromine atom. Although there is evidence for some degree of photolysis of the Tcmoc-caged ceramides upon UV irradiation, very long exposure times (> 30 min) are required in order to achieve an appreciable level of uncaging of the lipid molecules.

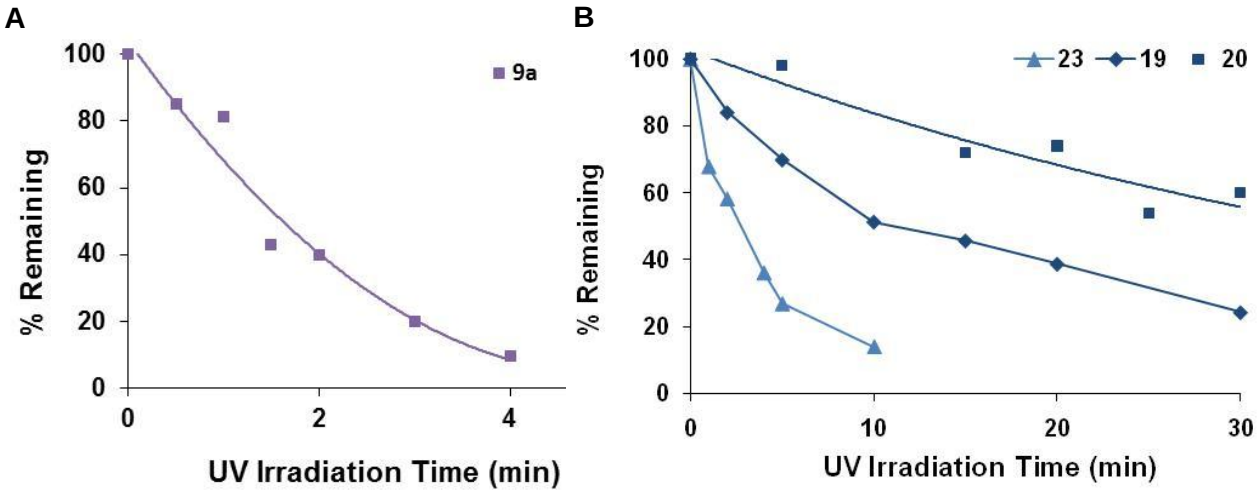

Figure 2-4. Time course of photolysis of the Bhc-caged C16 Dihydro-Cer (**9a**) in KMops (pH 7.4) containing 50% EtOH, from reference 8, (A) and time course of photolysis of the Btcmoc- and Tcmoc-caged Cers (**23**, **19** and **20**) in KMops containing 10% EtOH (B) with irradiation in a Rayonet photochemical reactor (4 lamps, 350 nm). Photolysis of the caged ceramides (4 mL sample in quartz cuvette) was quantified by HPLC analysis using Coumarin 480 as an internal standard.

For comparison, preparatory photolysis experiments with the Bhc-caged C16 Cer (**9b**) were carried out in a similar manner as described above, but the sample analysis was performed by fluorescence spectroscopy rather than by HPLC. Solutions of the caged ceramide **9b** and of the free coumarin **4** (20 uM) were prepared in KMops buffer containing ≤ 1% ethanol or serum-free cell culture medium containing ≤ 1% ethanol and placed in a 4 mL quartz cuvette for irradiation. Rather than collecting sample aliquots at the different time points, fluorescence emission spectra (between 385 and 600 nm) were recorded for the bulk sample with 374 nm excitation. In order to illustrate the time course of photolysis, fluorescence emission was quantified as the area under the curve and plotted against the UV irradiation time point. Control samples of the unirradiated caged ceramide **9b** and of the irradiated free Bhc-coumarin (**4**) were also analyzed in parallel for comparative purposes.

As shown in Figure 2-5 (A), an increase in fluorescence emission was measured for the irradiated Bhc-caged C16 Cer (**9b**) sample in KMops buffer (≤ 1% ethanol) during the first 60 seconds of UV irradiation, which was followed by a gradual decrease in the emission. This result is reasonable when we consider the very high fluorescence quantum yield of the free coumarin photo-product in comparison to the very weakly fluorescent caged compound. The peak in fluorescence emission at the beginning suggests that a large amount of photo-cleavage occurs within the first minute of UV exposure, generating the free Bhc-coumarin (**4**), which eventually begins to undergo photobleaching causing a marked decrease in fluorescence emission. As for the unirradiated caged ceramide control

sample, only a very low level of fluorescence emission was observed throughout the same time course. The slight increase observed with successive measurements could be due to the generation of a small amount of free coumarin photo-product from the excitation light. The free Bhc-coumarin control exhibited, initially, a very high level of fluorescence emission which decreased significantly with increasing UV exposure due to photo-bleaching. As seen in Figure 2-5 (B) below, the results that were obtained for an analogous experiment performed with the caged ceramide **9b** in serum-free medium (≤ 1% ethanol) were similar to those obtained for the sample in KMops buffer. This is reasonable considering that the two solvent systems are very similar, being aqueous in nature with a pH of about 7.4. Due to limited amounts of material, this type of spectroscopic analysis was not performed for the other caged ceramides.

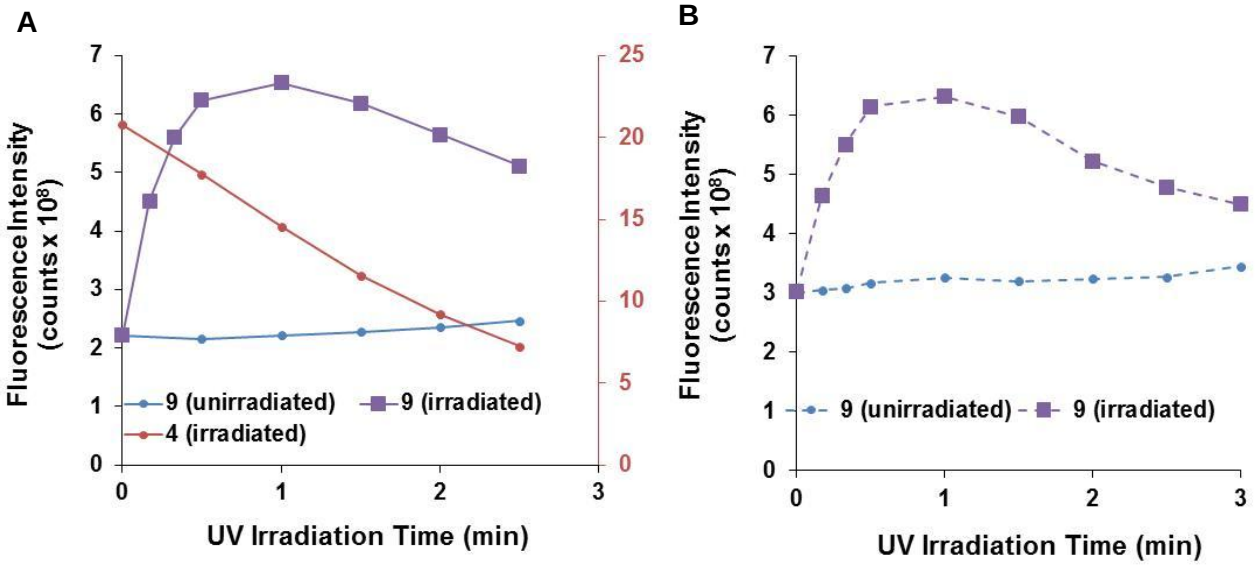

Figure 2-5. Fluorescence spectroscopic analysis of the time course of photolysis of the Bhc-caged C16 Cer (**9b**) in KMops (pH 7.4) containing ≤ 1% EtOH (A) and in serum-free medium containing ≤ 1% EtOH (B) with irradiation in a Rayonet photochemical reactor with 4 lamps (350 nm). Samples were placed in a 4 mL quartz cuvette. Fluorescence emission spectra were collected at different time points throughout the UV irradiation and fluorescence intensity was quantified as the area under the curve.

Since the goal of this work was to achieve uncaging of ceramide in cells, preparatory photolysis experiments (in solution) were also performed on a smaller scale, in a format analogous to that of cell experiments. These results are shown in Figure 2-6. For these experiments, a small volume (300 µL) of the sample solution was placed in the wells of a cell culture micro-well plate (96-well format) for irradiation and the samples were analyzed by HPLC. It was reasonable to see that these results followed the same trends as observed in the larger scale preparatory photolysis experiments (Figure 2-4). However, measurement of quantum yields of photolysis at low product conversion would be required in order to effectively compare the photolysis efficiency of the different caged ceramides. One difference was that the photolysis reactions performed on a smaller scale, in the micro-well plate, required approximately half of the UV exposure time as did the reactions done in the larger volume cuvette. Although the sample concentration and the number of UV lamps remained the same, differences in the irradiation geometry between the two different experimental set-ups (see chapter 5, section 5.3) could account for the differences in the amount of UV exposure required for uncaging.

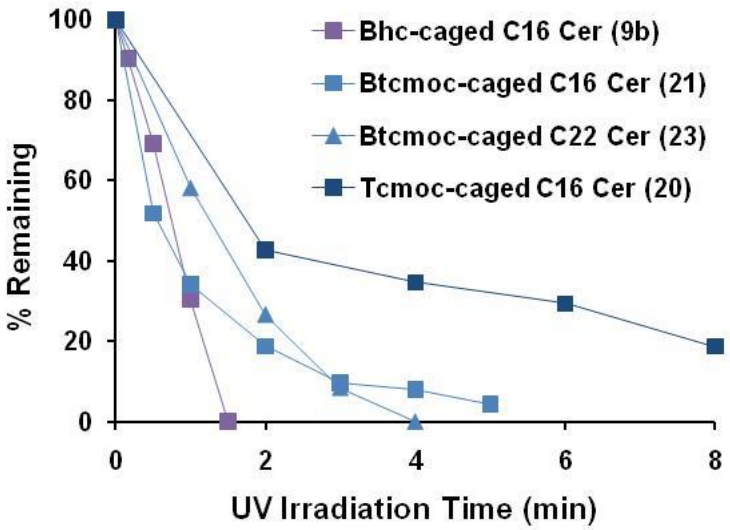

Figure 2-6. Time course of photolysis, in a micro-well plate, of the Bhc-caged C16 Cer (**9b**), the Btcmoc-caged Cers (**21**, **23**) and the Tcmoc-caged C16 Cer (**20**) in KMops (pH 7.4) containing 10% EtOH with irradiation in a Rayonet photochemical reactor with 4 lamps (350 nm). Photolysis was quantified by HPLC analysis using Coumarin 480 as an internal standard.

2.2.5 - Uptake of Coumarinyl-Caged Ceramides in HeLa Cells

In a previous report by our group, the Bhc-caged C16 Dihydro-Cer (**9a**) was shown to be internalized by J774 macrophages when these cells were incubated in the presence of the compound.[8] Here, the cervical cancer cell line HeLa was chosen for cell studies, based on other reports in which this cell line was used to investigate the biological effects of ceramide.[7,15-19] Before attempting to measure the biological effects of photochemically generated ceramide in HeLa cells, it was necessary to determine if the caged ceramides could be internalized by the cells. Since the coumarinyl moiety of the photocages emits fluorescence upon excitation, uptake could be assessed by fluorescence imaging of HeLa cells that were incubated with the caged ceramides.

Experiments were carried out in which the cells were incubated in the presence of the Bhc-caged C16 Cer (**9b**) for 2 hours, UV-irradiated for 6 minutes and washed with PBS buffer (1X) immediately before being imaged. The results shown in Figure 2-7 (B) suggest that the compound is in fact taken up by the cells, as assessed from the localized fluorescence emission. It is, however, noteworthy that the fluorescence emission that was observed with this sample is resulting in part from the free Bhc-coumarin photo-product, since UV irradiation of the sample was performed. Nonetheless, since the incubation was carried out in the dark and fluorescence imaging was performed immediately after the UV irradiation step, the results obtained are indicative of cellular uptake of the caged ceramide **9b**. The control sample, in which the cells were incubated in medium without the caged ceramide, showed no localized coumarin fluorescence, but a small amount of auto-

fluorescence of the cells was observed, as shown in Figure 2-7 (D). Some uptake experiments with the caged ceramide **9b** were performed where the samples were not UV-irradiated before fluorescence imaging. However, due to the very low quantum yield of fluorescence of the caged ceramide **9b**, the signal intensity was low resulting in poor image quality (data not shown).

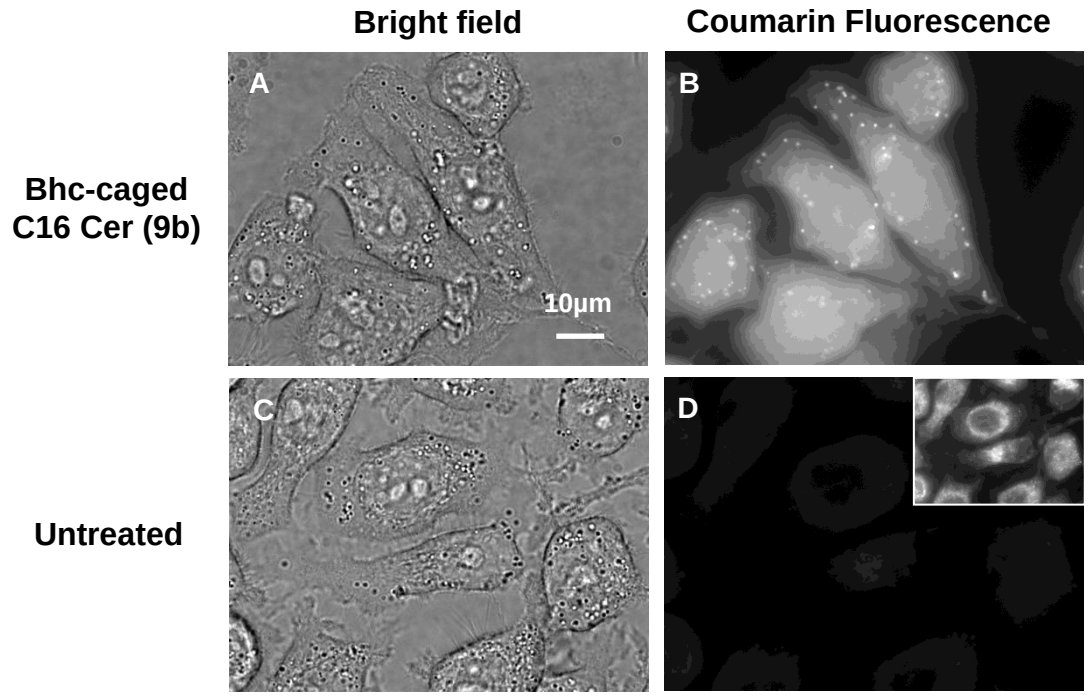

Figure 2-7. The Bhc-caged C16 Cer (**9b**) is taken up by HeLa cells with 2 hours of incubation, as assessed from the localized coumarin fluorescence in the cells. Bright field (A,C) and fluorescence images (B,D) of HeLa cells incubated with (top) and without (bottom) the caged ceramide **9b** in serum-free medium (20 µM) for 2 hours in the dark and irradiated in a UV reactor (350 nm) for 6 min. The medium was then removed and the cells were washed once with PBS buffer (1X) which was used as the imaging medium. Fluorescence images were acquired in the DAPI channel and are scaled at 200-1200 counts. The inset in image D is to illustrate the morphology of the control sample (Display: 200-350 counts).

Uptake of the pegylated Btcmoc-caged C22 Cer (**23**) was also assessed in a similar experiment and the results are displayed in Figure 2-8. In this experiment, which was performed by C. A. Lirette of the University of Ottawa, different incubation

times were tested, in order to ensure that a significant level of uptake of the compound could be achieved with an incubation of ~2 hours. The results indicated that after 2.5 hours of incubation with the caged ceramide **23**, a significant amount of the compound had been taken up by the cells. This was, once again, determined from the localized fluorescence emission in the cells, as observed in Figure 2-8 (F). One difference between the experiment presented here and the previous uptake experiment with the Bhc-caged C16 Cer (**9b**) was that the samples were not irradiated with UV light before imaging in this case. In light of this, the fluorescence emission that was observed was mostly from the intact caged ceramide **23** and was relatively low. This could be explained by the very low quantum yield of fluorescence of the caged ceramide **23**. In addition, the filter set that was available for the acquisition of the coumarin fluorescence images is not optimal for detecting fluorescence emission from the pegylated coumarinyl species. With this filter set, excitation is performed from 352-400 nm and emission is collected between 417 and 477 nm, whereas the absorption and emission maxima of the Btcmoc-caged C22 Cer (**23**) are 331 nm and 408 nm, respectively.

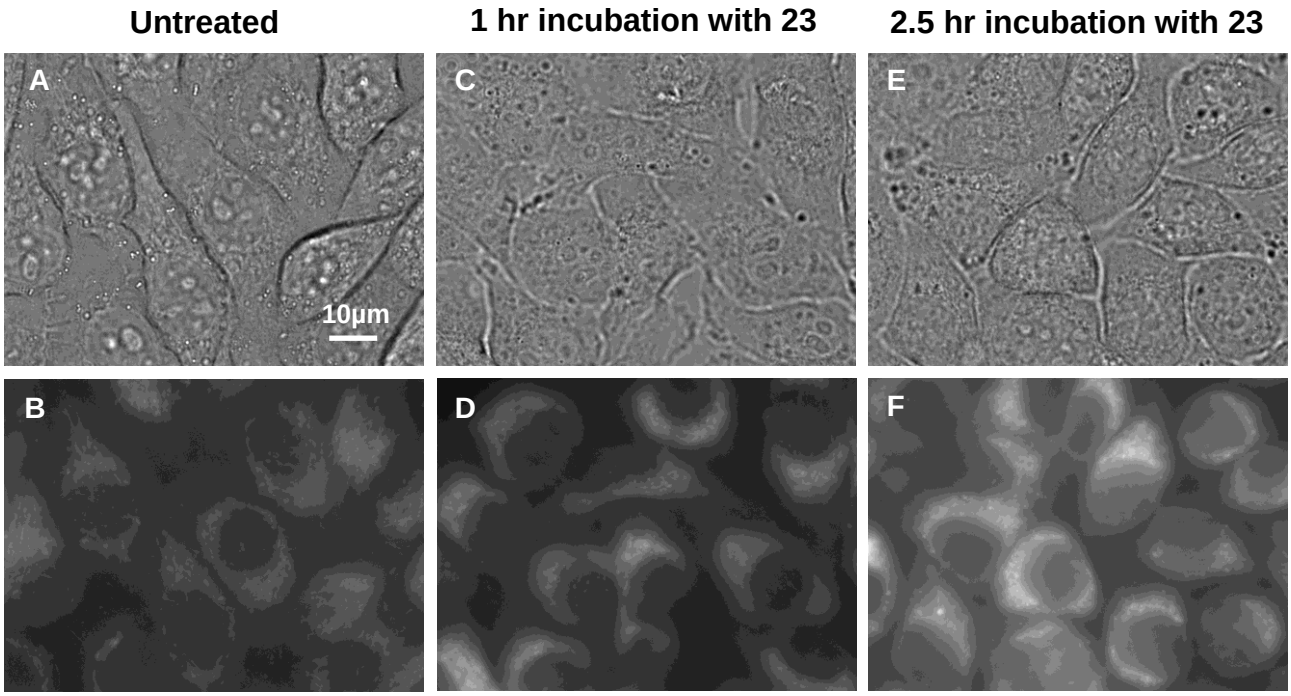

Figure 2-8. The Btcmoc-caged C22 Cer (**23**) is taken up by HeLa cells with 2.5 hours of incubation, as assessed from localized fluorescence emission in the cells. Bright field (A, C and E) and fluorescence images (B, D and F) of HeLa cells incubated with and without the Btcmoc-caged C22 Cer (**23**) in serum-free medium (20 µM) for up to 2.5 hours in the dark. Samples were washed and imaging was performed in PBS buffer (1X). Fluorescence images were acquired in the DAPI channel and are scaled at 500-1500 counts.

2.3 - Discussion and Conclusions

In order to effectively use caged ceramides to generate ceramide photochemically in the cellular environment, it was important to initially characterize the photophysical and photochemical properties of the compounds and to assess their uptake in cells. It has been shown elsewhere that the photophysical and photochemical properties of coumarinyl-caged compounds depend, to some extent, on the nature of the attached functional groups.[20] For example, the 7-hydroxy-4-

hydroxymethylcoumarin (Hcm) group exhibits two absorption maxima, one at around 325 nm corresponding to the protonated form of the C7 hydroxyl moiety and the other at 375 nm corresponding to the ionized form. Under physiological conditions (pH ~7.4), the protonated form of the phenolic hydroxyl group (pKa ~7.9) is predominant. The 6-bromo-7-hydroxy-4-hydroxymethylcoumarin (Bhc) caging group, which is a variant of the Hcm-coumarin, contains a bromine atom at the C6 position. The presence of this bromine atom lowers the pKa of the C7 hydroxyl group (pKa ~6.2) such that it is deprotonated at physiological pH.[21] This causes a red shift of about 60 nm in the absorption maximum of the compound, which is desirable for the purpose of uncaging a biomolecule in a biological system by the means of UV irradiation.[20]

The photophysical properties of different Bhc-caged compounds have been characterized previously by other groups.[22,23] In previous work by our group, it was determined that the free Bhc-coumarin (**4**) exhibits an absorption maximum at 366 nm[8] (see Table 2-1, section 2.2.3) in KMops buffer (pH 7.4), which is consistent with other results that are reported in the literature.[22] The Bhc-caged C16 Dihydro-Cer (**9a**) has an absorption maximum at 338 nm in KMops buffer containing ethanol (50%). The maximal absorption at the shorter wavelength exhibited by the caged dihydroceramide **9a** indicates predominance of the protonated form of the compound under these conditions. As mentioned earlier, this is likely due to hydrogen bonding between the coumarinyl and lipid moieties in the structure. Furthermore, the results obtained here are consistent with those presented in the literature for a similar Bhc-caged compound with shorter alkyl tails, where the

absorption maximum for the compound is reported to also be at the shorter wavelength.[23] The fluorescence emission of the Bhc-caged C16 Dihydro-Cer (**9a**) is highly suppressed in comparison to that of the free coumarin **4**, as indicated by its very low quantum yield of fluorescence (Φ_{fl}= 0.02). The 100-fold decrease in the quantum yield of fluorescence is consistent with the efficient photolysis reaction of the caged dihydroceramide **9a**. In fact, when photolysis of the related Bhc-caged C16 Cer (**9b**) was performed under conditions mimicking those that were to be used in cell experiments, it was observed that complete uncaging (100% conversion) can be achieved with just 90 seconds of UV irradiation (see Figure 2-6, section 2.2.4).

The spectral characteristics of the pegylated coumarinyl compounds present some differences when they are compared to the Bhc-related compounds. Namely, only one absorption peak near 330 nm is seen for these compounds, which is due to the lack of the ionizable hydroxyl group in their structure. Also, the fluorescence emission spectra of the Btcmoc- and Tcmoc-related compounds are blue-shifted by about 60 nm in comparison to the Bhc-related compounds (~400 nm versus 466 nm). In addition, it is noteworthy that the fluorescence emission maximum for the pegylated caged ceramides is at slightly longer wavelengths (~10 nm) than that of the parent coumarins, whereas for the Bhc-related compounds, the emission maxima for the caged dihydroceramide **9a** and for the parent Bhc-coumarin (**4**) are identical (466 nm). As for the fluorescence quantum yield values of the pegylated compounds, the Btcmoc-coumarin (**18**) and the related caged ceramides (**21**-**24**) all exhibit very low values on the order of 0.01. In fact, the quantum yield of fluorescence of the free Btcmoc-coumarin is significantly reduced in comparison to

that of the other free coumarins being studied here. The Tcmoc-coumarin (**17**) and the related caged ceramides (**19**-**20**) exhibit higher fluorescence quantum yield values (0.30, 0.06 and 0.05, respectively), but these compounds still are not as strongly fluorescent as the free Bhc-coumarin.

In terms of the photolysis reaction of coumarin photocages, the introduction of an electron-withdrawing substituent, such as a bromine atom, on the coumarin caging group is, to some extent, unfavourable. This is due to interference with the proposed through-bond electron transfer from the C7 oxygen to the carbonyl group at an electronically excited state. However, an increase in the rate of intersystem crossing (heavy atom effect) with a single bromine substitution compensates for the unfavourable electronic interaction by increasing the fraction of reactive triplet excited state. The time course of photolysis experiments revealed that the Btcmoc-caged ceramides can effectively release ceramide with relatively short UV exposure times (100% conversion with 4-5 min of UV irradiation, see Figure 2-6, section 2.2.4). These compounds do, however, require roughly twice the amount of irradiation time as the Bhc-caged C16 Cer (**9b**). Based on these results, the presence of the mTEG group on the coumarin could reduce the photolysis efficiency of coumarinyl-caged ceramides. It has, in fact, been reported for other Bhc-type photocages that acetylation of the C7 hydroxyl group causes a 10-fold decrease in the photo-release efficiency.[21] The photolytic cleavage of the Tcmoc-caged ceramides (**19**-**20**), which lack the bromine atom in the coumarinyl moiety, appears to not occur as efficiently as the photolysis of the other coumarinyl-caged ceramides.

This is consistent with the slightly higher fluorescence quantum yields of the caged ceramides **19** and **20**.

Coumarinyl-caged compounds have been shown, in other work, to be internalized by HeLa cells.[24] It has been proposed for other coumarinyl photocages that uptake into cells could occur through passive diffusion.[21] Fluorescence imaging allows for detection of coumarinyl-caged compounds in cells due to fluorescence emission from the coumarin moiety upon excitation. In our hands, coumarin fluorescence images revealed that the Bhc-caged C16 Cer (**9b**) is effectively taken up by the cells with 2 hours of incubation. Moreover, the pattern of the fluorescence emission within the cells was relatively diffuse. Therefore, it is not clear from these experiments whether the compound localizes to a specific subcellular compartment. Co-localization (co-staining) experiments utilizing different dyes are required in order to further investigate possible targeting of the caged ceramide **9b**. The free Bhc-coumarin (**4**) was also determined to be internalized by HeLa cells (data not shown). We are, however, reasonably confident that the fluorescence emission, which was observed for the cells incubated in the presence of the caged ceramide **9b**, is indicative of uptake of the intact photocage. Given the relatively slow rate of hydrolytic cleavage ($t_{1/2}$ = ~30 hrs at 25 ^{o}C in the dark), we do not expect significant degradation of the compound during the timeframe of the experiment.[8] The pegylated caged ceramide Btcmoc-caged C22 Cer (**23**) was also studied in uptake experiments and the results suggest that a minimum of ~2 hours of incubation is required in order to achieve an appreciable amount of internalization of the compound by the cells. When one hour of incubation is performed, the level of

coumarin fluorescence in the cells is very low and can't readily be distinguished from the autofluorescence exhibited by the untreated control cells.

In summary, the coumarinyl-caged ceramides were characterized with respect to their absorption and fluorescence emission properties, their time course of photolysis, as well as their ability to be taken up by HeLa cells. Due to the limited amounts of the synthesized caged ceramides, it was not possible to further characterize the photochemical properties of the compounds, such as the quantum yield of photolysis or photolysis reaction rate constants. Nonetheless, the results presented and discussed in this chapter suggest that coumarinyl-caged ceramides are potentially useful tools for studying the biological effects of specific ceramides in cells.

2.4 - References

(1) Ellis-Davies, G. C. R. *Nat Meth* **2007**, *4*, 619.
(2) Mayer, G.; Heckel, A. *Angewandte Chemie International Edition* **2006**, *45*, 4900.
(3) Fillet, M.; Bentires-Alj, M.; Deregowski, V.; Greimers, R.; Gielen, J.; Piette, J.; Bours, V.; Merville, M.-P. *Biochemical Pharmacology* **2003**, *65*, 1633.
(4) Hartfield, P. J.; Mayne, G. C.; Murray, A. W. *FEBS Letters* **1997**, *401*, 148.
(5) Engedal, N.; Saatcioglu, F. *The Prostate* **2001**, *46*, 289.
(6) Kim, W.; Choi, C.; Kang, S.; Kwon, C.; Kim, Y. *Neurochem Res* **2005**, *30*, 969.
(7) López-Marure, R.; Gutiérrez, G.; Mendoza, C.; Ventura, J. L.; Sánchez, L.; Reyes Maldonado, E.; Zentella, A.; Montaño, L. F. *Biochemical and Biophysical Research Communications* **2002**, *293*, 1028.
(8) Kim, Y. A.; Ramirez, D. M. C.; Costain, W. J.; Johnston, L. J.; Bittman, R. *Chemical Communications* **2011**, *47*, 9236.
(9) Karimi, B.; Zareyee, D. *Organic Letters* **2008**, *10*, 3989.
(10) Qiao, L.; Kozikowski, A. P.; Olivera, A.; Spiegel, S. *Bioorganic & Medicinal Letters* **1998**, *8*, 711.
(11) Swamy, K. C. K.; Kumar, N. N. B.; Balaraman, E.; Kumar, K. V. P. P. *Chemical Reviews* **2009**, *109*, 2551.
(12) Carter Ramirez, D. M., University of Ottawa, 2013.
(13) Jones Ii, G.; Jackson, W. R.; Halpern, A. M. *Chemical Physics Letters* **1980**, *72*, 391.
(14) Pal, H.; Nad, S.; Kumbhakar, M. *The Journal of Chemical Physics* **2003**, *119*, 443.

(15) Chipuk, Jerry E.; McStay, Gavin P.; Bharti, A.; Kuwana, T.; Clarke, Christopher J.; Siskind, Leah J.; Obeid, Lina M.; Green, Douglas R. *Cell* **2012**, *148*, 988.
(16) Dai, Q.; Liu, J.; Chen, J.; Durrant, D.; McIntyre, T. M.; Lee, R. M. *Oncogene* **2004**, *23*, 3650.
(17) Jiang, Z.; Hong, X.; Long, H.; Hu, J.; Zhai*, Z. *CMLS, Cell. Mol. Life Sci.* **2000**, *57*, 1117.
(18) Mesicek, J.; Lee, H.; Feldman, T.; Jiang, X.; Skobeleva, A.; Berdyshev, E. V.; Haimovitz-Friedman, A.; Fuks, Z.; Kolesnick, R. *Cellular Signalling* **2010**, *22*, 1300.
(19) Sassa, T.; Suto, S.; Okayasu, Y.; Kihara, A. *Biochimica et Biophysica Acta (BBA) - Molecular and Cell Biology of Lipids* **2012**, *1821*, 1031.
(20) Furuta, T. In *Dynamic Studies in Biology: Phototriggers, Photoswitches and Caged Biomolecules*; Givens, R., Goeldner, M., Eds.; Wiley-VCH: 2005, p 29.
(21) Furuta, T.; Takeuchi, H.; Isozaki, M.; Takahashi, Y.; Kanehara, M.; Sugimoto, M.; Watanabe, T.; Noguchi, K.; Dore, T. M.; Kurahashi, T.; Iwamura, M.; Tsien, R. Y. *ChemBioChem* **2004**, *5*, 1119.
(22) Furuta, T.; Wang, S. S.-H.; Dantzker, J. L.; Dore, T. M.; Bybee, W. J.; Callaway, E. M.; Denk, W.; Tsien, R. Y. *Proceedings of the National Academy of Sciences* **1999**, *96*, 1193.
(23) Suzuki, A. Z.; Watanabe, T.; Kawamoto, M.; Nishiyama, K.; Yamashita, H.; Ishii, M.; Iwamura, M.; Furuta, T. *Organic Letters* **2003**, *5*, 4867.
(24) Mentel, M.; Laketa, V.; Subramanian, D.; Gillandt, H.; Schultz, C. *Angewandte Chemie International Edition* **2011**, *50*, 3811.

Chapter 3: Effects of Photochemically Generated Ceramide on the Morphology and Viability of HeLa cells

Contributions: The dose response data presented was fitted by Dr. W. Costain of the National Research Council of Canada using the software GraphPad Prism.

3.1 - Introduction: Ceramide and Cell Death

The bioactive lipid ceramide is a critical mediator of apoptosis, a form of programmed cell death, as demonstrated in a large number of studies which were conducted in a variety cell types. Namely, treatment with short-chain ceramides has been shown to induce apoptotic cell death in the rat pheochromocytoma cell line PC12 and in the human colon carcinoma cell line HCT166.[1,2] Moreover, pancreatic cancer cells exposed to the cationic ceramide analogue LCL124 have been shown to undergo apoptotic cell death.[3] Although numerous reports have indicated that ceramide causes cell death through apoptosis, some studies have shown that ceramide-induced cell death can occur through necrosis, an alternate form of programmed cell death. For example, necrotic cell death with short-chain ceramide analogues was observed in the human cervix carcinoma cell line CALO, in the human glioblastoma cell line A172 and in the prostate cancer cell line LNCaP.[4-6] Although the nature of ceramide-induced cell death can vary, treatment with this bioactive sphingolipid is often associated with a measurable decrease in cell viability.

It has been suggested more recently that the biological activity of ceramide is dependent on the length of its N-acyl chain.[7] For instance, cellular levels of long-

chain C16 Cer have been shown to be elevated in cells undergoing apoptosis, which suggests that this sphingolipid exhibits pro-apoptotic effects in biological systems.[8,9] Due to the hydrophobicity of its long N-acyl chain, natural C16 Cer exhibits low solubility in aqueous media and poor membrane permeability. In light of this, many investigations of the biological effects of ceramide have relied on the use of C2 and C6 ceramides, which are short-chain analogues of natural ceramides. These water-soluble compounds, which form micelles in aqueous media, are commonly used in cell studies. Synthetic short-chain ceramides are available commercially and can be administered to cells exogenously. However, using short-chain analogues to study the biological effects of ceramide does present some disadvantages. Due to the difference in aqueous solubility, C2 Cer does not perfectly mimic endogenous long-chain ceramides in biological systems.[10] It has been shown that exogenous C2 Cer taken up at the plasma membrane can translocate to different subcellular compartments, whereas endogenous long-chain ceramides generally remain at the location where they are generated.[11,12] As an alternative to short-chain ceramides, photolabile compounds, such as caged ceramides, can be used for delivering natural long- and very long-chain ceramides to cells. A series of coumarinyl-caged ceramides were prepared, as described in the previous chapter, and used to assess the effects of specific ceramides on cell morphology and viability.

A variety of different methods can be used to evaluate the viability of cells that have been exposed to external stresses or stimuli or that have been subjected to treatment with a compound of interest. One method to assess cell viability is by examining and comparing the morphology of the treated cells to that of control cells

which were left untreated, under similar conditions. Cells undergoing apoptosis are known to exhibit distinct morphological features that are characteristic of this form of cell death, such as chromatin condensation, DNA fragmentation, cell shrinkage and membrane blebbing.[13] Alternatively, some of the morphological changes that are associated with necrosis are an increase in cell volume, as well as rupture of the plasma membrane followed by spilling of the cellular contents into the extracellular environment.[14] Scheme 3-1 depicts some of the morphological features that are observed during apoptotic and necrotic cell death.[15] Although some of the changes in morphology that are listed above can be visualized by bright field optical microscopy, the more intricate changes often require labelling of the structures with fluorescent dyes. For example, staining the nuclei of cells with Hoechst 33342 dye can allow for the detection of nuclear condensation or fragmentation, which are associated with apoptotic cell death.[16] In addition, assessing uptake of the fluorescent dye propidium iodide (PI) by the cells can provide information on the integrity of the plasma membrane.[17]

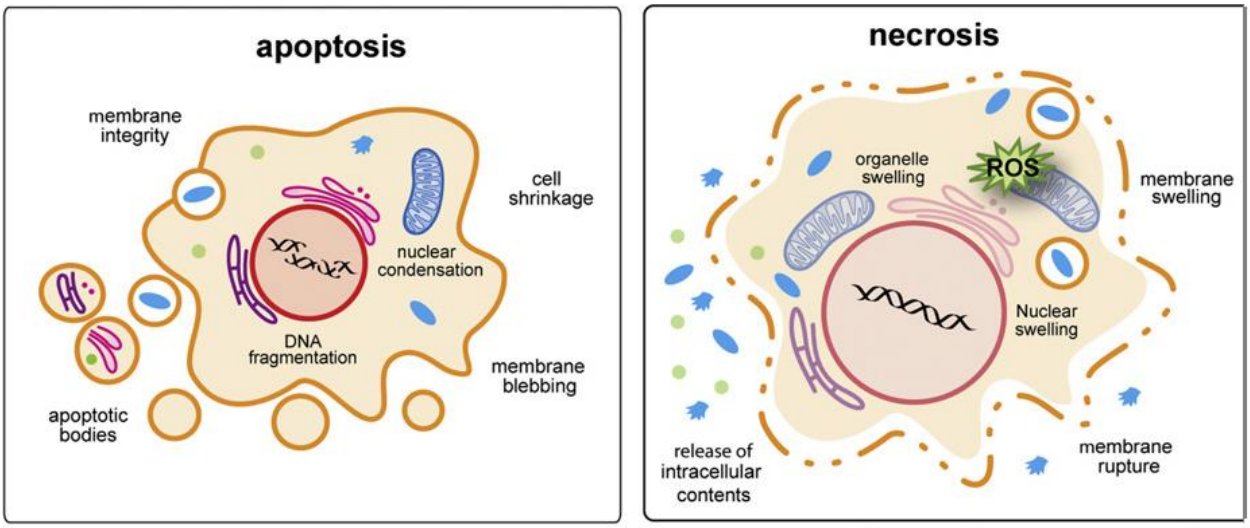

Scheme 3-1. Representation of the morphological features of apoptosis and necrosis. Reproduced from reference 15 with approval.

Although cell morphology can be used as a qualitative means of assessing cell viability, a variety of quantitative bioassays exist and can be used to measure the relative viability of cells exposed to different treatments. Cell viability is often evaluated by measuring the activity of metabolic enzymes, such as dehydrogenases. The MTT (3-(4,5-dimethylthiazol-2-yl)-2,5-diphenyl tetrazolium bromide) assay, which was developed by Mosmann in 1983, is a commonly used method for assessing cell death and proliferation in response to different treatments.[18] This assay, which is based on cellular reduction of the MTT tetrazolium salt to the formazan product, is outlined in Scheme 3-2.[19] The coloured formazan product produces a spectrophotometric signal, which is assumed to be proportional to the amount of living cells in the sample.

One drawback of this method, however, is that the dark purple formazan crystals, which are produced at the surface of the cell, require solubilization with an organic solvent (e.g. DMSO), such that the optical density can be measured. Although the mechanism of the cellular reduction of MTT has been extensively studied, it still remains to be fully elucidated. Some reports suggest that the MTT tetrazolium salt is converted to the formazan product by a mitochondrial succinate dehydrogenase enzyme[20], whereas others indicate that it is mainly reduced in the cytoplasm by NAD(P)H (nicotinamide adenine dinucleotide (phosphate)) and by dehydrogenases associated with the endoplasmic reticulum[21].

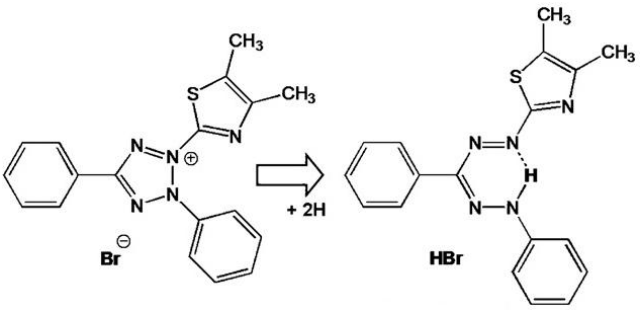

Scheme 3-2. Cellular conversion of the MTT tetrazolium salt to the MTT formazan product. Adapted from reference 19.

Despite the wide use of the MTT assay, some limitations have been observed with this method suggesting that it is not suitable in all systems. For example, the requirement for solubilizing the formazan product can be time-consuming and can introduce a certain error on the measurements.[22] In light of this, a variant of the MTT tetrazolium salt known as WST-1 (4-[3-(4-iodophenyl)-2-(4-nitrophenyl)-2H-5-tetrazolio]-1,3-benzene disulfonate, sodium salt) was developed and was first reported by Ishiyama et al.[23] Reduction of the WST-1 reagent to the respective formazan product is represented in Scheme 3-3.[23] This compound, which was termed WST for "water soluble tetrazolium" based on its ability to generate a formazan product that is soluble in aqueous solution, is a useful reagent for assessing cell viability. Conversion of the WST-1 tetrazolium salt to the corresponding formazan product generates a signal that can be measured directly at 450 nm. Like other tetrazolium salts, WST-1 is reduced to the formazan product by NADH, in the presence of an electron coupling agent.[23]

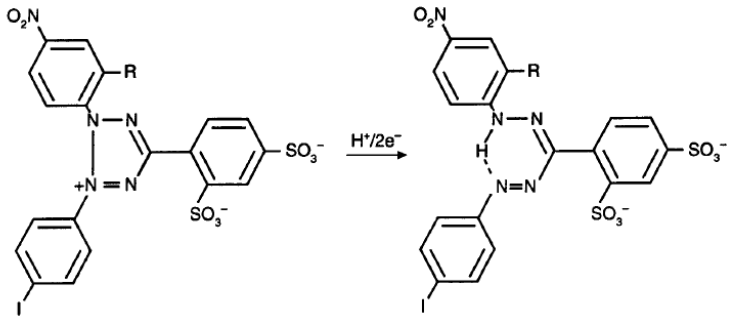

Scheme 3-3. Conversion of the WST-1 tetrazolium salt to the respective formazan product. Adapted from reference 23.

Several other methods for assessing cell viability have been reported in the literature, such as the trypan blue dye exclusion assay, the lactate dehydrogenase (LDH) activity assay and the fluorescent resazurin reduction assay.[4,24] However, these methods will not be described any further since they were not used in this

study. In the work presented in this chapter, bright field optical microscopy experiments and cell viability assays were conducted with the goal of assessing the effects of specific ceramides on the viability of HeLa cells. This was achieved through the use of coumarinyl-caged ceramides and the results from these experiments are presented and discussed in the pages that follow.

3.2 - Results

3.2.1 - Morphology of HeLa Cells Subjected to Ceramide Treatments

Since the goal of this study was to evaluate the biological effects of the photochemical generation of ceramide in HeLa cells, it was important to initially assess the morphological changes associated with different ceramide treatments. As a starting point, HeLa cells were subjected to treatments with exogenously added ceramides in a similar manner as outlined in the literature.[1,2,4-6] When the cells were exposed to short-chain C2 Cer (20 μM) and examined by bright field optical microscopy after 24 hours, they exhibited many of the morphological features that are characteristic of apoptosis, such as cell shrinkage, as well as the detachment of the cells from the surface of the culture plate. In contrast, cells incubated with long-chain C16 Cer appeared to be minimally affected by the treatment. Figure 3-1 displays representative bright field images of HeLa cells treated with exogenous ceramides, as well as an image of an untreated control for comparative purposes.

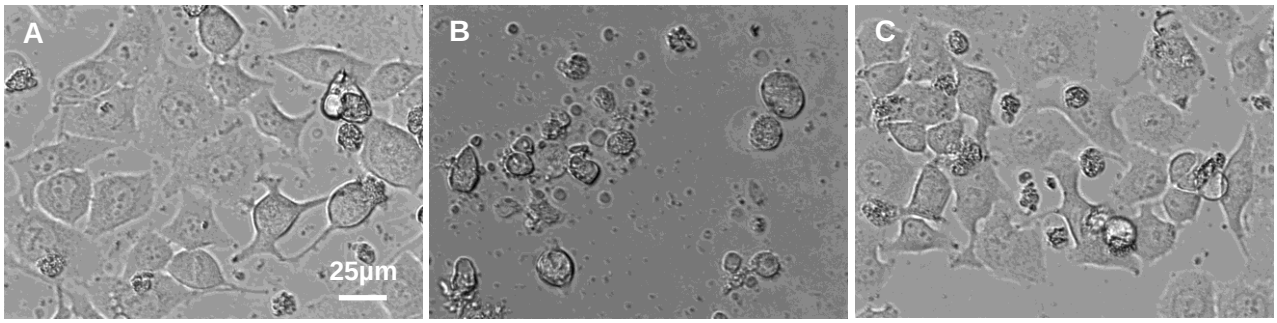

Figure 3-1. HeLa cells treated with C2 Cer exhibit morphological features that are consistent with apoptosis. Bright field images of HeLa cells incubated for 24 hours in the presence of C2 Cer (B) or C16 Cer (C), at a concentration of 20 µM, in serum-free medium. An untreated control sample (A) was included for comparison. The images were acquired using a 40X objective.

Next, the morphology of HeLa cells incubated with the Bhc-caged C16 Cer (**9b**), as well as with exogenous ceramides (for comparison) was assessed, in the absence and in the presence of UV irradiation. Exposure to UV irradiation, which is used to photolyze the caged ceramides, is reported to induce some biological effects in cells.[25] Therefore, it was necessary to determine whether any distinct morphological features were present in cells exposed to UV irradiation alone, in comparison to those that were left unirradiated. Since this experiment was meant to be a basic morphological assessment, no staining protocols were carried out. Bright field images of the samples were acquired after 24 hours of treatment and are displayed in Figure 3-2.

As observed in the preliminary imaging experiment with exogenous ceramides, C2 Cer treatment (20 µM) was very detrimental to the cells, which exhibited many apoptotic features (e.g. cell shrinkage, cell detachment, etc.). In contrast, cells incubated with C16 Cer (20 µM) did not appear to be significantly affected by the treatment. As mentioned previously, these results are reasonable

based on the differences in solubility and in membrane permeability of the two ceramides. Moreover, there did not appear to be any visible differences between the UV-irradiated and unirradiated samples that were treated with C2 Cer or with C16 Cer, and the same could be said for the untreated samples. This suggested that 4 minutes of UV irradiation does not cause significant damage to the cells under the conditions used here.

As for the cells incubated with the Bhc-caged C16 Cer (**9b**), the treatment appeared to cause some morphological changes in the samples, in the absence and in the presence of UV irradiation. However, the morphology that was observed did not resemble that of cells undergoing apoptosis and it was significantly different than the morphology of the cells treated with short-chain C2 Cer. The main difference between the untreated controls and the cells treated with the caged ceramide **9b** was the presence of some additional particulate matter within the treated samples. Moreover, this effect seemed to be larger in the presence of UV irradiation. The appearance of these morphological features could be indicative of plasma membrane rupture and spilling of the intracellular contents into the extracellular environment[14], which would suggest that some necrotic cell death occurs in response to treatment with the caged ceramide **9b**. Overall, the results showed that the caged ceramide **9b** causes changes in morphology that are not present in the untreated control or in the samples treated with C16 Cer, both with and without UV irradiation. However, careful examination of other biochemical factors is required in order to determine the effects of this caged ceramide on cell viability and its involvement in cell death.

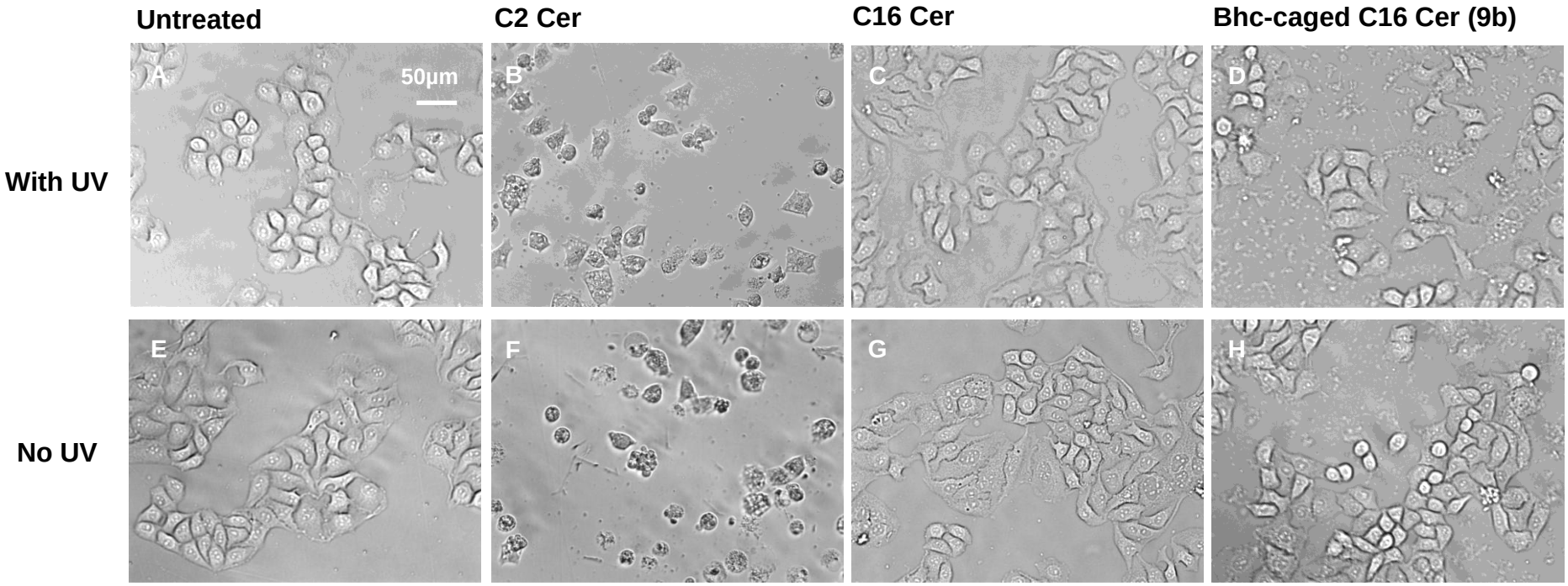

Figure 3-2. Treatment of HeLa cells with the Bhc-caged C16 Cer (**9b**) causes morphological changes that are different than those observed with C2 Cer treatment. Bright field images of HeLa cells treated with ceramide species in serum-free medium (20 µM) for 24 hrs (along with untreated vehicle controls). For UV-irradiated samples (A-D), the culture plate was removed from the incubator after 7.5 hrs and irradiated for 4 min (350 nm). The images were acquired using a 20X objective.

3.2.2 - Measuring the Viability of HeLa Cells Exposed to Bhc-Caged Cer

Having shown, with the results presented in the previous chapter, that coumarinyl-caged ceramides are taken up by HeLa cells and can effectively generate ceramide upon UV irradiation, the effects on cell viability were assessed quantitatively with the MTT assay. This assay, which was described earlier in this chapter, was selected based on the relative simplicity of the method. As a starting point, a concentration of 20 μM was chosen based on other studies where ceramide was used at similar concentrations.[1,2,5,6] In a preliminary assay, the cells were incubated in the presence of ceramides (or of a vehicle control, in the "Untreated" samples) for 24 hours before the viability assay was performed. In our hands, the MTT assay indicated that exogenous long-chain C16 Cer was causing a considerable decrease in cell viability, which was even larger than that observed with short-chain C2 Cer (data not shown). These results are inconsistent with what was observed in the bright field imaging experiments for HeLa cells treated with exogenous C2 and C16 ceramides under similar conditions (see Figures 3-1 and 3-2, section 3.2.1). Based on the fact that short-chain ceramides are known to be readily taken up by cells, it was reasonable to observe that C2 Cer caused a decrease in cell viability. However, the decrease in viability with C16 Cer was unexpected based on the very low aqueous solubility and poor membrane permeability of the long-chain ceramide. Other reports have shown that exogenous C16 Cer does not significantly affect the viability of cells since the long N-acyl chain in its structure prevents its uptake into cells.[2]

We next tested whether the presence of serum in the medium was facilitating the uptake of exogenous long-chain C16 Cer into the cells. Due to the pro-apoptotic nature of C16 ceramide, facilitated uptake of this species could account for the decrease in cell viability that was observed. Representative MTT assay results for HeLa cells treated with exogenous ceramides in serum-free medium are shown in Figure 3-3. It was observed, once again, that C16 Cer was causing a large decrease in viability (~55% viable), which was more significant than with C2 Cer (~65% viable). Again, the decrease in viability with C16 Cer was not consistent with the morphology of the cells, which exhibited no visible signs of apoptosis after 24 hrs of treatment (see Figure 3-1 (C), section 3.2.1). The viability of cells subjected to shorter ceramide treatments (6 or 12 hours) was also assessed by MTT assay and the same trends were observed (data not shown). Taken together, these results suggest that other factors, besides the presence of serum in the medium, were contributing to the reduced cell viability that was measured with the MTT assay. In light of this, it was important to cross-validate these findings using another assay.

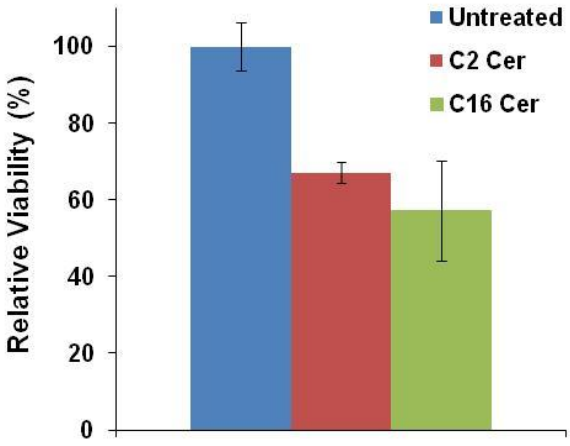

Figure 3-3. Effects of exogenously added C2 and C16 ceramides (20 µM in serum-free medium) on cell viability, as assessed by MTT assay after 24 hours of treatment in the dark (no UV). Data is from a single representative experiment (n=2) and error bars indicate the standard deviation within each treatment group (n = 12-18 values).

As an alternate approach, the WST-1 assay was chosen to assess the viability of HeLa cells treated with ceramides. This viability assay, as described earlier in this chapter, involves the reduction of the tetrazolium salt WST-1 to a water soluble formazan product for which a signal can be measured spectrophotometrically. Figure 3-4 shows the results from a preliminary WST-1 assay in which the effects of exogenously added ceramides on the viability of the cells were assessed. After 24 hours of treatment, it was observed that C2 Cer (20 µM) caused a large decrease in cell viability (~35% viable), which was consistent with the very pronounced morphological effects that were observed previously (see Figure 3-1 (B), section 3.2.1). In contrast, the assay revealed that treatment with C16 Cer (20 µM) for 24 hours had little or no effect on cell viability, as assessed from the relative viability near 100% that was measured for this treatment group. The fact that long-chain C16 Cer showed no significant effect on cell viability was reasonable based on its very low membrane permeability and poor aqueous solubility. These results suggested that the WST-1 assay is a suitable method for assessing the viability of HeLa cells exposed to ceramides. Hereafter, the WST-1 assay results that are presented will be referred to as "viability assay results".

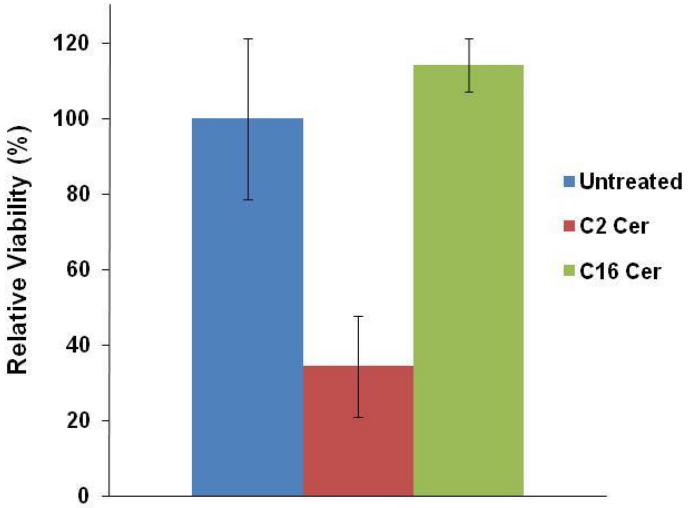

Figure 3-4. Effects of exogenously added C2 and C16 ceramides (20 µM in serum-free medium) on cell viability, as assessed by WST-1 assay after 24 hours of treatment in the dark (no UV). Data is from a single representative experiment and error bars indicate the standard deviation for each treatment group (n = 10 values).

In order to adequately assess the effects of ceramides on viability, it was important to determine the appropriate concentration for the treatment compounds through dose-response experiments. Fitting of the dose response data was performed by Dr. W. Costain of the National Research Council of Canada using the software GraphPad Prism. Figure 3-5 shows the dose-response profiles that were obtained for C16 Cer (+/- dodecane), C2 Cer and the Bhc-caged C16 Cer (**9b**) in HeLa cells subjected to 24 hours of treatment in the dark. From these results, the half-maximal effective concentration (EC_{50}), which is defined as the concentration at which 50% of the maximal response is observed, was determined for each of the compounds. Since EC_{50} is a measure of the cytotoxic potency of a compound, these experiments allowed for comparing the bioactivity of short- and long-chain exogenous ceramides, as well as of the caged ceramide **9b**, in the absence of UV irradiation. Furthermore, dose response analysis enabled the identification of sub-toxic concentrations of **9b** for use in subsequent uncaging studies ($\leq$ 20 µM). It is noteworthy, however, that the EC_{50} values were determined based on the results from a single experiment, which could affect the precision of these values.

The dose dependence of the effects of exogenous C16 Cer on cell viability was evaluated in two different systems. One system involved a co-solvent, dodecane, which was added to the delivery vehicle (ethanol) in order to facilitate the dispersion in aqueous solution and, therefore, the uptake of the long-chain ceramide into the cells. The presence of the co-solvent is expected to increase the toxicity of C16 Cer in the cells. This method of dispersion for long-chain ceramides, which was first reported by Ji et al., employs a 98:2 mixture of ethanol and dodecane to

dissolve the lipids which are to be added to aqueous medium.[26] The other system that was investigated, for comparison, was C16 Cer alone (in ethanol). As shown in Figure 3-5 (A), in the absence of dodecane, C16 Cer exhibited little toxicity, even at very high concentrations. Namely, the cells that were incubated with 100 µM of C16 Cer for 24 hours were still ~80% viable after the treatment. The EC_{50} of C16 Cer in HeLa cells with 24 hours of treatment was determined to be 71.7 µM. When dodecane was used as a co-solvent for C16 Cer, the cells were ~30% viable after being subjected to the 100 µM treatment, as shown in Figure 3-5 (B). The EC_{50} of "C16 Cer + dodecane" under these conditions was determined to be 48.1 µM, which is significantly lower than that of C16 Cer alone. This indicated that promoting cellular uptake with the co-solvent increases both the potency and the efficacy of the long-chain ceramide. Thus, low cellular uptake of long-chain ceramides appears to limit their toxicity. Notably, C2 Cer exhibited the greatest toxicity, where doses equal to and exceeding 30 µM appeared to almost completely eradicate viable cells, as displayed in Figure 3-5 (C). The EC_{50} of C2 Cer under the conditions used was determined to be 11.3 µM, suggesting that C2 Cer is approximately 4-fold more potent than "C16 Cer + dodecane". These results indicated that the concentration of 20 µM that was chosen initially and used in the preliminary cell viability experiments was adequate. This is illustrated in Figure 3-5, where the vertical lines show that 20 µM C16 Cer is sub-toxic, whereas 20 µM C2 Cer produces complete loss of cell viability.

A dose-response profile was also obtained for the Bhc-caged C16 Cer (**9b**) and these results are displayed in Figure 3-5 (D). It is important to note that UV

irradiation of the samples was not performed, and the compound should have mostly remained in the caged form for the duration of the experiment. The assay revealed that the EC_{50} of the caged ceramide **9b**, after 24 hours of treatment in the absence of UV irradiation, is 21.2 μM. Importantly, the dose-response curve that was obtained for the caged ceramide was qualitatively different than those obtained for the exogenous ceramides. The curves for the exogenous ceramides are best described using a 4 parameter model with Hill slopes in the -9.9 to -4.5 range. These very steep Hill slopes indicate that exogenous ceramides elicit their toxicity over a very narrow concentration range. Conversely, the dose-response curve for the caged ceramide **9b** is best described using a 3 parameter model, with a Hill slope set to -1. Therefore, the toxicity range of the caged ceramide is much wider, indicating that caging alters the toxicity profile of ceramides. The low cytotoxicity that was observed for the caged ceramide under the conditions used is reasonable considering that the bioactive C16 Cer was not photochemically uncaged. The decrease in cell viability that was observed with high concentrations of the caged ceramide **9b** in the absence of UV irradiation could be explained by the release of a certain amount of C16 Cer due to hydrolytic cleavage or due to minimal exposure of the compound to ambient light during one or more of the experimental steps. It is expected that photorelease of the caged ceramide **9b** in cells will result in the pharmacological characteristics reverting to those of the parent compound (i.e. steep dose-response curve).

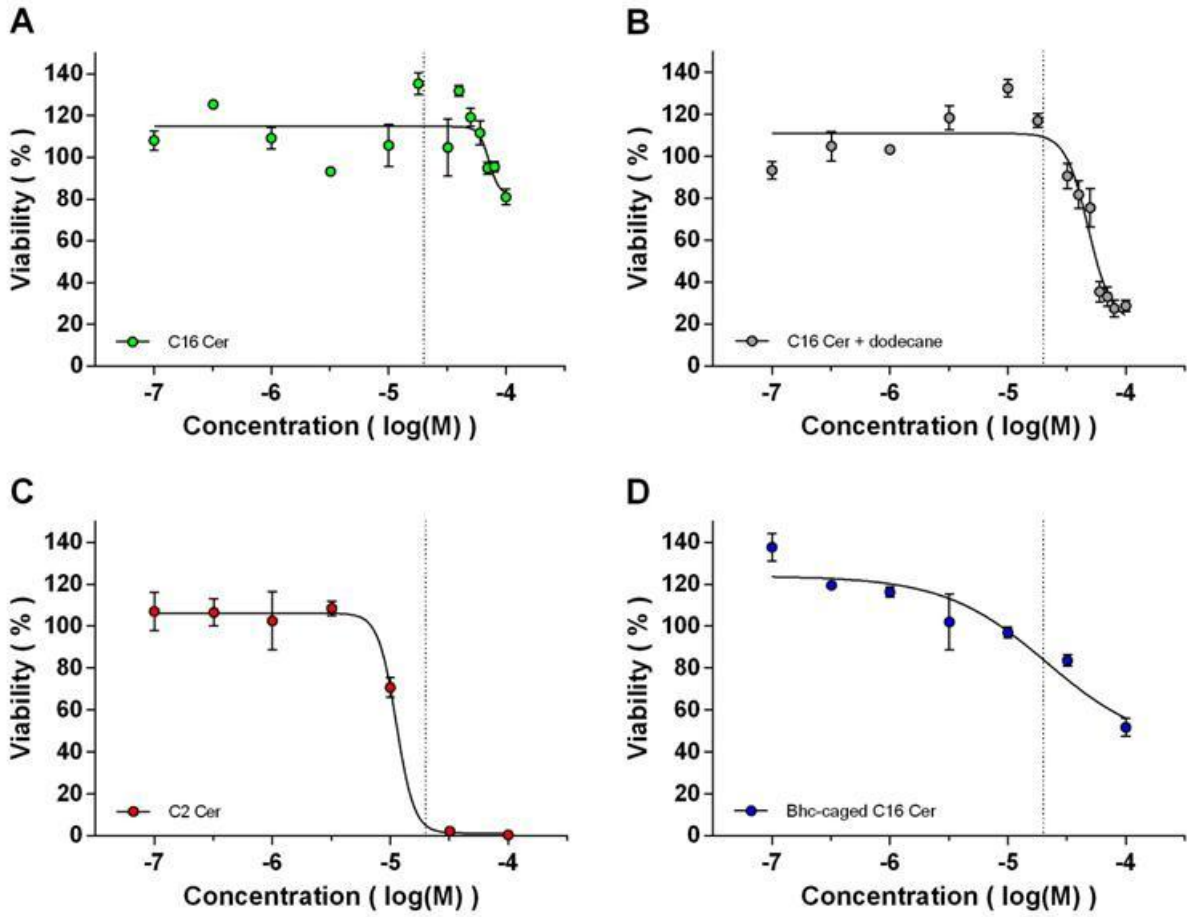

Figure 3-5. Dose-response profiles of exogenously added C2 and C16 ceramides and of the Bhc-caged C16 Cer (**9b**), as assessed by WST-1 assay after 24 hours of treatment in the dark (no UV). Data is from a single experiment and error bars indicate the standard deviation (n = 4-6 values).

Aside from the concentration of the compounds, it was important to consider the photophysical and photochemical properties of the caged ceramides in order to achieve effective photorelease of ceramide in HeLa cells. These parameters were investigated earlier in this study and the results are presented in chapter 2. It was hypothesized that the photolysis of caged ceramides in cells would require slightly longer UV irradiation times than those required for uncaging in solution. This is because some cellular components may absorb some of the UV light that is used for photolyzing the compounds. In order to determine the length of UV irradiation time

to be used in the cell viability experiments, it was necessary to perform some optimization experiments.

An experiment was designed in which HeLa cells were incubated with 20 µM of the Bhc-caged C16 Cer (**9b**), or left untreated, and exposed to 0, 4 or 12 minutes of UV irradiation. A viability assay was performed after a total of 24 hours of treatment. As shown in Figure 3-6, the results suggested that 4 minutes of UV irradiation is sufficient to photolyze the caged ceramide **9b** in the cells in order to generate C16 Cer. This was assessed from the large decrease in cell viability (~45% viable) that was observed for the samples treated with the caged ceramide and irradiated, when compared to the untreated or unirradiated samples. This decrease in viability can be explained by the known biological activity of C16 Cer, as well as its involvement in different cell death pathways. Moreover, this result is reasonable based on the amount of UV exposure (1.5 min) that was determined, from preparatory photolysis experiments, to be required for complete (100%) uncaging of the caged ceramide **9b** in solution (see Figure 2-6, section 2.2.4, chapter 2). With the longer UV irradiation time of 12 minutes, the untreated control cells exhibited a significant decrease in viability (~75% viable). This was indicative of UV damage caused to the cells as a result of the irradiation. In light of this, it was necessary to utilize shorter UV exposure times for the purpose of uncaging in cells.

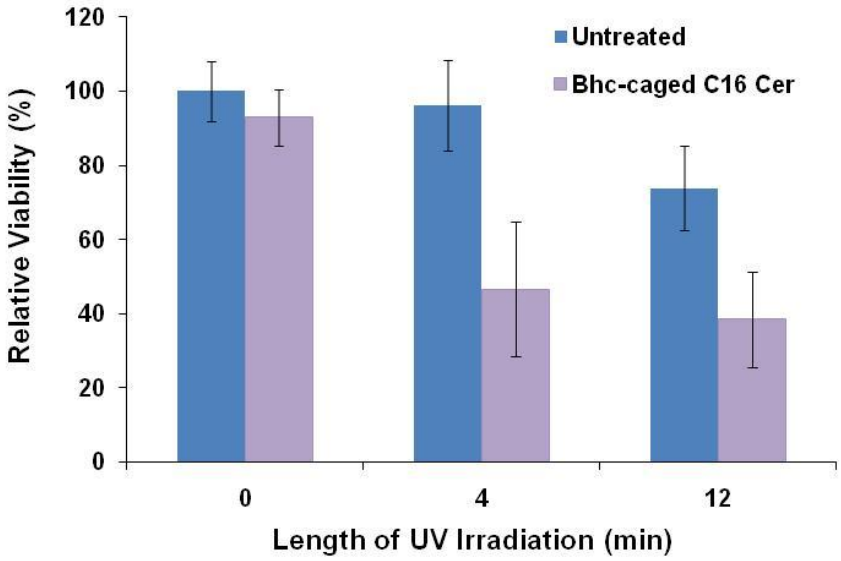

Figure 3-6. Effects of the Bhc-caged C16 Cer (**9b**) on cell viability when different lengths of UV irradiation were used for uncaging, after 4 hours of incubation. Viability was assessed by WST-1 assay after 24 hours of treatment. Data is from a single experiment and error bars indicate the standard deviation for each treatment group (n = 12 values).

Having determined the appropriate length of incubation with the compounds, as well as their effective dose and the amount of UV exposure time required for uncaging in HeLa cells, the effects of the photochemical generation of ceramide on cell viability could be thoroughly assessed and compared to the effects exerted by exogenously added ceramides. Viability assays were performed after 24 hours for samples that were treated and subjected to UV irradiation, as well as for samples that were treated and left unirradiated (or left untreated, in both cases). Where applicable, UV irradiation was performed after 2 hours of incubation with the compounds. Although 4 minutes of UV irradiation appeared to allow for effective uncaging of the Bhc-caged C16 Cer (**9b**) in the cells (see Figure 3-6 of this section), a standard UV irradiation time of 6 minutes was chosen in order to maximize the photorelease of ceramide while minimizing UV-induced damage. Average values (from several experiments) for the relative viability of HeLa cells, which were treated for 24 hours with the caged ceramide **9b** and with other control compounds (exogenous ceramides and the free Bhc-coumarin (**4**)), are presented in Figure 3-7.

The cells treated with exogenous C2 and C16 ceramides gave results that are consistent with those obtained in the preliminary cell viability experiments (see Figure 3-4 of this section). It was observed that C2 Cer, at a concentration of 20 μM, causes a very large decrease in cell viability (~40% viable) in the absence and in the presence of UV irradiation. Long-chain C16 Cer (20 μM), once again, was shown to cause little or no effect on cell viability in the absence and in the presence of UV irradiation. These results are reasonable based on the relative aqueous solubility and membrane permeability of these different ceramides.

It was also important to test for any effects of the free coumarin **4** on cell viability, in the absence and in the presence of UV irradiation, since this compound is generated as a by-product of the photolysis of the caged ceramide **9b**. This was required in order to be able to effectively attribute to C16 Cer the decrease in viability that is observed upon the photochemical generation of this lipid in HeLa cells. The samples treated with the free coumarin **4** and subjected to 6 minutes of UV irradiation showed slightly decreased cell viability (~90% viable) in comparison to the untreated control. However, no significant decrease in cell viability was observed in the absence of UV irradiation. The slight toxicity of the free coumarin could be due to the generation of reactive oxygen species (ROS) in the cells upon UV irradiation. This was investigated in later experiments, which will be discussed in the next chapter.

With the appropriate controls in place, the effects of the photochemical generation of ceramide on the viability of HeLa cells could be measured. In the presence of UV irradiation, the Bhc-caged C16 Cer (**9b**) caused a decrease in cell

viability (~70% viable), which is statistically significant ($p < 0.05$), after 24 hours of treatment. Moreover, this decrease in cell viability was not observed in the absence of UV irradiation. Taken together, these results suggest that the caged ceramide **9b** can effectively be used to photochemically generate C16 Cer in the cells with a certain level of spatial temporal control, by the means of UV irradiation. In addition, the difference in the magnitude of the effects caused by the caged ceramide **9b** and by the free Bhc-coumarin control, in the presence of UV, was determined to be statistically significant ($p < 0.05$). It is also noteworthy that the extent of the decrease in viability determined here, with the caged ceramide **9b**, is smaller than that observed in the optimization experiment (see Figure 3-6, section 3.2.2). This could be due to differences in cell density during plating or in UV lamp intensity during the photolysis. However, since the earlier result was based on a single experiment, the average value for the relative viability, which is presented here, is more reliable.

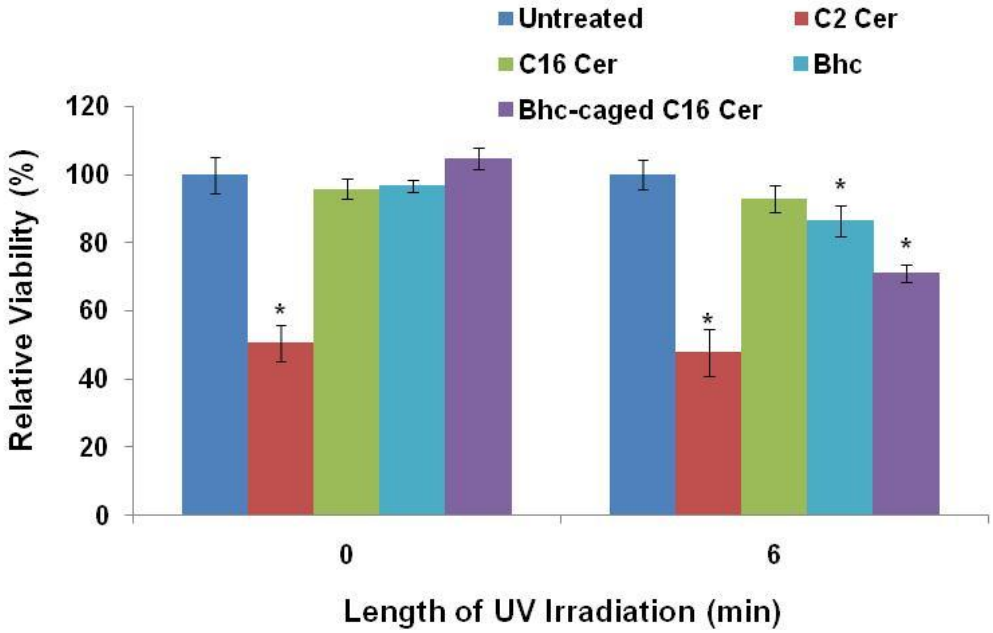

Figure 3-7. UV irradiation of the Bhc-caged C16 Cer (**9b**) in HeLa cells causes a decrease in viability that is not observed in the absence of UV. Relative viability (%) of cells treated with the caged ceramide **9b** or with the control compounds C2 Cer, C16 Cer and Bhc (20 µM) in serum-free medium, as assessed by WST-1 assay after 24 hours of treatment. Data is from several experiments (n=3-10) and error bars indicate the standard error mean. * Indicates statistical significance ($p < 0.05$) of the difference in the relative viability, with reference to the respective (0 and 6 min UV) untreated controls.

3.2.3 – Measuring the Effects of Btcmoc-Caged Cers on Viability

The effects of the pegylated Btcmoc-caged ceramides on the viability of HeLa cells were also investigated. In order to optimize the length of UV irradiation to be used for uncaging these compounds in the cells, the viability of cells treated with the Btcmoc-caged C22 Cer (**23**) was assessed in an experiment where different lengths of UV irradiation time were used. The cells were incubated in the presence of the caged ceramide **23** (20 μM) and exposed to 0, 4 or 6 minutes of UV irradiation. Cell viability was measured after 24 hours of treatment and the results from this experiment are displayed in Figure 3-8. It was observed that the cells that were treated with the caged ceramide **23** and UV-irradiated for 4 minutes were considerably less viable (~75% viable) than those which were left untreated or unirradiated. These results suggested that 4 minutes of UV irradiation allows for photolysis of the caged ceramide **23** in the cells. Due to the large error on the measurements, it was not possible to distinguish any significant effect of the caged ceramide with 6 minutes of UV irradiation.

The fact that 4 minutes of UV irradiation was determined to be sufficient for uncaging the Btcmoc-caged C22 Cer (**23**) in the cells was reasonable based on the results from the preparatory photolysis experiments, where complete (100%) photolysis of the compound was achieved with 4 minutes of irradiation (see Figure 2-6, section 2.2.4, chapter 2). Again, in order to maximize the response that is observed upon the photochemical generation of ceramide in the cells, a standard UV irradiation time of 6 minutes was selected and was used in most of the viability assays with the Btcmoc-caged ceramides.

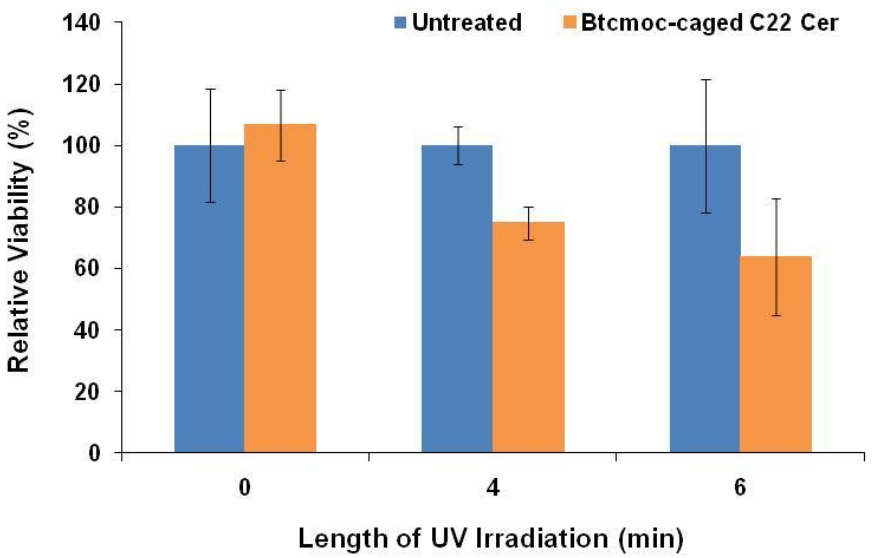

Figure 3-8. Effects of the Btcmoc-caged C22 Cer (**23**) on cell viability when different lengths of UV irradiation were used, after 2 hours of incubation. Viability was assessed by WST-1 assay after 24 hours of treatment. Data is from a single experiment and error bars indicate the standard deviation for each treatment group (n = 10-12 values).

Average values for the relative viability of HeLa cells treated with the different Btcmoc-caged ceramides (**21**-**24**) or with the free Btcmoc-coumarin (**18**) were determined from several experiments and the results are displayed in Figure 3-9. In these assays, C2 Cer (20 µM) was included as a positive control and the samples treated with this ceramide exhibited a similar decrease in cell viability (30-50% viable with 0, 6 and 9 min of UV irradiation) as observed earlier. Since the cytotoxicity of C16 Cer was assessed in previous experiments, it was omitted here in order to simplify these assays which evaluated several treatment groups. When the samples were subjected to 6 minutes of UV irradiation, no significant effects on cell viability could be detected with any of the Btcmoc-caged ceramides. In addition, the free coumarin **18**, which was included as a control, did not cause any significant decrease in viability under these conditions. Furthermore, no differences between the various treatment groups were observed. Possibly, a more specific assay is required for investigating the N-acyl chain length dependence of the biological

effects of ceramides using this series of coumarinyl-caged ceramides. It is also noteworthy that these results are in contrast to those obtained from the optimization experiment with the Btcmoc-caged C22 Cer (**23**), where 4 minutes of UV irradiation was sufficient to cause reduced cell viability (see Figure 3-8, section 3.2.3). Once again, this discrepancy could be due to differences in cell density during plating or in UV lamp intensity during the photolysis. Due to the larger number of experimental replicates presented here for the average relative viability, these results should be considered more representative than the earlier results.

A longer UV exposure time of 9 minutes was also tested with some of the compounds and the results are shown in Figure 3-9. Cells treated with the Btcmoc-caged C16, C18 and C24 ceramides (**21**, **22** and **24**) and UV-irradiated for 9 minutes exhibited decreased viability (~75-80% viable), which was, in each case, statistically significant ($p < 0.05$) with reference to the respective (9 min UV) untreated control (see page 134, section 5.6, chapter 5 for details on statistical analysis). However, under the same conditions, the free coumarin **18** caused a similar decrease in viability (~80% viable) as the caged ceramides. It is therefore difficult to determine whether the photo-release of ceramide from the Btcmoc-caged compounds significantly affects the viability of HeLa cells.

As for the Tcmoc-caged ceramides, they were not used for assessing the biological effects of specific ceramides in HeLa cells. Based on the low efficiency of photolytic cleavage of these compounds in solution, which was assessed from preparatory photolysis experiments (see Figure 4, section 2.2.4, chapter 2), it was determined that these compounds would not be as useful for cell studies. It is more

than likely that the very long UV exposure times that are required for achieving an appreciable level of photolysis of these caged ceramides would be detrimental to the cells.

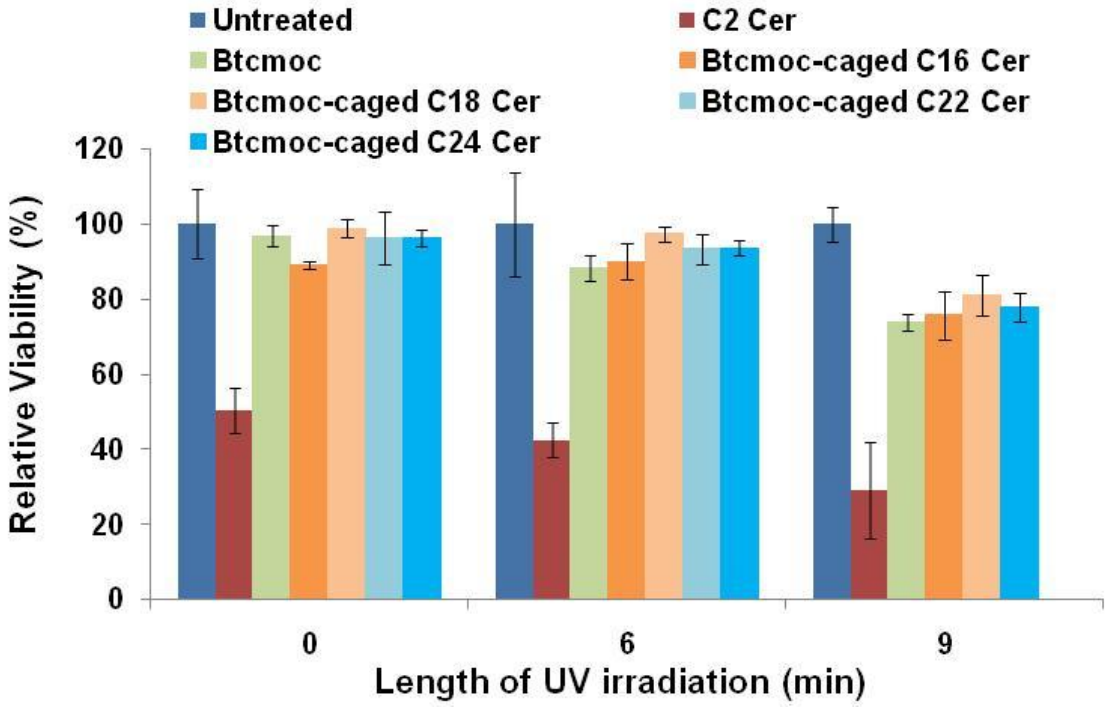

Figure 3-9. UV irradiation of the Btcmoc-caged ceramides (**21**-**24**) and of the free Btcmoc-coumarin (**18**) causes similar effects on the viability of HeLa cells. Relative viability (%) of cells treated with the Btcmoc-caged ceramides or with the control compounds C2 Cer and the free coumarin **18** (20 μM), as assessed by WST-1 assay after 24 hours of treatment. Data is from 1-3 experiments and error bars indicate the standard error mean (for n=1 experiment, SEM is from 6-12 absorbance values for a given treatment group).

3.3 - Discussion and Conclusions

The results presented in this chapter demonstrate that UV irradiation of coumarinyl-caged ceramides in HeLa cells causes morphological changes, as well as decreases in viability which can be detected after 24 hours of treatment. In obtaining these results, different experiments, which included treatments with

exogenous short- and long-chain ceramides as controls, were performed. The morphological assessment of cells incubated with exogenous C2 Cer for 24 hours, which showed cell shrinkage and cell detachment from the surface of the culture plate (see Figure 3-1 (B), section 3.2.1), is consistent with literature reports of apoptotic cell death with ceramide.[1,2] The lack of morphological changes with long-chain C16 Cer (see Figure 3-1 (C), section 3.2.1) can be explained by its poor solubility in aqueous solution and its low membrane permeability. As per Small's classification of lipids, long-chain ceramides are considered "insoluble non-swelling amphiphiles", which means that these molecules are unable to give rise to hydrated aggregates in aqueous suspensions. Due to these properties, it is almost impossible for them to cross the cell membrane.[27,28] Given the hydrophobicity of their long N-acyl chains, long-chain ceramides accumulate at the cell surface when they are administered exogenously and are therefore not delivered into the cytosol.[29-31] Short-chain ceramides, such as C2 Cer, are more amphiphilic in nature, which allows them to reach the cytosol as well as other subcellular compartments where they can exert different biological effects. The findings from studies that are performed using exogenous short-chain ceramides must, however, be interpreted carefully since these analogues of natural ceramides may localize in a non-physiological manner within cellular compartments.[28]

As demonstrated in this work, coumarinyl-caged ceramides can be used to investigate the biological activity of ceramide in cells. A key result was that no distinct changes in cell morphology resulted from the exposure to UV irradiation alone, under the conditions used for uncaging the Bhc-caged C16 Cer (**9b**) (see

Figure 3-2 (A,E), section 3.2.1). This suggests that the dose of UV irradiation to which the cells are exposed for the uncaging of ceramide is not damaging. When the cells were incubated with the caged ceramide **9b** and UV-irradiated in order to generate C16 Cer, there were no visible signs of apoptotic morphology. However, some additional particulate matter was present among the cells (see Figure 3-2 (D), section 3.2.1), which could be indicative of necrosis. During necrotic cell death, rupture of the plasma membrane and spilling of the cell's contents into the extracellular environment are often observed.[14,32] However, in order to gain further insight into the cell death pathway that is involved with the UV-irradiated caged ceramide **9b**, additional bioassays were required and the results from those experiments will be presented in the next chapter.

When the MTT assay was used to quantitatively assess the effects of different ceramide treatments on the viability of HeLa cells, it proved to be an inappropriate method to be used in our system. In several preliminary MTT assays with exogenous ceramides, long-chain C16 Cer appeared to cause a significant decrease in the viability of the cells with 24 hours of incubation (see Figure 3-3, section 3.2.2), which was inconsistent with other reports from the literature.[2] The fact that MTT is reported to be reduced non-specifically by numerous intracellular agents may explain why this assay was found to be an unsuitable method for measuring cell viability in the context of our study, as well as in other studies.[19,33,34]

The WST-1 assay, which has been used previously to measure the viability of cells treated with ceramides[2], was determined to be a suitable method for quantitatively assessing the viability of HeLa cells subjected to ceramide treatments.

The results from preliminary assays revealed that cells treated with exogenous C2 Cer exhibit a large decrease in viability, whereas those treated with exogenous C16 Cer are not significantly affected (see Figure 3-4, section 3.2.2). The differential responses generated by the short- and long-chain ceramides can be explained by the relative aqueous solubility and membrane permeability of these lipids.

Dose-response studies were performed to determine the effective concentration of the different ceramide-related compounds that were under investigation (see Figure 3-5, section 3.3.2). The results can be used to compare the different compounds in terms of their biological activity (potency and efficacy). Due to differences in aqueous solubility and membrane permeability, which were discussed above, it was reasonable to observe that the EC_{50} of short-chain C2 Cer in HeLa cells (11.3 µM) was significantly lower than that of long-chain C16 Cer (71.7 µM). Moreover, although the extent of the response with C2 Cer is known to depend on cell type and cell density[11], the effective concentration that was determined in our system is reasonable. Reports from other studies indicate that roughly a 50% decrease in viability is seen with a C2 Cer concentration of 50 µM in HCT116 cells[2], 45 µM in LNCaP cells[6] and 10 µM in A172 cells[5]. When dodecane was added to the solvent as a vehicle for the delivery of long-chain C16 Cer to the cells, a large decrease in the EC_{50} (48.1 µM) was seen. This result is reasonable and suggests that the solvent mixture of ethanol and dodecane (98:2) facilitates cellular uptake of the lipid, increasing its cytotoxicity. In fact, this technique has been used in previous studies that were conducted in U937 cells and in HL-60 cells and was shown to be effective in these systems.[26,35]

When the Bhc-caged C16 Cer (**9b**) was tested, in the absence of UV irradiation, it exhibited an EC_{50} of 21.2 µM. However, **9b** did not exhibit the steep slope in the dose-response curve that was observed with the exogenous ceramides. This suggests that caging produces qualitative differences in the pharmacological properties of this compound. Furthermore, uncaging is expected to restore the natural toxicity profile of C16 Cer. These results suggest that the ceramide photocage has the potential to offer a certain level of spatial and temporal control, which is a desirable characteristic for a caged compound. Hereafter, the concentration of each of the compounds under investigation was matched to 20 µM.

A direct comparison of the effects observed with the UV-irradiated (6 min) Bhc-caged C16 Cer (**9b**) and those exerted by exogenous ceramides revealed that the decrease in cell viability caused by the caged ceramide, although significant, was less than that caused by C2 Cer (see Figure 3-7, section 3.2.2). The fact that a larger response was observed with C2 Cer than with the caged ceramide **9b** could be due to differences in solubility, membrane permeability and intracellular localization of the compounds. Although the presence of the coumarin cage in **9b** is thought to increase the aqueous solubility and membrane permeability of the lipid, short- and long-chain ceramides are known to have different physico-chemical properties, as mentioned earlier in this chapter. As for the intracellular localization of these lipids, it has been reported in the literature that exogenous long-chain C16 Cer can be recovered in lysosomes and in mitochondria, whereas C2 Cer is mainly recovered in microsomes.[35] The intracellular localization of the caged ceramide **9b**, which contains a coumarinyl moiety, remains to be investigated further (see Figure

2-7, section 2.2.5, chapter 2). Perhaps the most significant finding from these experiments was that the caged ceramide **9b** causes a decrease in cell viability only in the presence of UV irradiation. This indicates that the compound allows for achieving spatially and temporally controlled biological effects in cells, which is a key attribute of all photocages and represents an advantage to using coumarinyl-caged ceramides over short-chain ceramides in these types of studies.[36]

The N-acyl chain length dependence of the biological effects of ceramide was investigated using a series of Btcmoc-caged long- and very long-chain ceramides. With each of the Btcmoc-caged compounds (**21**-**24**), there was little or no effect of the photochemically generated ceramide on the viability of HeLa cells when the samples were subjected to 6 minutes of UV irradiation (see Figure 3-9, section 3.2.3). However, when a longer UV exposure time of 9 minutes was used, a decrease in viability was observed with each of the Btcmoc-caged ceramides that was tested under these conditions (Note: caged ceramide **23** was not included), but no significant differences between the various treatment groups were detected. The requirement for longer UV irradiation times with the Btcmoc-caged ceramides is consistent with the results from the preparatory photolysis experiments, which showed, qualitatively, that these caged ceramides require about double the amount of UV exposure time as the Bhc-caged C16 Cer (**9b**) (see Figure 2-6, section 2.2.4, chapter 2). Since a similar decrease in viability was caused by the free Btcmoc-coumarin (**18**), which may be due to ROS generation in the cells, it is not possible to determine whether the decreased viability observed upon UV irradiation of the

Btcmoc-caged ceramides in the cells is due to ceramide generation or due to the coumarin cage.

The viability assay results obtained for the two different caged C16 ceramides, Btcmoc-caged C16 Cer (**21**) and Bhc-caged C16 Cer (**9b**) can be used to assess whether the pegylated caging moiety, Btcmoc-coumarin (**18**), offers any advantages over the Bhc-coumarin (**4**) caging moiety. Based on these results (see Figures 3-7 and 3-9, sections 3.2.2 and 3.2.3), there is no evidence that the pegylated cage is an improvement. In designing the pegylated caged ceramides, it was hypothesized, based on previous reports from the literature, that the presence of a short methoxytriethylene glycol (mTEG) moiety on the coumarin caging group would allow for enhanced solubility, membrane permeability and biocompatibility of the compounds.[37] Such differences inferred by the caging moiety could increase the biological activity of the compound. The results obtained here, however, suggest that including the mTEG moiety on the coumarin does not offer the advantages that were anticipated. The pegylation could be allowing for increased solubility and membrane permeability, but also altering the intracellular localization of the compounds. If the Btcmoc caging moiety is preventing the caged ceramides from reaching a specific target site within the cell, their biological activity could be significantly reduced.

In summary, the Bhc-caged C16 Cer (**9b**) can be used to generate long-chain C16 Cer in HeLa cells, which causes a significant decrease in viability. Furthermore, this approach allows for C16 Cer to be delivered to the cells without using an additive (i.e. dodecane), by dissolving the caged ceramide in aqueous

medium. Based on the lack of activity of the compound in the absence of UV irradiation, these biological effects can be achieved with a certain level of spatial and temporal control. With longer UV irradiation times, the pegylated Btcmoc-caged ceramides (**21**-**24**) cause decreases in cell viability that are not more significant than the effects exerted by the free Btcmoc-coumarin (**18**) alone, which suggests that the pegylated photocages do not offer any advantages over the Bhc photocages .

3.4 - References

(1) Hartfield, P. J.; Mayne, G. C.; Murray, A. W. *FEBS Letters* **1997**, *401*, 148.

(2) Fillet, M.; Bentires-Alj, M.; Deregowski, V.; Greimers, R.; Gielen, J.; Piette, J.; Bours, V.; Merville, M.-P. *Biochemical Pharmacology* **2003**, *65*, 1633.

(3) Beckham, T. H.; Lu, P.; Jones, E. E.; Marrison, T.; Lewis, C. S.; Cheng, J. C.; Ramshesh, V. K.; Beeson, G.; Beeson, C. C.; Drake, R. R.; Bielawska, A.; Bielawski, J.; Szulc, Z. M.; Ogretmen, B.; Norris, J. S.; Liu, X. *Journal of Pharmacology and Experimental Therapeutics* **2013**, *344*, 167.

(4) López-Marure, R.; Gutiérrez, G.; Mendoza, C.; Ventura, J. L.; Sánchez, L.; Reyes Maldonado, E.; Zentella, A.; Montaño, L. F. *Biochemical and Biophysical Research Communications* **2002**, *293*, 1028.

(5) Kim, W.; Choi, C.; Kang, S.; Kwon, C.; Kim, Y. *Neurochem Res* **2005**, *30*, 969.

(6) Engedal, N.; Saatcioglu, F. *The Prostate* **2001**, *46*, 289.

(7) Hannun, Y. A.; Obeid, L. M. *Journal of Biological Chemistry* **2011**, *286*, 27855.

(8) Osawa, Y.; Uchinami, H.; Bielawski, J.; Schwabe, R. F.; Hannun, Y. A.; Brenner, D. A. *Journal of Biological Chemistry* **2005**, *280*, 27879.

(9) Seumois, G.; Fillet, M.; Gillet, L.; Faccinetto, C.; Desmet, C.; François, C.; Dewals, B.; Oury, C.; Vanderplasschen, A.; Lekeux, P.; Bureau, F. *Journal of Leukocyte Biology* **2007**, *81*, 1477.

(10) van Blitterswijk, W. J.; van der Luit, A. H.; Veldman, R. J.; Verheij, M.; Borst, J. *Biochemical Journal* **2003**, *369*, 199.

(11) Hannun, Y. A.; Luberto, C. *Trends in Cell Biology* **2000**, *10*, 73.

(12) Venkataraman, K.; Futerman, A. H. *Trends in Cell Biology* **2000**, *10*, 408.

(13) Vaux, D. L.; Strasser, A. *Proceedings of the National Academy of Sciences* **1996**, *93*, 2239.

(14) Berghe, T. V.; Vanlangenakker, N.; Parthoens, E.; Deckers, W.; Devos, M.; Festjens, N.; Guerin, C. J.; Brunk, U. T.; Declercq, W.; Vandenabeele, P. *Cell Death Differ* **2010**, *17*, 922.

(15) Lamkanfi, M.; Dixit, V. M. *Cell Host & Microbe* **2010**, *8*, 44.

(16) Hu, W.; Xu, R.; Zhang, G.; Jin, J.; Szulc, Z. M.; Bielawski, J.; Hannun, Y. A.; Obeid, L. M.; Mao, C. *Molecular Biology of the Cell* **2005**, *16*, 1555.

(17) Yoshimura, S.-i.; Banno, Y.; Nakashima, S.; Takenaka, K.; Sakai, H.; Nishimura, Y.; Sakai, N.; Shimizu, S.; Eguchi, Y.; Tsujimoto, Y.; Nozawa, Y. *Journal of Biological Chemistry* **1998**, *273*, 6921.
(18) Mosmann, T. *Journal of Immunological Methods* **1983**, *65*, 55.
(19) Stockert, J. C.; Blázquez-Castro, A.; Cañete, M.; Horobin, R. W.; Villanueva, Á. *Acta Histochemica* **2012**, *114*, 785.
(20) Yamaue, H.; Tanimura, H.; Tsunoda, T.; Tani, M.; Iwahashi, M.; Noguchi, K.; Tamai, M.; Hotta, T.; Arii, K. *European Journal of Cancer and Clinical Oncology* **1991**, *27*, 1258.
(21) Berridge, M. V.; Tan, A. S. *Archives of Biochemistry and Biophysics* **1993**, *303*, 474.
(22) Ngamwongsatit, P.; Banada, P. P.; Panbangred, W.; Bhunia, A. K. *Journal of Microbiological Methods* **2008**, *73*, 211.
(23) Ishiyama, M.; Sasamoto, K.; Shiga, M.; Ohkura, Y.; Ueno, K.; Nishiyama, K.; Taniguchi, I. *Analyst* **1995**, *120*, 113.
(24) O'Brien, J.; Wilson, I.; Orton, T.; Pognan, F. *European Journal of Biochemistry* **2000**, *267*, 5421.
(25) Dai, Q.; Liu, J.; Chen, J.; Durrant, D.; McIntyre, T. M.; Lee, R. M. *Oncogene* **2004**, *23*, 3650.
(26) Ji, L.; Zhang, G.; Uematsu, S.; Akahori, Y.; Hirabayashi, Y. *FEBS Letters* **1995**, *358*, 211.
(27) Small, D. *J Am Oil Chem Soc* **1968**, *45*, 108.
(28) Sot, J.; Goñi, F. M.; Alonso, A. *Biochimica et Biophysica Acta (BBA) - Biomembranes* **2005**, *1711*, 12.
(29) Birbes, H.; El Bawab, S.; Hannun, Y. A.; Obeid, L. M. *The FASEB Journal* **2001**, *15*, 2669.
(30) Grassmé, H.; Jekle, A.; Riehle, A.; Schwarz, H.; Berger, J.; Sandhoff, K.; Kolesnick, R.; Gulbins, E. *Journal of Biological Chemistry* **2001**, *276*, 20589.
(31) Mimeault, M. *FEBS Letters* **2002**, *530*, 9.
(32) Festjens, N.; Vanden Berghe, T.; Vandenabeele, P. *Biochimica et Biophysica Acta (BBA) - Bioenergetics* **2006**, *1757*, 1371.
(33) Ahmad, S.; Ahmad, A.; Schneider, B. K.; White, C. W. *International Journal of Toxicology* **2006**, *25*, 17.
(34) Niu, Q.-x.; Zhao, C.-y.; Jing, Z.-a. *Journal of Immunological Methods* **2001**, *251*, 11.
(35) Ardail, D.; Popa, I.; Bodennec, J.; Famy, C.; Louisot, P.; Portoukalian, J. *Biochimica et Biophysica Acta (BBA) - Molecular and Cell Biology of Lipids* **2002**, *1583*, 305.
(36) Ellis-Davies, G. C. R. *Nat Meth* **2007**, *4*, 619.
(37) Pandey, M. K.; Kumar, S.; Thimmulappa, R. K.; Parmar, V. S.; Biswal, S.; Watterson, A. C. *European Journal of Pharmaceutical Sciences* **2011**, *43*, 16.

Chapter 4: Investigation of the Mechanism of Cell Death Involved with the Photochemical Generation of Ceramide *in Vitro*

4.1 - Introduction: The Role of Ceramide in Cell Death

Ceramide is a lipid second messenger that plays a key part in cell death. In response to elevations in ceramide concentrations, cell death frequently occurs through an apoptotic pathway. However, in some cases, ceramide has been shown to cause cell death through necrosis. Each of these cell death pathways is regulated by distinct cellular events, some of which are not fully understood. Elucidating the molecular mechanisms that are implicated during cell death with ceramide is important in understanding the pathogenesis of different diseases, such as cancer and Alzheimer's disease.[1,2] Apoptosis, which is a type of programmed cell death, allows for the elimination of unwanted cells from a biological system for the purpose of development, homeostasis, defence or aging.[3] Necrosis is an alternate form of cell death, which often results from exposure to conditions of intense physico-chemical stress.[4] Necrotic cell death was long viewed as a mode of cell death that took place in an uncontrolled manner. However, it has been recognized more recently as a type of programmed cell death implicating specific molecular targets.[5] The different signal transduction pathways that are involved in apoptosis and necrosis with ceramide have been the subject of many studies. Although these studies have provided insight into the underlying mechanisms, several aspects still require further investigation.

The intrinsic pathway of apoptosis, which can be initiated by ceramide, involves specific cell signalling events at the level of the mitochondria.[6] A key event in this pathway is "mitochondrial outer membrane permeabilization" (MOMP). MOMP promotes the release of critical proteins, such as cytochrome *c*, into the cytosol. In addition, a decrease in the mitochondrial membrane potential ($\Delta\psi_m$) can be detected. The formation of pores in the mitochondrial outer membrane is thought to be regulated by the Bcl-2 family of proteins, which partition in mitochondrial ceramide-rich macrodomains. More specifically, the pro-apoptotic protein Bax inserts itself, oligomerizes and functionalizes as a pore in the membrane (see Scheme 1-7, section 1.3, chapter 1).[7] It has also been suggested that the permeabilization of the mitochondrial outer membrane occurs through the formation of ceramide channels.[8]

Alterations in mitochondrial function can be probed in cells through the use of cationic dyes that accumulate in the mitochondria in a manner that is proportional to the $\Delta\psi_m$. An example of one of these dyes is tetramethylrhodamine methyl ester (TMRM), which exhibits strong fluorescence emission near 560 nm when concentrated in the mitochondria and otherwise very diffuse fluorescence emission at this wavelength.[9] Upon mitochondrial membrane depolarization, dye leakage from the mitochondria causes a decrease in the fluorescence emission. Despite the widespread use of single-wavelength fluorescence techniques for detecting changes in $\Delta\psi_m$, one drawback of using these techniques is that the measurements are dependent on certain other factors, such as mitochondrial size, shape, and density.[10]

As an alternative to using TMRM for measuring changes in mitochondrial function in response to ceramide treatment, the dye 5,5',6,6'-tetrachloro-1,1',3,3'-tetraethylbenzimidazolylcarbocyanine iodide (JC-1) can be utilized. In fact, JC-1, for which the structure is shown in Scheme 4-1 (A), has been used previously to measure mitochondrial depolarization in cells treated with the cationic ceramide analogue LCL-124.[11] JC-1 exhibits concentration-dependent formation of red fluorescent J-aggregates in healthy mitochondria. Since different absorption maxima are observed for the monomeric (~529 nm) and aggregated (~590 nm) forms of the dye, ratiometric measurements of fluorescence can be performed.[12] Mitochondrial depolarization can be detected as a decrease in the red to green fluorescence intensity ratio, which is due to a decrease in the amount of red fluorescent J-aggregates and an increase in the amount of green fluorescent monomers upon leakage of the dye from the mitochondria. When using JC-1, carbonyl cyanide-4-(trifluoromethoxy)phenylhydrazone (FCCP) can be utilized as a control compound for inducing mitochondrial depolarization. FCCP, for which the structure is shown in Scheme 4-1 (B), is an uncoupler of oxidative phosphorylation. When administered to cells, it causes dissipation of the $\Delta\psi_m$ and a decrease in the red to green JC-1 fluorescence ratio is observed.[13]

A **B**

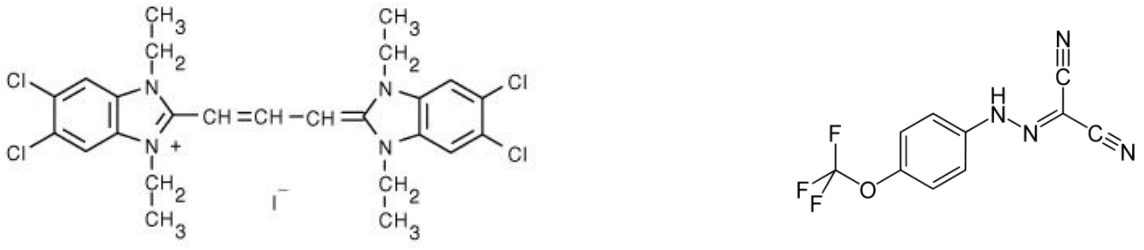

Scheme 4-1. Structure of the mitochondrial membrane potential probe JC-1 (A) and of the uncoupling agent FCCP (B).

Downstream of the mitochondrial effects, another critical signalling event that takes place during apoptotic cell death with ceramide is the activation of a series of cysteine protease enzymes called "caspases".[14-16] Caspases are proteolytic enzymes which are known to cleave a wide variety of substrates. They are, therefore, largely responsible for many of the morphological changes that are observed during apoptosis.[17] Different members of the caspase family play different roles during apoptosis. For example, initiator caspases, such as caspase 8, are responsible for cleaving pro-caspases 3 and 7, in order to yield the active form of the executioner (i.e. 3 and 7) caspases. Once proteolytically activated, caspases 3 and 7 are responsible for cleaving different components in the cell.[18] In the intrinsic pathway of apoptosis, the release of cytochrome *c* activates initiator caspases (e.g. 8) in order to start the caspase signalling cascade. In the extrinsic pathway of apoptosis, the signalling cascade is triggered by the binding of extracellular death receptor ligands to transmembrane receptors causing receptor aggregation. This promotes the formation of a "death-inducing signalling complex" (DISC), which serves as a platform for the recruitment and activation of initiator caspases, such as caspase 8 (see Scheme 1-7, section 1.3, chapter 1).

When investigating caspase activation in cells, synthetic caspase inhibitors are routinely employed as probes for these enzymes.[19] Prior to being treated with different compounds of interest, the cells can be pre-incubated with caspase inhibitors, in order to determine whether blocking the caspase signalling cascade has an effect on the extent of the biological effects that are observed. The caspase inhibitor z-VAD-fmk (carbobenzoxy-valyl-alanyl-aspartyl-[O-methyl]-

fluoromethylketone) is commonly used in these types of studies. This inhibitor is considered a “pan-caspase inhibitor” since it is not specific for any particular member of the caspase family. The caspase inhibitor Z-DEVD-fmk is a caspase 3/7-specific inhibitor, given that the tetrapeptide sequence DEVD is recognized by these particular caspases.[20]

Different methods have been established for probing caspase activity during cell death. For example, one study showed that an immunochemical assay can be used to measure caspase activation in response to treatment with a cationic ceramide analogue.[21] Another study indicated that caspase activation can be detected by a spectrophotometric assay, where a caspase substrate labelled with *p*-nitroanilide is used and the absorbance at 405 nm is measured.[22] Furthermore, many studies have demonstrated that fluorescently-tagged caspase substrates can be used to probe caspase activity in cells treated with ceramides and ceramide analogues.[11,14,23,24] However, the major drawback of these commonly used techniques is the requirement for several experimental steps, such as washing and removing the medium, in order to achieve a measurable result. A luminescence-based assay for caspase 3/7 activity was developed as an alternative method. A schematic representation of the biochemical reactions that occur during the caspase 3/7 luminescence assay is shown in Scheme 4-2.[25] This assay, which is based on the cleavage of a luciferase-conjugated caspase substrate by active caspases, involves no additional experimental steps at the end of the treatment period. The specificity of this assay for detecting caspases 3 and 7 arises from the nature of the

caspase substrate in the reagent, which consists of the tetrapeptide sequence DEVD.

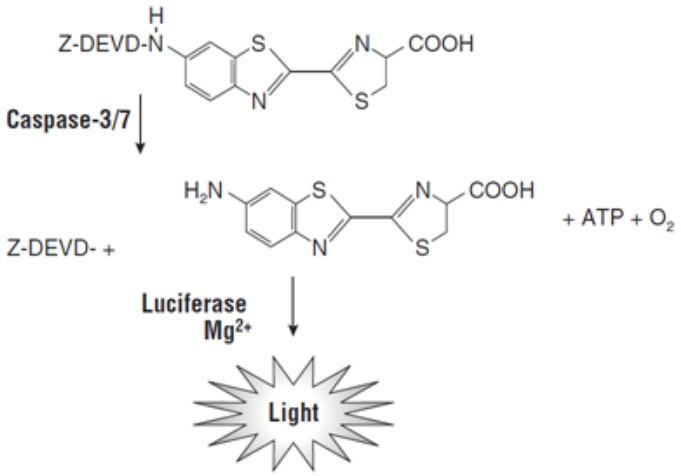

Scheme 4-2. Biochemical reactivity of the probe used for the caspase 3/7 luminescence assay. From reference 25.

Although ceramide is known to play a role in apoptosis, this bioactive lipid can also induce non-apoptotic cell death, depending on the cellular context. Ceramide has been shown, in some cases, to induce cell death in a manner that resembles necrosis, rather than apoptosis. Particularly, when B-CLL cells were treated with C2 ceramide, the addition of the caspase inhibitor z-VAD-fmk did not decrease the amount of ceramide-mediated cell death, which suggested that a caspase-independent mechanism was involved.[26] In addition, a switch from apoptosis to necrosis has been shown to occur in some cell types, under certain conditions. For example, this phenomenon has been observed in the presence of the caspase inhibitor Z-VAD-fmk or in the case of ATP depletion in the cells.[27,28]

Necrotic cell death is thought to involve the tumour necrosis factor (TNF) receptor-1 and to occur in a receptor-interacting protein (RIP)1- and/or RIP3-dependent manner (see Scheme 1-8, section 1.3, chapter 1).[5,29] The occurrence of

necrosis can be probed in cells through the use of a class of specific RIP1 kinase inhibitors called necrostatins. Particularly, the small molecule inhibitor Necrostatin-1 (Nec-1) is a selective allosteric inhibitor of RIP1.[30] Recently, the specificity of Nec-1 was questioned when it was shown to inhibit not only RIP1, but also the immunomodulatory enzyme indoleamine 2,3-dioxygenase (IDO).[31] In light of this, Nec-1s, a more specific analogue, for which the structure is shown in Scheme 4-3, was developed.

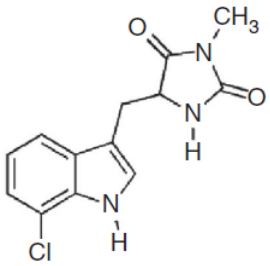

Scheme 4-3. Structure of the RIP1 inhibitor Nec-1s. From reference 31.

Another phenomenon that has been shown to occur in the cell during necrotic cell death with ceramide is reactive oxygen species (ROS) generation.[4,32] Different methods can be used to probe ROS generation in cells. Namely, the fluorescent dye 5-(and-6)-carboxy-2',7'-dichlorodihydro-fluorescein diacetate (carboxy-H_2DCFDA) is commonly used for detecting ROS in cells.[33] Scheme 4-4 depicts the cellular conversion of this probe to the fluorescent end product, in the presence of ROS.[34] In this assay, the non-fluorescent, cell permeable substrate is initially cleaved by cellular esterases to the carboxylate anion and then converted to a highly fluorescent product, dichlorofluorescein (DCF) through a two-electron oxidation process.[35] The fluorescence signal, which is measured at 529 nm with 495 nm excitation, is considered to be proportional to the amount of ROS in the system.

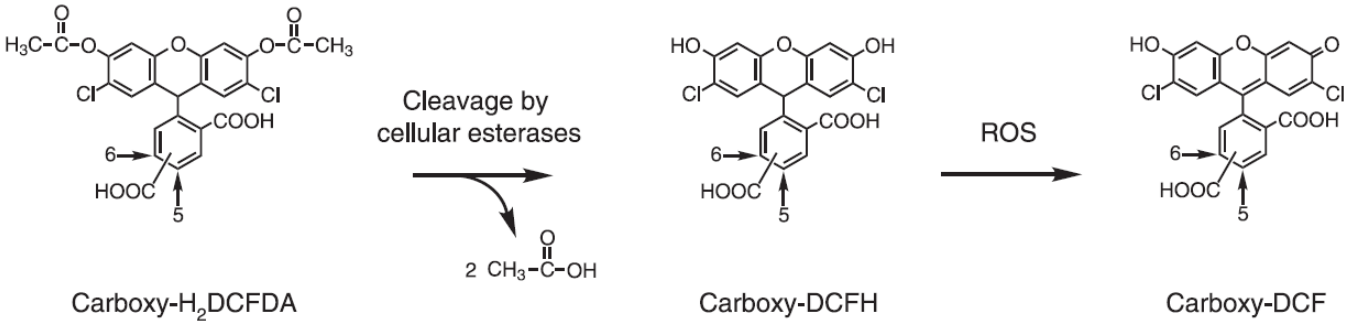

Scheme 4-4. Intracellular conversion of carboxy-H_2DCFDA to the fluorescent product. From reference 34.

With the results presented in the previous chapter, we have shown that cell death occurs in response to generating ceramide photochemically in HeLa cells. The work that is presented in the pages that follow was performed with the goal of determining the molecular mechanisms that are involved during cell death induced by coumarinyl-caged ceramides. This chapter includes the presentation and discussion of results that were acquired using some of the assays described above. We first investigated the occurrence of the intrinsic pathway of apoptosis, by performing mitochondrial staining experiments with the dyes JC-1 and TMRM. Caspase 3/7 activation, which is typical of apoptotic cell death, was then probed in the cells, by the means of a luminescence-based assay. Since the results from the caspase assay revealed that cell death with coumarinyl-caged ceramides takes place in a caspase-independent manner, the occurrence of necrosis was then investigated by probing RIP1 activity and by measuring ROS generation in the cells. Overall, the results from each of these assays provided insight into the cell death pathway that takes place when ceramide is generated photochemically in HeLa cells.

4.2 - Results

4.2.1 - Probes for Assessing Mitochondrial Membrane Potential

In order to probe the biological effects of ceramide at the level of the mitochondria, the cationic fluorophore JC-1 was selected and used to measure changes in mitochondrial membrane potential ($\Delta\psi_m$) in HeLa cells treated with different ceramides. In a preliminary experiment, the effects of an uncoupler of oxidative phosphorylation, FCCP, were assessed in cells stained with JC-1 (5 µg/mL). In the context of our study, FCCP was used as a positive control for mitochondrial depolarization. Upon treatment with the uncoupler, we observed, qualitatively, a large decrease in the red fluorescence (mitochondrial aggregates) accompanied by a large increase in the green fluorescence (cytosolic monomers) of the JC-1 dye within the cells, as shown in Figure 4-1. This was indicative of mitochondrial depolarization in response to treatment with FCCP. It is also noteworthy that the red aggregates within the mitochondria exhibited a punctate pattern of fluorescence, whereas the green monomers showed a very diffuse pattern of fluorescence. When the effects of FCCP were quantified by extracting fluorescence intensity values from individual cells in the images, a 5-fold decrease in the red/green fluorescence ratio was observed. The JC-1 fluorescence ratio that was calculated for the cells treated with FCCP was 0.44 ± 0.03 (10 min after treatment), which is very low in comparison to the value of 2.4 ± 0.4 that was obtained for the untreated control cells (before FCCP addition). The results from this experiment effectively demonstrated that JC-1 fluorescence can be used to detect changes in $\Delta\psi_m$ in HeLa cells, under these conditions.

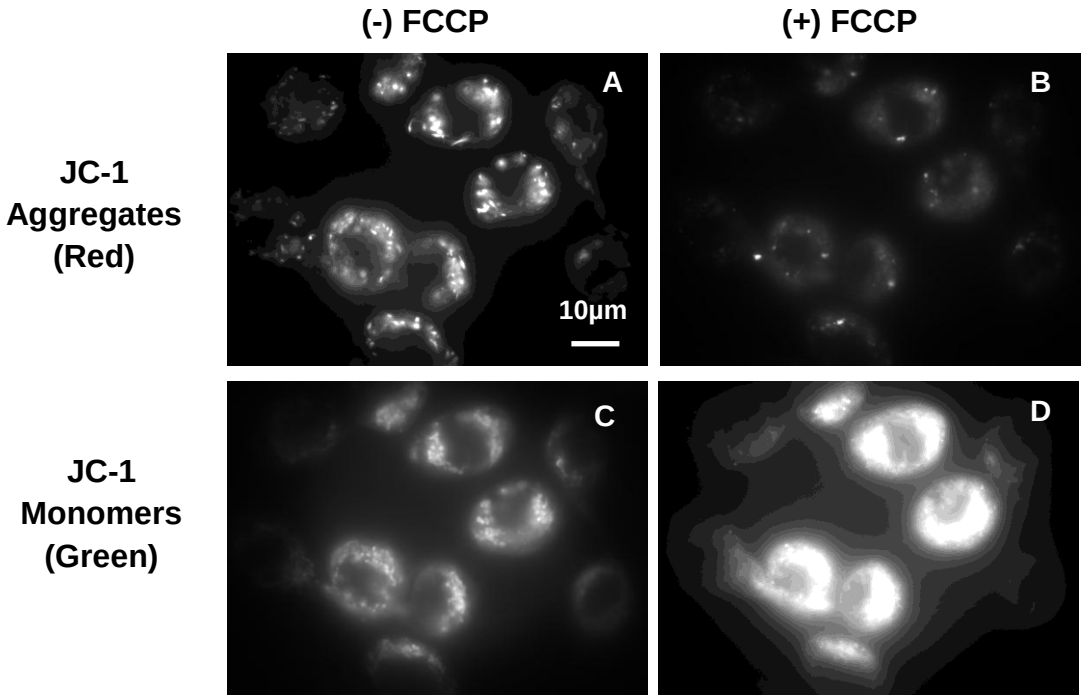

Figure 4-1. Treatment of HeLa cells with FCCP causes a decrease in the red to green JC-1 fluorescence ratio. Fluorescence images of HeLa cells stained with JC-1 (5 µg/mL) in serum-free medium, before (A,C) and after (B,D) treatment with FCCP (7 µM) on the microscope stage. Samples were washed (after staining) before imaging in PBS buffer (1X). Fluorescence images were acquired using a 100X oil immersion objective in the red channel (100 ms exposure) and in the green channel (200 ms exposure) and are scaled appropriately (red: 100-2500 counts; green: 100-1200 counts). Quantification of red and green fluorescence intensity, as well as of the red/green ratio, was performed within individual cells. Fluorescence intensity was quantified as the blank-corrected mean intensity.

Once the appropriate staining conditions were established, JC-1 could be used to detect changes in $\Delta\psi_m$ upon generating ceramide photochemically in HeLa cells. The cells were incubated in the presence of the Bhc-caged C16 Cer (**9b**) for 4 hours in the dark before being stained with JC-1 (5 µg/mL). In order to release ceramide photochemically in the cells, UV irradiation was performed on the microscope by illuminating a small area of the sample for 30 seconds, using the appropriate filter set. Fluorescence images were acquired in the red and green channels and two-color composite images are shown in Figure 4-2. Prior to UV

irradiation, both the control and treated cells demonstrated a punctuate pattern of red fluorescence, which was indicating accumulation of the dye inside healthy mitochondria, accompanied by diffuse green fluorescence (Figure 4-2 (A,E)). Immediately after UV exposure, red fluorescent J-aggregates were still present in both the control cells and the caged ceramide-treated cells, but some changes were observed over time. Qualitatively, we saw a decrease in the amount and intensity of the red fluorescent aggregates, over time, in the cells treated with the UV-irradiated caged ceramide **9b**, whereas the red aggregates remained present in the untreated control cells. These effects could be detected as early as 10 minutes post-irradiation and were more significant at 20 minutes post-irradiation (see Figure 4-2 (E,F)). These results suggest that mitochondrial depolarization occurs in HeLa cells in response to the photorelease of C16 Cer from the caged ceramide **9b**. It is, however, noteworthy that the fluorescence intensity in both channels was significantly reduced after UV irradiation (note adjustment of image display range). This decrease in fluorescence intensity indicated that photobleaching of JC-1 occurs with exposure to UV irradiation and needs to be considered when conducting these experiments.

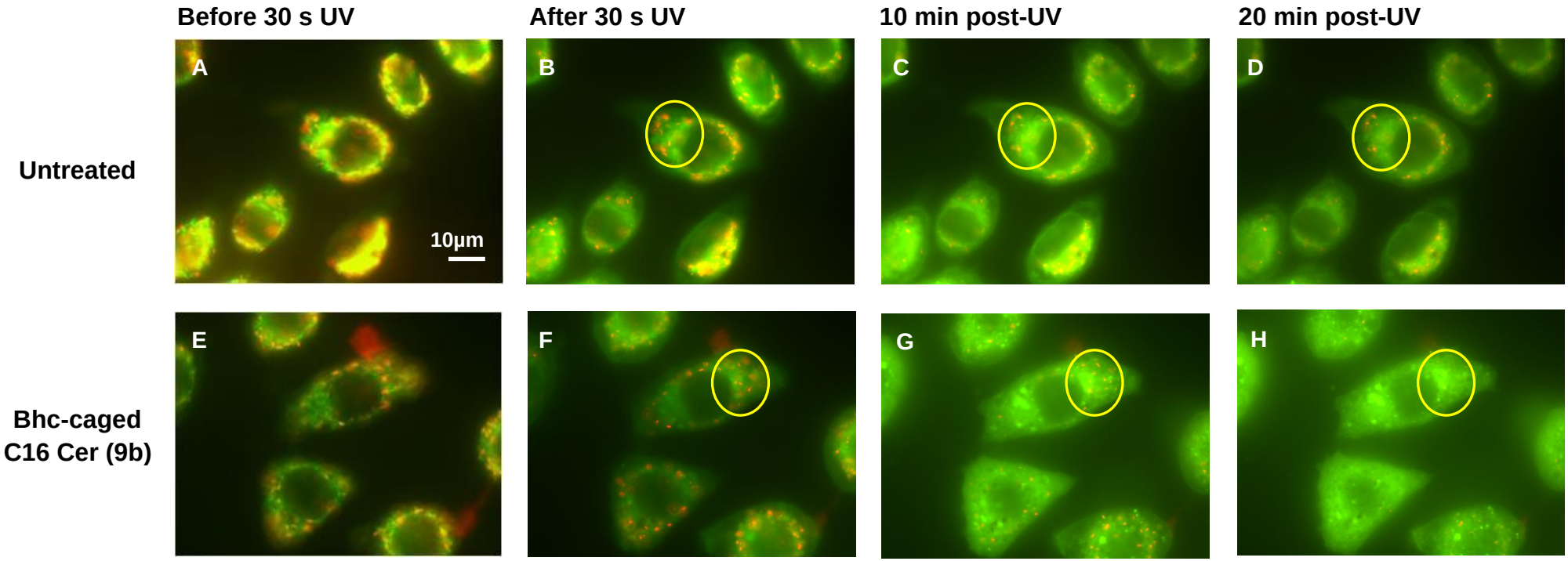

Figure 4-2. The Bhc-caged C16 Cer (**9b**) causes a decrease in the mitochondrial membrane potential, as assessed using JC-1 staining. Two-colour (red/green) composite fluorescence images of HeLa cells incubated with (E-H) and without (A-D) **9b** in serum-free medium (20 µM) for 4 hours in the dark and then stained with JC-1 (5 µg/mL). Samples were washed and imaging was done in PBS buffer (1X). UV irradiation was performed on the microscope with an appropriate filter. Images were acquired in the red and green channels using a 100X oil immersion objective. The images have been scaled with matched display ranges (Untreated – red: 100-2400 counts, green: 100-2800 counts; **9b** – red: 100-900 counts, green: 100-800 counts). Note: display range for "Before UV" images was adjusted due to photobleaching (for both samples - red: 100-3600 counts, green: 100-1400 counts).

In order to examine the reasons for the decrease in fluorescence intensity after UV irradiation, additional control experiments were required. The effects of UV exposure alone on the fluorescence of JC-1 in HeLa cells were examined. Untreated cells were subjected to 30 seconds of UV irradiation on the microscope and fluorescence images were acquired in the red and green channels. As shown in Figure 4-3 (A), a large decrease in JC-1 fluorescence intensity was observed after UV irradiation, which occurred in both the red and green channels. This result demonstrates that UV exposure causes a significant amount of photobleaching of the dye.

The decrease in the fluorescence intensity of JC-1 was also quantified as a function of UV exposure. The fluorescence intensity was measured in individual cells, in a series of images (100 ms exposure) that were acquired sequentially with increasing UV exposure. As a control, an unirradiated area from the same sample was also imaged for the same time points. The fluorescence intensity measured for each time point was compared to the initial fluorescence intensity. This experiment was repeated for both the red and green channels (different areas within the same sample). The results, which are displayed in Figure 4-3 (B), showed that the fluorescence intensity exhibited by the JC-1 aggregates (red channel) decreased by roughly 60% with 30 seconds of UV exposure. Based on this result, it appears that the significant amount of photobleaching that occurs with UV exposure is problematic when trying to measure decreases in fluorescence intensity (of the JC-1 aggregates) as an indication of mitochondrial membrane depolarization. Although

photobleaching of the dye occurs with visible light (e.g. lamp excitation light), it is not as significant as with UV light.

Some photobleaching of the JC-1 monomers (green channel) was also observed, but it occurred with a different pattern compared to that observed for the aggregates (red channel). As displayed in Figure 4-3 (B), UV exposure resulted in a decrease in intensity (photobleaching) for the green monomer fluorescence, followed by an increase and subsequent decrease in intensity. The increase in intensity in the green fluorescence with UV irradiation may indicate dissociation of the JC-1 aggregates, forming JC-1 monomers, which are subsequently photobleached. The combination of rapid UV-induced photobleaching and possible equilibration of monomers and aggregates means that it is not straightforward to obtain quantitative red/green ratios as a measure of mitochondrial depolarization. Thus, UV-induced photobleaching appears to be producing an artefact in JC-1 fluorescence that is unlikely to be related to mitochondrial function as similar control experiments (i.e. WST-1 assay measuring mitochondrial succinate dehydrogenase activity; see Figure 3-7) did not show UV-induced effects at the level of the mitochondria.

In an attempt to overcome these issues, another mitochondrial dye, TMRM, was tested in HeLa cells exposed to UV irradiation. However, similarly to JC-1, TMRM is significantly photobleached upon UV irradiation, where roughly a 20% decrease in fluorescence intensity can be seen with 30 seconds of UV exposure (data not shown). In light of this, no further experiments were performed using TMRM.

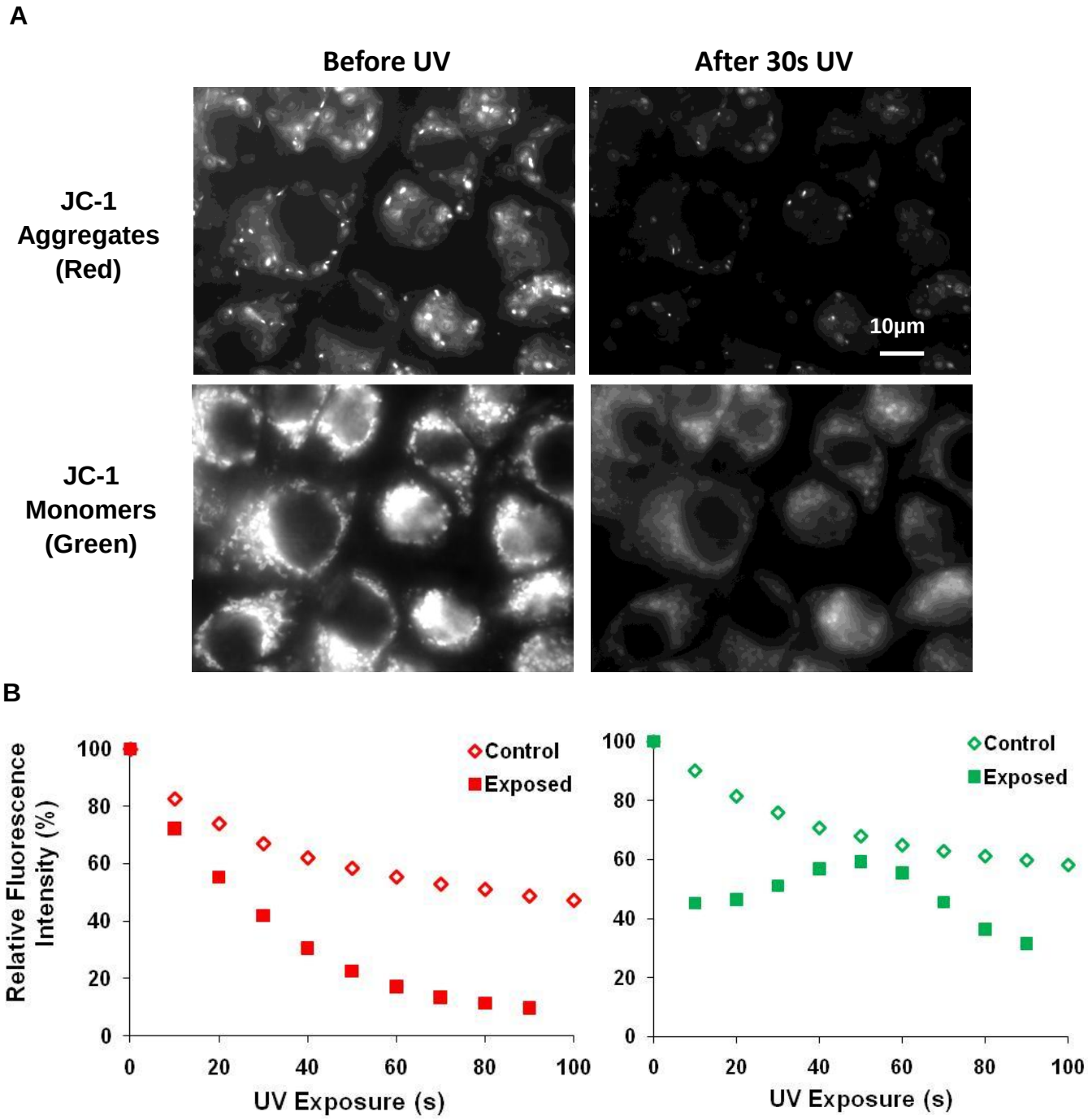

Figure 4-3. The mitochondrial dye JC-1 is significantly photobleached in HeLa cells exposed to UV irradiation. A) Fluorescence images (Before and After UV) of HeLa cells stained with JC-1 (5 µg/mL) in serum-free medium and exposed to UV irradiation. Samples were washed and imaging was performed in PBS buffer (1X). Fluorescence images were acquired with a 100X oil immersion objective, in the red and green channels and are scaled appropriately (red: 100-1000 counts; green: 200-800 counts). B) Quantification of the relative fluorescence intensity as a function of UV exposure for an irradiated sample (Exposed) and an unirradiated sample (Control). Fluorescence images were acquired in the red and green channels with a series of sequential exposures and the fluorescence intensity was quantified in each channel as the blank-corrected mean intensity. The fluorescence intensity measured from the initial image was set to 100%, in each case, for quantification.

4.2.2 – Probing Caspase Activation

In order to assess the involvement of caspase activation in the mode of cell death that is observed with photochemically generated ceramide in HeLa cells, we utilized a luminogenic assay for caspase 3/7 activity, which is described briefly in the introduction of this chapter. It was important to initially determine whether this assay was an appropriate method to be used in our experimental system. This was assessed from a preliminary caspase 3/7 assay that was performed by incubating the cells with exogenous C2 and C16 ceramides, as well as with the Bhc-caged C16 Cer (**9b**) for a total of 18 hours. For each treatment group, some samples were UV-irradiated for 9 minutes after 2 hours of incubation, whereas others were left unirradiated.

As shown in Figure 4-4, a high degree of caspase activation was observed with the short-chain C2 Cer (20 µM). The samples treated with this exogenous ceramide exhibited roughly a 4-fold increase in caspase 3/7 activity in the absence of UV irradiation and a 6-fold increase in the presence of UV irradiation. This increase in caspase 3/7 activity is indicative of apoptotic cell death. In contrast, HeLa cells treated with the long-chain C16 Cer (20 µM) showed no significant increase in caspase 3/7 activity. The lack of caspase activation with C16 ceramide is reasonable based on the poor solubility and low membrane permeability of the long-chain ceramide. Furthermore, the caged ceramide **9b** did not significantly increase caspase 3/7 activity, either in the presence or in the absence of UV irradiation. This suggests that caspase activation does not occur in response to the photochemical generation of C16 Cer in HeLa cells.

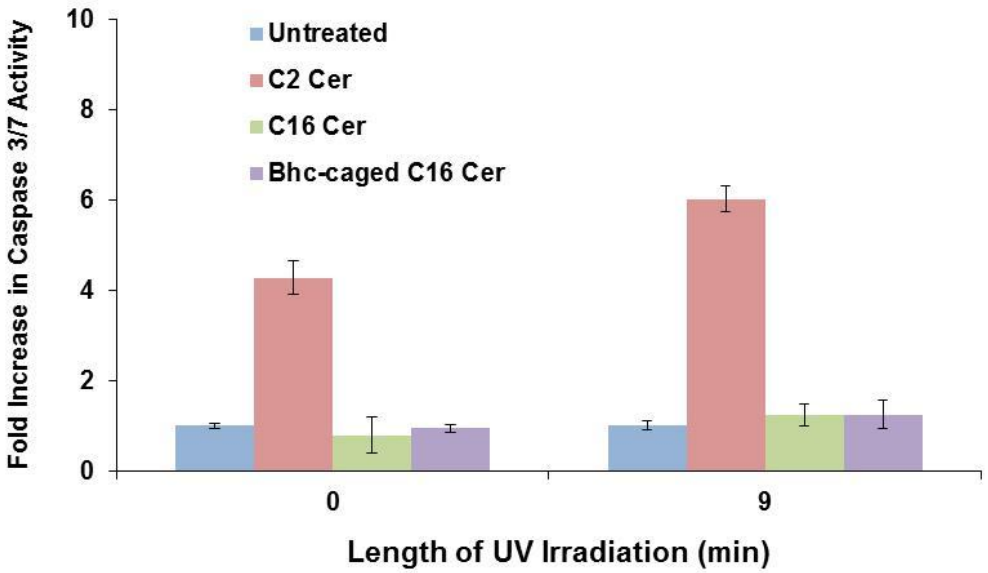

Figure 4-4. Caspase 3/7 activity assay results for HeLa cells treated with C2 Cer, C16 Cer or Bhc-caged C16 Cer (**9b**), at a concentration of 20 μM, in serum-free medium. Samples were incubated in the dark for 2 hours, irradiated in a UV reactor (350 nm) for 9 min (or left unirradiated) and an assay was performed after 18 hours. Data shown are mean values from a single experiment and error bars indicate the standard deviation (n=5 values per treatment group).

Since cell death often involves a precise series of biochemical events within the cell, it is crucial that appropriate timing is employed when performing a particular assay in order to accurately probe the parameter in question. Caspase 3/7 activity was measured at different time points (8, 14, 18 or 24 hours of total incubation time, in separate experiments) in order to optimize the timing of the assay. In these experiments, the cells were incubated with the Bhc-caged C16 Cer (**9b**), with the exogenous ceramide controls, or left untreated and UV irradiation (9 min) was performed after 2 hours of incubation, where applicable. The results followed the same trends as those described above, where C2 Cer was the only compound to cause caspase 3/7 activation in HeLa cells (data not shown).

Furthermore, some optimization of the length of UV irradiation was required. Although this was investigated for the viability assay in the previous chapter, it was necessary to determine the proper irradiation conditions to be used for the caspase 3/7 activity assay which was done in different tissue culture plates. The tissue culture plates that were used for caspase assays were white in color and opaque, whereas the ones used for viability assays were clear. With the clear tissue culture plates, the samples are irradiated from above and from below, whereas with the opaque tissue culture plates, the samples are irradiated from above only, which may require longer irradiation times.

In order to determine the appropriate UV irradiation conditions, an experiment was performed in which 20 µM of exogenous C2 Cer or 20 µM of the Bhc-caged C16 Cer (**9b**) was added to the cells and the samples were incubated for 2 hours before being UV-irradiated for different lengths of time. For comparative purposes, an untreated control was also included for each set of conditions. As shown in Figure 4-5, treatment with C2 Cer caused a large increase (roughly 5-10 fold) in caspase 3/7 activity, under each of the sets of conditions used (0, 9, 12 and 15 min UV). As for the samples treated with the caged ceramide **9b**, no significant increase in caspase 3/7 activity was observed under any of the sets of conditions used. These results, which are consistent with those presented in the previous figure, suggest that caspase activation does not occur during cell death with photochemically generated ceramide in HeLa cells.

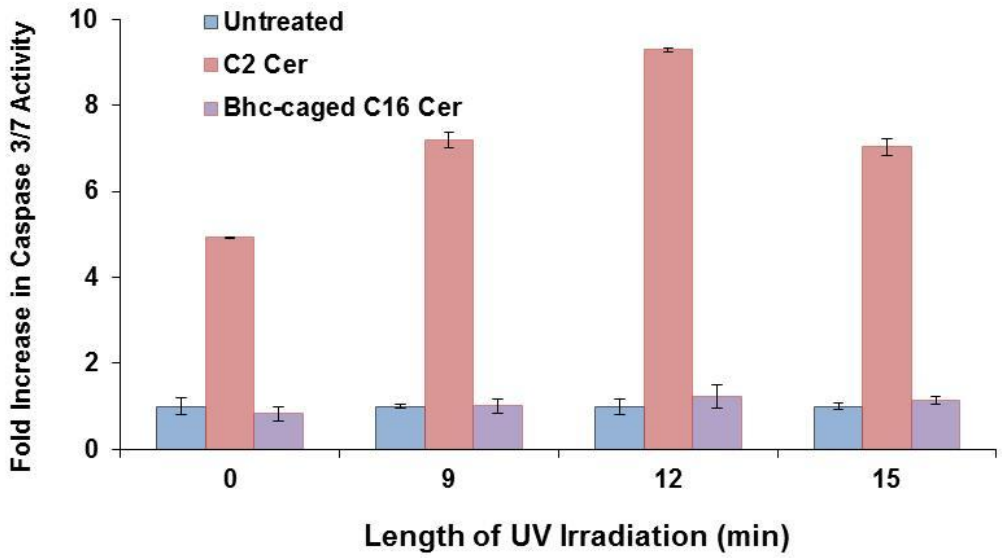

Figure 4-5. Caspase 3/7 activity assay results for HeLa cells treated with C2 Cer or with the Bhc-caged C16 Cer (**9b**), at a concentration of 20 μM, in serum-free medium. Samples were incubated in the dark for 2 hours, irradiated in a UV reactor (350 nm) for 0, 9, 12 or 15 min and an assay was performed after 24 hours. Data shown are mean values from a single experiment and error bars indicate the standard deviation (n=4 values per treatment group).

In order to further investigate the occurrence of caspase activation during cell death with photochemically generated ceramide in HeLa cells, a caspase 3/7-specific inhibitor was used. The synthetic peptide Z-DEVD-fmk, which consists of a sequence of four O-methylated amino acids with a terminal fluoromethylketone moiety, is a potent inhibitor of caspases 3 and 7.[19] In our study, this inhibitor was first tested in the caspase 3/7 luminescence assay and these results are shown in Figure 4-6 (A). For these experiments, the cells were pre-incubated for 1 hour with Z-DEVD-fmk (100 μM) before ceramide treatment solutions were added. The results showed that C2 Cer (20 μM) caused a very large increase in caspase 3/7 activity (roughly 5-fold), which could be blocked by the inhibitor Z-DEVD-fmk, in the absence and in the presence of UV irradiation. At the same concentration, the Bhc-

caged C16 Cer (**9b**), once again, caused no caspase activation, in the presence or in the absence of the inhibitor.

By including the caspase 3/7 inhibitor in viability assays which are used to assess the effects of different ceramide treatments, further insight into the involvement of caspase activation in ceramide-induced cell death can be gained. When a WST-1 cell viability assay incorporating the Z-DEVD-fmk was conducted, it was observed that cell death caused by C2 Cer is not significantly blocked by the inhibitor, as shown in Figure 4-6 (B). This implies that, although C2 Cer causes caspase activation, other cell death pathways must be involved. The UV-irradiated caged ceramide **9b** was shown to cause cell death in the absence and in the presence of the inhibitor Z-DEVD-fmk. This suggests that cell death resulting from treatment with the UV-irradiated caged ceramide is primarily caspase-independent.

A

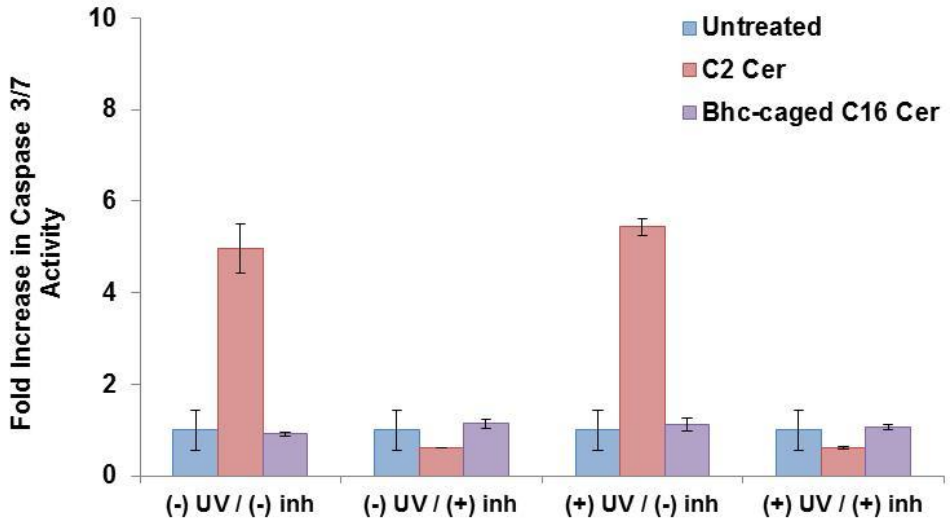

B

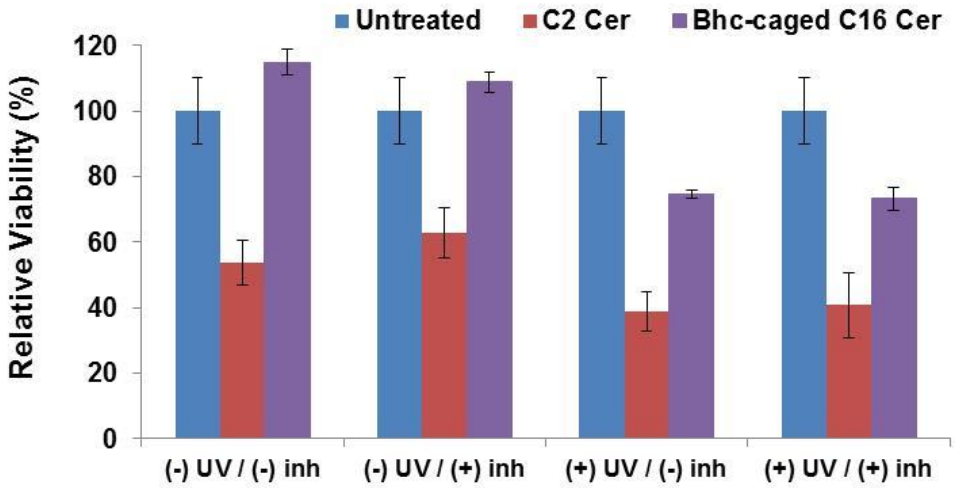

Figure 4-6. C2 Ceramide causes caspase 3/7 activation in HeLa cells which can be blocked by the caspase inhibitor Z-DEVD-fmk, whereas cell death with the Bhc-caged C16 Cer (**9b**) occurs independently of caspase 3/7 activation. Caspase 3/7 activity assay results (A) and WST-1 cell viability assay results (B) for HeLa cells treated with C2 Cer or with the caged ceramide **9b**, at a concentration of 20 µM, in serum-free medium. Samples were pre-treated with Z-DEVD-fmk (100 µM) for 1 hour, incubated in the dark for 2 hours with the compounds, irradiated in a UV reactor (350 nm) for 9 min (caspase assay) / 6 min (viability assay) and an assay was performed after 24 hours. Data shown are average values for the fold increase in caspase 3/7 activity and for the relative cell viability, which were obtained from 2 independent experiments and error bars indicate the standard deviation.

Caspase activation was also probed in HeLa cells treated with pegylated caged ceramides. Particularly, the cells were incubated with the Btcmoc-caged C18

Cer (**22**) or with the Btcmoc-caged C22 Cer (**23**) and UV-irradiated for 9 minutes (or left unirradiated) after 2 hours of incubation. The samples were subjected to a caspase 3/7 activity assay after 24 hours and the results from this experiment are displayed in Figure 4-7. The results that were obtained are consistent with those from other caspase 3/7 assays, where C2 Cer (20 µM) caused a large increase in caspase 3/7 activity (roughly 4-fold, with and without UV) and the UV-irradiated caged ceramides caused no significant increase in activity. These results suggest that the photochemical generation of long-chain C18 Cer and very long-chain C22 Cer in HeLa cells does not cause caspase activation, which is consistent with what was observed for the Bhc-caged C16 Cer (**9b**).

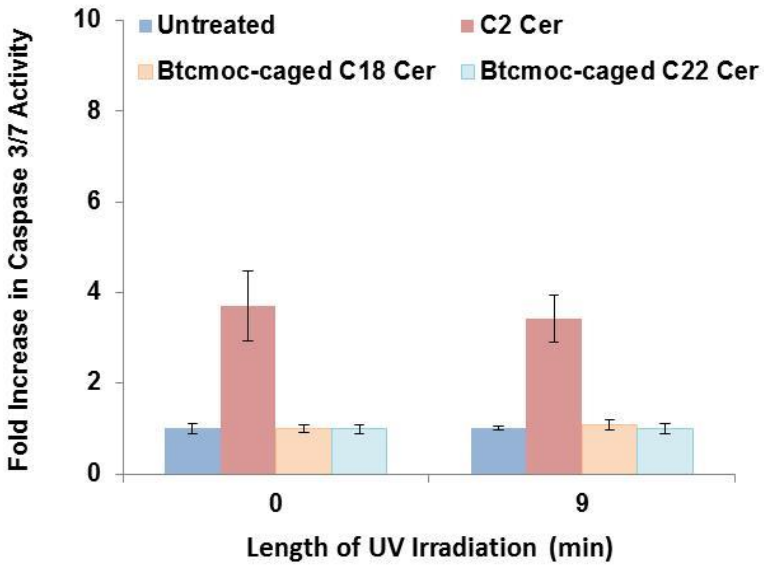

Figure 4-7. Caspase 3/7 activity assay results for HeLa cells treated with C2 Cer or with the Btcmoc-caged ceramides (**22** and **23**), at a concentration of 20 µM, in serum-free medium. Samples were incubated in the dark for 2 hours, irradiated in a UV reactor (350 nm) for 9 min and an assay was performed after 24 hours. Data shown are mean values from a single experiment and error bars indicate the standard deviation (n=6 values per treatment group).

4.2.3 – Probing the Involvement of the RIP1 Kinase

Since the results presented in the previous section have shown that cell death induced by photochemically generated ceramide in HeLa cells proceeds in a caspase-independent manner, the occurrence of necrotic cell death was

investigated by probing the involvement of the RIP1 kinase. As described earlier, this kinase has been implicated in mediating necrosis in different systems. RIP1 signalling was probed through the use of a small molecule inhibitor termed necrostatin-1s (Nec-1s), which was described at the beginning of this chapter. Determining the ability of the inhibitor to block the decrease in cell viability that is observed as a result of treatment with the Bhc-caged C16 Cer (**9b**), at a concentration of 20 µM, can provide insight into the mechanism of cell death. In order to be able to directly compare these viability assay results to the results presented in Figure 4-6 (section 4.2.2), the caspase inhibitor Z-DEVD-fmk was also included in this experiment. The cells were pre-incubated in the presence of the necrosis inhibitor Nec-1s (100 µM) and the caspase inhibitor (100 µM) for 1 hour before the ceramide treatment solutions were added. The samples were then UV-irradiated after 2 hours of incubation (or left unirradiated) and incubated for 22 more hours. The results from this preliminary experiment, which are displayed in Figure 4-8, showed that the decrease in cell viability that is observed with the UV-irradiated caged ceramide **9b** can't be attenuated by inhibiting the RIP1 kinase, which suggests that RIP signalling is not implicated in cell death induced by coumarinyl-caged ceramides.

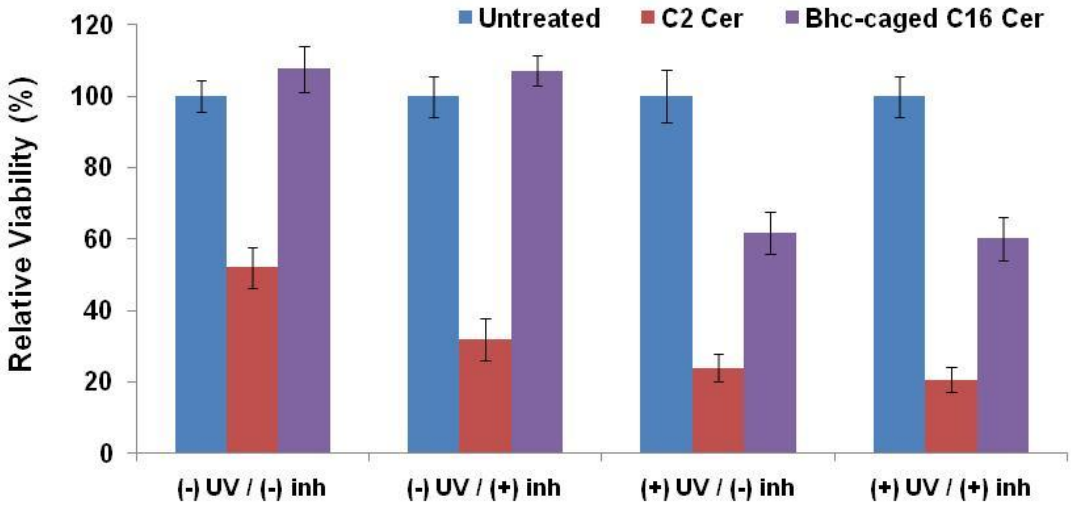

Figure 4-8. The Bhc-caged C16 Cer (**9b**) exhibits a form of cell death that is not blocked by the necrosis inhibitor Nec-1s. WST-1 cell viability assay results for HeLa cells treated with C2 Cer or the caged ceramide **9b**, at a concentration of 20 µM, in serum-free medium. The samples were pre-treated with the inhibitors Z-DEVD-fmk and Nec-1s (100 µM each) for 1 hour, incubated in the dark for 2 hours, irradiated in a UV reactor (350 nm) for 6 min and an assay was performed after 24 hours. Data shown are mean values for relative cell viability from a single experiment and error bars indicate the standard deviation (n= 6-12 values per treatment group).

4.2.4 - ROS Detection Assay and Use of Scavengers

In order to probe ROS generation in response to the photochemical generation of ceramide in HeLa cells, a fluorescence-based assay was used. It was observed earlier in this work that the free Bhc-coumarin (**4**), which was used as a control in this study of the biological effects of coumarinyl-caged ceramides, causes a small decrease in the viability of HeLa cells (see chapter 3, section 3.2.2, Figure 3-7). Similarly, the free Btcmoc (**18**) was shown to affect the viability of the cells and to a larger extent than the free coumarin **4** (see chapter 3, section 3.2.3, Figure 3-9). It was hypothesized that these effects could be due to the generation of ROS upon

excitation of the coumarins in the cells. In order to investigate ROS generation upon UV exposure, the cells were labelled with carboxy-H_2DCFDA (10 μM), incubated with the compounds for 2 hours and subjected to 6 minutes of UV irradiation (or left unirradiated).

In a preliminary ROS assay, the cells were treated with the positive control compound tert-butyl hydroperoxide (TBHP) at a concentration of 100 μM, the free Bhc-coumarin (**4**) at a concentration of 20 μM, the free Btcmoc-coumarin (**18**) at a concentration of 20 μM, or left untreated. As shown in Figure 4-9, TBHP caused roughly a 3-fold increase in the fluorescence emission of the probe in the absence and in the presence of UV irradiation. This increase in fluorescence emission suggested that ROS generation occurred upon treatment with the peroxide, which indicated that the assay was functioning appropriately. As for the results with the free coumarins **4** and **18**, the fluorescence emission increased by about 9-fold in the presence of UV irradiation, in each case, but remained at the baseline level in the absence of UV irradiation. These results suggest that ROS are generated upon exciting the coumarin cages within the cells, which needs to be considered when attempting to assess the biological effects of photochemically generated ceramide.

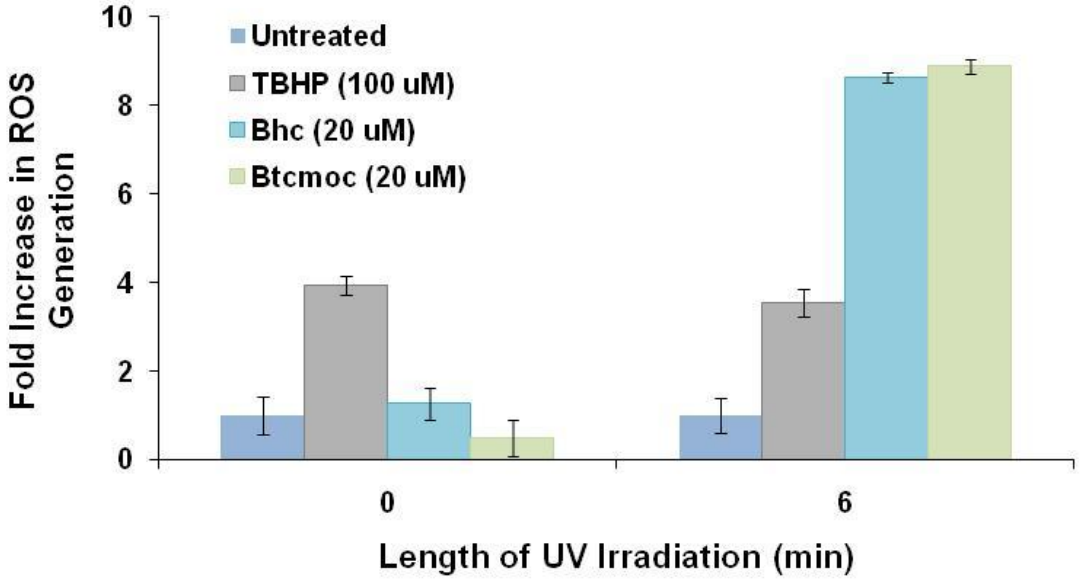

Figure 4-9. UV irradiation of the free coumarins Bhc (**4**) and Btcmoc (**18**) causes ROS generation in HeLa cells. Carboxy-H_2DCFDA fluorescence assay results for ROS detection in HeLa cells treated with the control species TBHP (100 µM), with the free coumarin **4** (20 µM), or with the free coumarin **18** (20 µM) in HBSS buffer. The cells were stained with carboxy-H_2DCFDA (10 µM) for 45 min in the dark and washed once with buffer. Treatment solutions were added and the samples were incubated in the dark for 2 hours, irradiated in a UV reactor (350 nm) for 6 min (or left unirradiated) and the fluorescence emission at 520 nm (with 485 nm excitation) was measured. Data is normalized to the untreated control for each set of conditions (0 and 6 min UV irradiation). Data shown are mean values for the fold increase in fluorescence intensity from a single experiment and error bars are indicate the standard deviation (n= 12 values per treatment group).

ROS scavengers can be used to attenuate the effects of ROS in different systems. In order to investigate this in our system, different ROS scavengers were selected and tested using the carboxy-H_2DCFDA fluorescence assay in HeLa cells incubated with the Bhc-coumarin (**4**), at a concentration of 20 µM, for 2 hours and exposed to UV irradiation (6 min). The ROS scavengers that were selected were ascorbic acid (200 µM), alpha-tocopherol (100 µM) and Trolox (100 µM). The concentrations were chosen based on those reported in other studies in which similar experiments were carried out.[36-38] Each of the scavengers was tested in the absence and in the presence of the free coumarin **4**, as well as in the absence and in the presence of UV irradiation. The results from this experiment are displayed in Figure 4-10. It was observed that only a moderate increase in the fluorescence

emission of the probe occurred with the UV-irradiated free coumarin **4** when ascorbic acid or Trolox were present in the samples. This suggested that these hydrophilic antioxidants were able to effectively scavenge ROS in this system. In contrast, ROS generation could not be blocked by the antioxidant alpha-tocopherol. The highly lipophilic nature of this antioxidant could make it ineffective as a ROS scavenger in this system. In light of these results, Trolox was selected and used in subsequent ROS assay experiments with coumarinyl-caged ceramides.

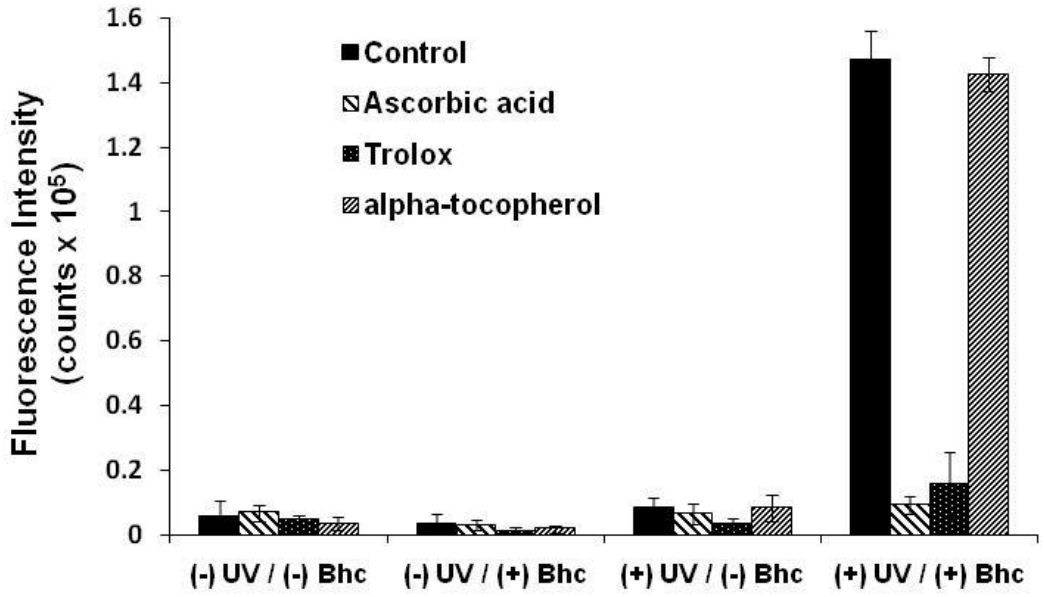

Figure 4-10. ROS generation upon UV irradiation of the Bhc-coumarin (**4**) in HeLa cells can be blocked by the scavengers ascorbic acid and Trolox. Carboxy-H_2DCFDA fluorescence assay results for ROS detection in HeLa cells treated with the free coumarin **4** (20 µM) in HBSS buffer. The cells were stained with carboxy-H_2DCFDA (10 µM) for 45 min in the dark and washed once with buffer. The samples were then pre-treated for 1 hour with ascorbic acid (200 µM), alpha-tocopherol (100 µM) or Trolox (100 µM). Incubation in the dark for 2 hours with the free coumarin **4** and irradiation in a UV reactor (350 nm) for 6 min were then performed. The fluorescence emission at 520 nm (with 485 nm excitation) was measured. Data shown are mean values for the fluorescence intensity from a single experiment and error bars indicate the standard deviation (n= 6-12 values per treatment group).

With all of the appropriate controls in place, ROS generation as a result of the photochemical generation of ceramide in HeLa cells could be probed using the

carboxy-H_2DCFDA dye. As shown in Figure 4-11 (A), the Bhc-coumarin (**4**), in the presence of UV irradiation (6 min), caused roughly a 10-fold increase in the fluorescence emission of the dye, which was consistent with the results from preliminary experiments. However, when the cells were pre-incubated with Trolox (100 μM), an increase in fluorescence of only 2.5-fold was observed due to ROS scavenging. As for the Bhc-caged C16 Cer (**9b**), it also caused a large increase (10-fold) in fluorescence intensity, which could be only partially blocked by the incorporation of Trolox (5-fold increase). This suggests that the photochemical generation of C16 Cer in HeLa cells using the caged ceramide **9b** produces some ROS species which are not scavenged by the antioxidant Trolox.

In order to correlate these results to those obtained from the viability assays that were performed with the caged ceramide **9b**, a WST-1 assay incorporating the ROS scavenger Trolox was carried out and the results are presented in Figure 4-11 (B). It was observed that Trolox is not able to block the decrease in cell viability that occurs with the UV-irradiated caged ceramide **9b**. This suggests cell death induced by the photolytic cleavage of coumarinyl-caged ceramides in HeLa is mediated by other cellular events besides ROS generation. It is also noteworthy that the free Bhc-coumarin (**4**) did not cause a significant decrease in viability here, which is in contrast to the averaged viability data presented in the previous chapter (see Figure 3-7, section 3.2.2, chapter 3). Differences in the method of preparation of the treatment solutions are responsible for this effect (see experimental procedures in section 5.6, chapter 5).

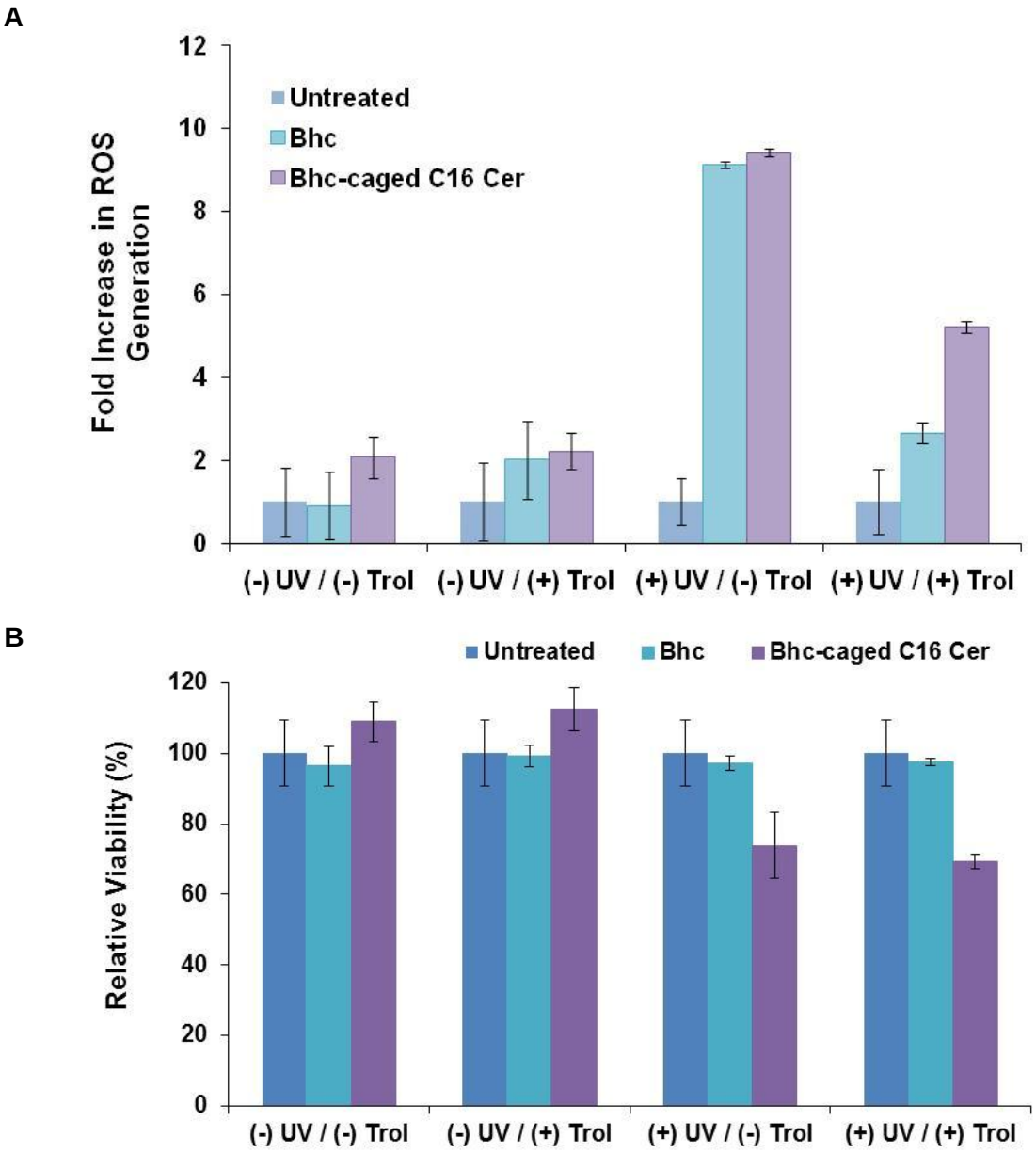

Figure 4-11. A) Carboxy-H_2DCFDA fluorescence assay results for ROS detection in HeLa cells treated with the Bhc-coumarin (**4**) or with the Bhc-caged C16 Cer (**9b**) (20 µM) in HBSS buffer. The cells were stained with carboxy-H_2DCFDA (10 µM) for 45 min in the dark and washed once with buffer. The samples were then pre-treated for 1 hour with Trolox (100 µM), incubated in the dark for 2 hours with the compounds and irradiated in a UV reactor (350 nm) for 6 min (or left unirradiated). The fluorescence emission at 520 nm (with 485 nm excitation) was measured. Data is normalized to the untreated control for each set of conditions. Data shown are mean values for the fold increase in fluorescence intensity from a single experiment and error bars indicate the standard deviation (n= 6-12 values per treatment group). B) WST-1 cell viability assay results for HeLa cells treated with the free coumarin **4** and with the caged ceramide **9b** (20 µM) in serum-free medium. The samples were then pre-treated for 1 hour with Trolox (100 µM), incubated in the dark for 2 hours with the compounds and irradiated in a UV reactor (350 nm) for 6 min (or left unirradiated). The assay was performed after 24 hours. Data shown are average values for relative cell viability from two experiments and error bars indicate the standard deviation.

4.3 – Discussion and Conclusions

The results presented in the previous chapter showed that a decrease in cell viability occurs as a result of generating ceramide photochemically in HeLa cells. In order to elucidate the mechanism by which cell death occurs with caged ceramides, apoptotic and necrotic cell death were probed in the cells using different methods. The occurrence of apoptosis was first investigated by assessing mitochondrial function with the mitochondrial dye JC-1. A preliminary experiment with the control compound FCCP revealed that the JC-1 staining method employed was capable of detecting decreases in mitochondrial membrane potential ($\Delta\psi_m$) in HeLa cells. This suggested that JC-1 staining could be used to assess the mitochondrial effects of different ceramide treatments.

When JC-1 was used in cells subjected to UV irradiation, however, it was observed that UV exposure causes a significant amount of photobleaching of the fluorescent dye. Particularly, the aggregated form of the dye exhibited a 60% decrease in fluorescence intensity with 30 seconds of UV exposure (see Figure 4-3, section 4.2.1). Reports from other studies in the literature have suggested that the red fluorescent J-aggregates formed by the JC-1 dye are very photosensitive, even in the absence of prolonged UV irradiation. Moreover, it is advised that photobleaching of JC-1 be restricted by performing minimal illumination of the sample (i.e. by using short exposure times for image acquisition).[39] The photobleaching of the probe with UV exposure is therefore problematic in measuring decreases in $\Delta\psi_m$ as a result of photochemically generated ceramide in cells.

The efficient photobleaching and the apparent monomer-aggregate equilibration complicate the analysis of the results that were obtained for JC-1 staining of HeLa cells incubated with the UV-irradiated Bhc-caged C16 Cer (**9b**). A decrease in the fluorescence of the red J-aggregates was observed in the treated cells, which suggests that mitochondrial depolarization occurs as a result of treatment with the caged ceramide **9b** (see Figure 4-2, section 4.2.1). For control (untreated) cells that were exposed to UV irradiation, the relative changes in the aggregate and monomer fluorescence intensities indicate that the red/green fluorescence ratio increases for short UV irradiation times and then decreases after ~30-40 s (see Figure 4-3 (B), section 4.2.1). Therefore, it can be concluded that the large decrease in the amount of red aggregate emission after 30 s of UV irradiation of the cells treated with the caged ceramide provides evidence for mitochondrial depolarization, although it is not possible to quantify this without correcting for changes induced by UV irradiation alone. Additional optimization of this assay would be required, possibly by exploring whether it is possible to add the JC-1 dye after the UV irradiation. The photobleaching of another mitochondrial dye, TMRM, with UV exposure was determined to occur to a lesser extent than with JC-1, but it was nonetheless significant. Although these mitochondrial dyes may be used under some conditions, it was necessary to use other assays for probing apoptotic cell death in HeLa cells treated with caged ceramides.

Apoptosis was further investigated by probing the activation of executioner caspases 3 and 7 with a luminescence-based caspase 3/7 activity assay. A preliminary experiment revealed that treatment with exogenous short-chain C2 Cer

for 24 hours causes caspase 3/7 activation in the cells (see Figure 4-4, section 4.2.2). This result is consistent with what was observed in other studies. Namely, an increase in caspase activity in response to C2 ceramide treatment has been observed in PC12 cells.[16] Also, another short-chain ceramide, C6 Cer, has been shown to induce caspase activation in HCT116 cells.[14] In contrast, we observed that exogenous long-chain C16 Cer does not activate caspases 3 and 7. This is consistent with the lack of any significant effect of exogenous C16 Cer on cell viability, as assessed by WST-1 assay earlier in this work (see Figures 3-4 and 3-7, section 3.2.2, chapter 3). Moreover, this result is reasonable based on the poor aqueous solubility and the low membrane permeability of long-chain C16 Cer.

In the preliminary experiment, it was observed that no increase in caspase 3/7 activity occurs with the Bhc-caged C16 Cer (**9b**), in the absence or in the presence of UV irradiation. The results from other experiments (see Figure 4-5, section 4.2.2) also revealed that caspase 3/7 activation does not occur with the caged ceramide **9b**, even when UV exposure times of up to 15 minutes are used and regardless of whether the assay is performed after 8, 14, 18 or 24 hours of incubation. The fact that complete (100%) photolysis of the caged ceramide **9b** can be achieved with just 1.5 minutes of UV irradiation, based on the results from preparatory photolysis experiments (see Figure 2-6, section 2.2.4, chapter 2), further supports the conclusion that caspase activation does not occur in response to photochemically generated C16 Cer in HeLa cells.

Furthermore, a caspase 3/7-specific inhibitor, Z-DEVD-fmk, was included in a caspase 3/7 activity assay and in a corresponding WST-1 cell viability assay in order

to probe caspase activation through enzyme inhibition. In the luminescence assay, it was observed that Z-DEVD-fmk can effectively block caspase activation in response to C2 Cer treatment (see Figure 4-6 (A), section 4.2.2). However, in the viability assay, the Bhc-caged C16 Cer (**9b**) caused a decrease in cell viability that could not be attenuated by the inhibitor Z-DEVD-fmk (see Figure 4-6 (B), section 4.2.2). These results confirmed that ceramide which is generated photochemically in HeLa cells does not activate the executioner caspases 3 and 7. In addition, when caspase activation was probed in HeLa cells treated with other UV-irradiated caged ceramides, such as the pegylated Btcmoc-caged C18 Cer (**22**) and Btcmoc-caged C22 Cer (**23**), no increase in caspase 3/7 activity was observed (see Figure 4-7, section 4.2.2). These results suggest that cell death resulting from the photochemical generation of long- and very long-chain ceramides in HeLa cells occurs in a caspase-independent manner.

Caspase-independent cell death with ceramide has been observed previously, in other studies.[40,41] In some cases, ceramide induces cell death in the absence of any of the biochemical and morphological markers of apoptosis and the mode of cell death that is undergone more closely resembles necrosis.[42,43] More and more studies are suggesting that RIP1, a kinase, is a key regulator of necrotic cell death.[5,29,44] When RIP1 signalling was probed in our system with the small molecule inhibitor Nec-1s, the inhibitor did not appear to block the decrease in cell viability that occurs with the UV-irradiated Bhc-caged C16 Cer (**9b**) (see Figure 4-8, section 4.2.3). This suggests that cell death caused by photochemically generated C16 Cer does not involve the RIP1 kinase. However, this experiment was only done

once and further experiments are required in order to confirm the validity of this observation.

Necrotic cell death with ceramide has also been shown to involve the generation of ROS.[40,45] In addition, it was hypothesized earlier in this study that ROS generation could account for the small decrease in cell viability that is observed with the UV-irradiated free Bhc-coumarin (**4**). ROS generation can be probed in cells through the use of carboxy-H_2DCFDA, which was confirmed in our system using the peroxide TBHP. The results from these experiments revealed that the free coumarin **4** does, in fact, generate ROS in the cells in the presence of UV irradiation. It is, however, noteworthy that this effect could mostly be attenuated in the presence Trolox, which has been shown to be an effective ROS scavenger in other systems.[36]

Trolox has, however, been shown to be ineffective in preventing ROS generation in response to ceramide treatment in A20 B lymphoma cells and in Jurkat T cells.[46] This is useful in distinguishing between the biological effects of ceramide and the UV-induced effects of the coumarin when cells are treated with the Bhc-caged C16 Cer (**9b**) and UV-irradiated. In fact, the caged ceramide **9b** was shown to generate ROS upon UV irradiation in the cells, which could be only partially blocked by the antioxidant Trolox. This suggests that ROS generation with the caged ceramide **9b** could be occurring partially as a result of UV-irradiating the coumarin but also as a result of ceramide bioactivity. When an analogous viability assay was performed, it was observed that the presence of Trolox, which was shown to block UV-induced ROS generation, does not significantly reduce the

amount of cell death that is caused by the UV-irradiated caged ceramide **9b**. This suggests that ROS generation is not the main event involved during this mode of cell death. In summary, the photochemical generation of ceramide, particularly C16 Cer, in HeLa cells results in a caspase-independent form of cell death that appears to implicate mitochondrial depolarization and some ROS production, but not RIP1 signalling.

4.4 - References

(1) He, X.; Huang, Y.; Li, B.; Gong, C.-X.; Schuchman, E. H. *Neurobiology of Aging* **2010**, *31*, 398.
(2) Reynolds, C. P.; Maurer, B. J.; Kolesnick, R. N. *Cancer Letters* **2004**, *206*, 169.
(3) Vaux, D. L.; Strasser, A. *Proceedings of the National Academy of Sciences* **1996**, *93*, 2239.
(4) Festjens, N.; Vanden Berghe, T.; Vandenabeele, P. *Biochimica et Biophysica Acta (BBA) - Bioenergetics* **2006**, *1757*, 1371.
(5) Fulda, S. *Cancer Biol Ther* **2013**, *14*, 999.
(6) Morad, S. A. F.; Cabot, M. C. *Nat Rev Cancer* **2013**, *13*, 51.
(7) Lee, H.; Rotolo, J. A.; Mesicek, J.; Penate-Medina, T.; Rimner, A.; Liao, W.-C.; Yin, X.; Ragupathi, G.; Ehleiter, D.; Gulbins, E. *PLoS One* **2011**, *6*, e19783.
(8) Ganesan, V.; Colombini, M. *FEBS Letters* **2010**, *584*, 2128.
(9) Novgorodov, S. A.; Szulc, Z. M.; Luberto, C.; Jones, J. A.; Bielawski, J.; Bielawska, A.; Hannun, Y. A.; Obeid, L. M. *Journal of Biological Chemistry* **2005**, *280*, 16096.
(10) Cossarizza, A.; Ceccarelli, D.; Masini, A. *Experimental Cell Research* **1996**, *222*, 84.
(11) Beckham, T. H.; Lu, P.; Jones, E. E.; Marrison, T.; Lewis, C. S.; Cheng, J. C.; Ramshesh, V. K.; Beeson, G.; Beeson, C. C.; Drake, R. R.; Bielawska, A.; Bielawski, J.; Szulc, Z. M.; Ogretmen, B.; Norris, J. S.; Liu, X. *Journal of Pharmacology and Experimental Therapeutics* **2013**, *344*, 167.
(12) Smiley, S. T.; Reers, M.; Mottola-Hartshorn, C.; Lin, M.; Chen, A.; Smith, T. W.; Steele, G. D.; Chen, L. B. *Proceedings of the National Academy of Sciences* **1991**, *88*, 3671.
(13) Dispersyn, G.; Nuydens, R.; Connors, R.; Borgers, M.; Geerts, H. *Biochimica et Biophysica Acta (BBA) - General Subjects* **1999**, *1428*, 357.
(14) Fillet, M.; Bentires-Alj, M.; Deregowski, V.; Greimers, R.; Gielen, J.; Piette, J.; Bours, V.; Merville, M.-P. *Biochemical Pharmacology* **2003**, *65*, 1633.
(15) Jiang, Z.; Hong, X.; Long, H.; Hu, J.; Zhai*, Z. *CMLS, Cell. Mol. Life Sci.* **2000**, *57*, 1117.
(16) Yoshimura, S.-i.; Banno, Y.; Nakashima, S.; Takenaka, K.; Sakai, H.; Nishimura, Y.; Sakai, N.; Shimizu, S.; Eguchi, Y.; Tsujimoto, Y.; Nozawa, Y. *Journal of Biological Chemistry* **1998**, *273*, 6921.

(17) Thornberry, N. A.; Lazebnik, Y. *Science* **1998**, *281*, 1312.
(18) Lamkanfi, M.; Dixit, V. M. *Cell Host & Microbe* **2010**, *8*, 44.
(19) Ekert, P. G.; Silke, J.; Vaux, D. L. *Cell death and differentiation* **1999**, *6*, 1081.
(20) Garcia-Calvo, M.; Peterson, E. P.; Leiting, B.; Ruel, R.; Nicholson, D. W.; Thornberry, N. A. *Journal of Biological Chemistry* **1998**, *273*, 32608.
(21) Syed, I.; Szulc, Z. M.; Ogretmen, B.; Kowluru, A. *Cellular Physiology and Biochemistry* **2012**, *30*, 1051.
(22) Sassa, T.; Suto, S.; Okayasu, Y.; Kihara, A. *Biochimica et Biophysica Acta (BBA) - Molecular and Cell Biology of Lipids* **2012**, *1821*, 1031.
(23) Dahm, F.; Bielawska, A.; Nocito, A.; Georgiev, P.; Szulc, Z. M.; Bielawski, J.; Jochum, W.; Dindo, D.; Hannun, Y. A.; Clavien, P. A. *Br J Cancer* **2007**, *98*, 98.
(24) Dindo, D.; Dahm, F.; Szulc, Z.; Bielawska, A.; Obeid, L. M.; Hannun, Y. A.; Graf, R.; Clavien, P.-A. *Molecular Cancer Therapeutics* **2006**, *5*, 1520.
(25) "Caspase-Glo® 3/7 Assay" – Technical Bulletin (Promega). [Online Access]. Published Online: 2003.
(26) Mengubas, K.; Riordan, F. A.; Bravery, C. A.; Lewin, J.; Owens, D. L.; Mehta, A. B.; Hoffbrand, A. V.; Wickremasinghe, R. G. *Oncogene* **1999**, *18*, 2499.
(27) Leist, M.; Single, B.; Castoldi, A. F.; Kühnle, S.; Nicotera, P. *The Journal of Experimental Medicine* **1997**, *185*, 1481.
(28) Lemaire, C.; Andréau, K.; Souvannavong, V.; Adam, A. *FEBS Letters* **1998**, *425*, 266.
(29) Ofengeim, D.; Yuan, J. *Nat Rev Mol Cell Biol* **2013**, *14*, 727.
(30) Degterev, A.; Hitomi, J.; Germscheid, M.; Ch'en, I. L.; Korkina, O.; Teng, X.; Abbott, D.; Cuny, G. D.; Yuan, C.; Wagner, G.; Hedrick, S. M.; Gerber, S. A.; Lugovskoy, A.; Yuan, J. *Nat Chem Biol* **2008**, *4*, 313.
(31) Takahashi, N.; Duprez, L.; Grootjans, S.; Cauwels, A.; Nerinckx, W.; DuHadaway, J. B.; Goossens, V.; Roelandt, R.; Van Hauwermeiren, F.; Libert, C.; Declercq, W.; Callewaert, N.; Prendergast, G. C.; Degterev, A.; Yuan, J.; Vandenabeele, P. *Cell Death Dis* **2012**, *3*, e437.
(32) Schulze-Osthoff, K.; Bakker, A. C.; Vanhaesebroeck, B.; Beyaert, R.; Jacob, W. A.; Fiers, W. *Journal of Biological Chemistry* **1992**, *267*, 5317.
(33) Bartosz, G. *Clinica Chimica Acta* **2006**, *368*, 53.
(34) "Image-iT LIVE Green ROS Detection kit" - Product Information (Molecular Probes). [Online Access]. Published Online: 2004..
(35) Kalyanaraman, B.; Darley-Usmar, V.; Davies, K. J. A.; Dennery, P. A.; Forman, H. J.; Grisham, M. B.; Mann, G. E.; Moore, K.; Roberts Ii, L. J.; Ischiropoulos, H. *Free Radical Biology and Medicine* **2012**, *52*, 1.
(36) Distelmaier, F.; Valsecchi, F.; Forkink, M.; van Emst-de Vries, S.; Swarts, H. G.; Rodenburg, R. J. T.; Verwiel, E. T. P.; Smeitink, J. A. M.; Willems, P. H. G. M.; Koopman, W. J. H. *Antioxidants & Redox Signaling* **2012**, *17*, 1657.
(37) Drummen, G. P. C.; Makkinje, M.; Verkleij, A. J.; Op den Kamp, J. A. F.; Post, J. A. *Biochimica et Biophysica Acta (BBA) - Molecular and Cell Biology of Lipids* **2004**, *1636*, 136.
(38) Du, C.-B.; Liu, J.-W.; Su, W.; Ren, Y.-H.; Wei, D.-Z. *Life Sciences* **2003**, *74*, 771.
(39) Nicholls, D. G.; Ward, M. W. *Trends in Neurosciences* **2000**, *23*, 166.
(40) Thon, L.; Möhlig, H.; Mathieu, S.; Lange, A.; Bulanova, E.; Winoto-Morbach, S.; Schütze, S.; Bulfone-Paus, S.; Adam, D. *The FASEB Journal* **2005**, *19*, 1945.
(41) Zhao, S.; Yang, Y.-N.; Song, J.-G. *Journal of Cellular Physiology* **2004**, *199*, 47.
(42) Engedal, N.; Saatcioglu, F. *The Prostate* **2001**, *46*, 289.

(43) López-Marure, R.; Gutiérrez, G.; Mendoza, C.; Ventura, J. L.; Sánchez, L.; Reyes Maldonado, E.; Zentella, A.; Montaño, L. F. *Biochemical and Biophysical Research Communications* **2002**, *293*, 1028.
(44) Festjens, N.; Vanden Berghe, T.; Cornelis, S.; Vandenabeele, P. *Cell Death Differ* **2007**, *14*, 400.
(45) Kim, W.; Choi, C.; Kang, S.; Kwon, C.; Kim, Y. *Neurochem Res* **2005**, *30*, 969.
(46) Villena, J.; Henriquez, M.; Torres, V.; Moraga, F.; Díaz-Elizondo, J.; Arredondo, C.; Chiong, M.; Olea-Azar, C.; Stutzin, A.; Lavandero, S.; Quest, A. F. G. *Free Radical Biology and Medicine* **2008**, *44*, 1146.

Chapter 5: Experimental Procedures

5.1 – Chemicals

The Bhc-caged C16 Dihydro-Cer (**9a**) and the Bhc-caged C16-Cer (**9b**) were synthesized by our collaborators in the Bittman group, as described previously.[1] The series of mTEGylated caged ceramides (**19**-**24**) were more recently prepared by the same group (see Chapter 2). Reversed-phase HPLC was used to monitor samples of the caged lipids for degradation and to purify them as required. All aqueous solutions were prepared using 18.3 MΩ cm *Milli-Q* water. KMops buffer (100 mM KCl, 10 mM 3-(N-morpholino)-propanesulfonate (Mops), pH 7.4) was used for most of the photophysical and photochemical characterization experiments. The buffered solution was passed through a 0.22 μm filter (Millipore, Billerica, MA) before being used. The laser dyes 7-amino-4-methyl-2*H*-1-benzopyran-2-one (Coumarin 440), 7-(diethylamino)-4-methyl-2*H*-1-benzopyran-2-one (Coumarin 460) and 2,3,6,7-tetrahydro-9-methyl-1*H*,5*H*-quinolizino(9,1-*gh*)coumarin (Coumarin 480) were obtained from Exciton (Dayton, OH) and used as standards for photophysical and photochemical characterization. All organic solvents used were HPLC grade from EMD Chemicals (Philadelphia, PA).

Dubelco's modified Eagles medium (DMEM), fetal bovine serum (FBS) and 0.25% trypsin / ethylenediaminetetraacetic acid (EDTA) were purchased from Wisent Bioproducts (St-Bruno, PQ, Canada). Phosphate buffered saline (PBS) solution (pH 7.4) was prepared (137 mM NaCl, 2.7 mM KCl, 10 mM Na_2HPO_4, 1.8 mM KH_2PO_4) and autoclaved for sterility. The cell proliferation reagent MTT (3-[4,5-

dimethylthiazol-2-yl]-2,5- diphenyltetrazolium bromide) and tissue culture grade dimethyl sulfoxide (DMSO) were purchased from Sigma-Aldrich (St-Louis, MO). The cell proliferation reagent WST-1 (4-[3-(4-iodophenyl)-2-(4-nitrophenyl)-2*H*-5-tetrazolio]-1,3-benzene disulfonate) was obtained from Roche Diagnostics (Laval, PQ, Canada).

The mitochondrial membrane potential probe JC-1 (5,5',6,6'-tetrachloro-1,1',3,3'-tetraethylbenzimidazolylcarbocyanine iodide) and the "Image-iT^{TM} LIVE Green Reactive Oxygen Species Detection Kit" (containing carboxy-H_2DCFDA (5-(and-6)-carboxy-2',7'-dichlorodihydrofluorescein diacetate) as well as the inducer of reactive oxygen species (ROS) production *tert*-butyl hydroperoxide (TBHP)) were purchased from Molecular Probes (Eugene, OR). Hank's balanced salt solution (HBSS) with calcium and magnesium and without phenol red was obtained from Invitrogen (Carlsbad, CA). The mitochondrial oxidative phosphorylation uncoupler FCCP (carbonyl cyanide-4-(trifluoromethoxy)phenylhydrazone) and the mitochondrial membrane potential dye TMRM (tetramethylrhodamine methyl ester) were kindly provided by Dr. Willard Costain of the National Research Council of Canada. The ROS scavengers Trolox, ascorbic acid and alpha-tocopherol were purchased from Sigma-Aldrich (St-Louis, MO).

The "Caspase-Glo® 3/7 Assay" kits were obtained from Promega (Madison, WI). The caspase inhibitor Z-DEVD-fmk (Z-Asp(OMe)-Glu(OMe)-Val-DL-Asp(OMe)-fluoromethylketone) was purchased from Bachem (Bubendorf, Switzerland) and the necrosis inhibitor Nec-1s (5-((7-chloro-1H-indol-3-yl)methyl)-3-methyl-2,4-imidazolidinedione) was obtained from Calbiochem (Billerica, MA).

5.2 - Absorbance and Fluorescence Spectroscopy

Absorption spectra were recorded with a Cary 5000 UV-vis/NIR spectrophotometer (Agilent Technologies, Santa Clara, CA). Emission spectra were acquired using a Fluorolog-3 spectrofluorometer (Horiba Jobin Yvon, Edison, NJ) with slit widths of 1-3 nm. All spectral measurements were performed at room temperature using a quartz cuvette with a pathlength of 1 cm. Fluorescence quantum yields were calculated with reference to Coumarin 460 in ethanol (Φ_{fl} = 0.59)[2] for Bhc-related compounds or Coumarin 440 in ethanol (Φ_{fl} = 0.56)[3] for mTEGylated compounds from sample solutions having an absorbance ≤ 0.25. Working solutions of the compounds were prepared at 10-20 μM to match the absorbance of the standard. The excitation wavelengths were 374 nm for the Bhc-related compounds and 330 nm for the mTEGylated compounds. Quantum yields were calculated by measuring the integrated fluorescence intensity for both the standard and the compound.

5.3 - Photolysis and Photoproduct Analysis

Photolysis of the caged lipid (20 μM) in KMops buffer (pH 7.4) containing 10 or 50% ethanol (as specified in results) was performed in a 4 mL quartz cuvette or in a 96-well plate (multiple wells with 300 μL of solution per well). In these experiments, the sample was subjected to 350 ± 25 nm irradiation in a Rayonet photochemical reactor (Southern New England Ultraviolet Company, Branford, CT) equipped with four lamps. For preparatory photolysis experiments performed in a

microwell plate, the UV reactor was turned on its side and the microwell plate was placed on an aluminum cradle, with two lamps above the plate and two lamps below the plate. Aliquots (20-50 µL) were removed from the sample at defined time points and analyzed by reversed-phase HPLC with a HP 1090 system (Agilent Technologies, Santa Clara, CA) set up with a SunFire C18 column (Waters Corporation, Milford, MA). A solution of Coumarin 480 with a known concentration was prepared and a defined amount was added to each aliquot as an internal standard. Sample aliquots were eluted with an ethanol/water gradient (75% ethanol increasing to 95% over 3 min) at a flow rate of 0.5-0.8 mL/min in order to monitor the loss of starting material and the formation of the free coumarin photo-product. Detection was by absorbance at 325 nm and fluorescence at 480 nm.

5.4 - Cell Culture of the HeLa Cell Line

HeLa cells were kindly provided by Dr. Willard Costain of the National Research Council of Canada. The cells were maintained in Dulbecco's modified Eagle's medium (DMEM) supplemented with 10% fetal bovine serum (FBS), 10 mM glutamine and 100 units/mL of penicillin/streptomycin ("complete medium") in a humidified incubator with 5% CO_2. The cells were subcultured periodically in T75 flasks (BD Biosciences, Billerica, MA) when the confluence was around 80%. The cells were used between passages 7 and 20 for experiments. Ibidi µ-slide 8 well uncoated dishes (Ibidi, Verona, WI) were used in cellular uptake experiments and in mitochondrial staining experiments. Alternatively, black-walled/clear (glass)

uncoated bottom 96-well plates (In Vitro Scientific, Sunnyvale, CA) were used in other JC-1 experiments. Clear plastic tissue culture treated 96-well plates (BD Biosciences, Billerica, MA) were used for experiments in which cell morphology (imaging) and cell viability (MTT and WST-1 assays) were assessed. White (opaque) tissue culture treated 96-well plates (BD Biosciences, Billerica, MA) were used for caspase 3/7 activity assays. Black-walled/clear (plastic) bottom tissue culture treated 96-well plates (BD Biosciences, Billerica, MA) were used for carboxy-H_2DCFDA reactive oxygen species (ROS) detection assays.

5.5 - Bright Field and Fluorescence Microscopy

Bright field and fluorescence imaging were performed for assessing uptake of caged ceramides in HeLa cells, as well as cell morphology. The experiments were conducted on an IX81 inverted optical microscope (Olympus Corporation, Tokyo, Japan). Bright field images were acquired with different Olympus UPlanSApo (100x, NA= 1.4; 40x, NA= 0.95; 20x, NA= 0.75) objectives and a high resolution CoolSNAP CCD camera (Photometrics, Tucson, AZ). Epifluorescence images were obtained using lamp excitation with an Olympus UPlanSApo (100x, NA= 1.4) oil immersion objective and the same camera. The filter sets used were DAPI, Cy3 and FITC WF (Semrock, Rochester, NY). Image analysis was performed using Image J freeware (NIH, Bethesda, MD).

For uptake experiments, HeLa cells were seeded at a density of $6x10^4$ cells per well and cultured for 24 hours in complete medium prior to adding caged

ceramides (20 μM). The cells were incubated with caged ceramides in serum-free medium (DMEM + 100 units/mL of penicillin/streptomycin) for 1-3 hours (as specified) and washed once with PBS (1X) before imaging in this buffer. In these experiments, the samples were placed in an ONICS stage-top incubator (Tokai Hit, Japan) for imaging (37 ^{o}C, 5% CO_2). Images of coumarin fluorescence were acquired in the DAPI channel.

For cell morphology experiments, HeLa cells were seeded at a density of 5000 cells per well and cultured for 24 hours in complete medium before being treated with exogenous ceramides (20 μM) or with the caged ceramide **9b** (20 μM) in serum-free medium for 24 hours and imaged in bright field mode without washing. In one experiment, the cells were subjected to 350 nm irradiation (4 min) in a Rayonet photochemical reactor equipped with four lamps after 7.5 hours of incubation. For all cell-based experiments involving an irradiation step with the photochemical reactor, the same set-up was used as described for preparatory photolysis experiments in microwell plates. An untreated (vehicle) control in which the cells were exposed to serum-free medium (or buffer, where applicable) containing only matched amounts (≤ 1%) of the organic solvents used to solubilize the compounds was included in all experiments.

5.6 - Cell Viability Assays

For MTT assays, HeLa cells were seeded at a density of 5000 cells per well in 96-well plates and cultured for 24 hours in complete medium before being treated

with ceramides (20 µM) in serum-free medium for 24 hours. At the end of the treatments, the medium was removed and replaced with 100 µL of a solution of the MTT reagent (1 mM final concentration from stock in PBS) in serum-free medium. After 4 hours of incubation with the reagent, the solution was removed from the wells and 50 µL of DMSO was added to solubilize the purple formazan crystals. The absorbance at 540 nm was measured in each well with a SpectraMax M2 multi-mode microplate reader (Molecular Devices, Sunnyvale, CA).

For the WST-1 assay, HeLa cells were seeded at a density of 5000 cells per well and cultured for 24 hours in complete medium or at a density of 2500 cells per well and cultured for 48 hours in complete medium before being treated with exogenous ceramides (20 µM), free coumarins (20 µM) or caged ceramides (20 µM) in serum-free medium for 24 hours (2-4 hours of incubation before 4-12 minutes of UV irradiation + 20-22 subsequent hours of treatment, as specified). Treatment solutions were prepared by dissolving the compounds in ethanol (or ethanol:dodecane, 98:2) and diluting to the appropriate concentration. The final amount of organic solvent did not exceed 1% (v/v). UV irradiation (350 nm) was performed in a Rayonet photochemical reactor equipped with four lamps (same set up as described earlier). Treatment solutions of the free coumarins were prepared either from a bulk stock solution (Chapter 3 results) or from small dried aliquots of a predetermined amount (Chapter 4 results). In some experiments, the caspase inhibitor Z-DEVD-fmk was diluted to 100 µM in serum-free medium (≤ 2% v/v DMSO) and 50 µL was added to the cells 1 hour before the treatment with exogenous ceramides or caged ceramides (50 µL of 2X concentrated ceramide

treatment solutions to yield a final concentration of 20 µM). In other cases, the cells were pre-treated for 1 hour with the antioxidant Trolox (100 µM in serum-free medium, ≤ 1% v/v ethanol) before ceramide treatments were performed, in a similar fashion. At the end of the treatments, the medium was removed and replaced with 100 µL of the WST-1 reagent diluted 11-fold in serum-free medium. The cells were incubated with the reagent for 3 hours and the absorbance at 450 nm was measured in each well with a SpectraMax M2 multi-mode microplate reader or with a FLUOstar Omega microplate reader (BMG Labtech, Cary, NC).

Data analysis was performed using Microsoft Excel. Relative cell viability was determined for each treatment group by dividing the mean absorbance for the group by the mean absorbance of the untreated control (x 100%). The number of wells per treatment group was 6-12 wells. In most cases, the "0 min UV" and "6 min UV" categories were analyzed separately (i.e. all values are relative to the untreated control for the respective category). The error on the calculated values represents the standard deviation between independent experiments, the standard deviation between sample wells (for single experiments) or the standard error mean (SEM) between independent experiments, as specified. Where applicable, the statistical significance of the differences in relative viability, with reference to the untreated control (or as otherwise specified) was estimated using Student's t-test. A p-value of <0.05 was considered significant. For the Bhc-related results, the t-test was performed using the average viability (%) values. For the Btcmoc-related results, the t-test was performed using the absorbance values obtained from individual experiments.

5.7 - Mitochondrial Staining Experiments with JC-1 and TMRM

For JC-1 staining experiments, HeLa cells were seeded at a density of $1x10^4$ cells per well and cultured for 24 hours in complete medium before being incubated with a 20 µM solution of the caged ceramide **9b** (in a glass-bottom plate). Alternatively, HeLa cells were seeded at a density of $6x10^4$ cells per well and cultured for 24 hours in complete medium before imaging (FCCP control experiment, in an Ibidi µ-slide 8 well dish). At the end of the incubation period, the medium was removed and the cells were stained with JC-1 (5 µg/mL) in serum-free medium for 30 minutes in the dark at 37 ^oC. After staining, the cells were washed once with PBS and imaging was performed in this buffer. When Ibidi µ-slide 8 well dishes were used, the samples were placed in an ONICS stage-top incubator for imaging (37 ^oC, 5% CO_2). Bright field and fluorescence imaging were performed with the optical microscope described above. Precisely, an Olympus UPlanSApo (100x, NA= 1.4) oil immersion objective and the Cy3 (Exc.: 514-555 nm; Em.: 570-616 nm) and FITC (Exc.: 465-499 nm; Em.: 516-556 nm) filter sets were used for imaging. Short exposure times of 100-200 ms were used for image acquisition. Image analysis was done with Image J freeware.

In some experiments (as specified), UV irradiation was performed on the microscope stage using the DAPI filter set (Exc.: 352-402 nm; Em.: 417-477 nm). For control experiments with FCCP (7 µM in serum-free medium), the uncoupler was added to the cells on the microscope stage and fluorescence images were acquired at 1 minute intervals after the addition (up to 10 minutes). The fluorescence emission of JC-1 was quantified in the cells by measuring the mean

intensity values for several individual cells (n=3), with background subtraction. The mitochondrial dye TMRM (100 nM in serum-free medium) was used in some experiments and images were acquired with the Cy3 WF filter set in a similar fashion as with the JC-1 dye.

5.8 - Caspase 3/7 Activity Assays

For the caspase 3/7 activity assays, HeLa cells were seeded at a density of 2500 cells per well in complete medium and cultured for 48 hours before being treated with exogenous ceramides (20 µM) or caged ceramides (20 µM) in serum-free medium. In some experiments, the caspase inhibitor Z-DEVD-fmk (100 µM) was added 1 hour prior to adding the treatment solutions. UV irradiation (350 nm) was performed in a Rayonet photochemical reactor equipped with four lamps (same set up as described earlier), after 2 hours of incubation with the exogenous ceramides or caged ceramides (where applicable). At the end of the treatment period, 50 µL of the caspase 3/7 assay reagent, which was prepared by mixing the lyophilized luminogenic caspase 3/7 substrate (Z-DEVD-aminoluciferin) with the assay buffer (as per the manufacturer's instructions), was added to the wells. The reconstituted reagent from "Caspase-Glo® 3/7 Assay" kits was always used in its entirety for a single experiment. After 1 hour of incubation, luminescence was measured on a FLUOstar omega microplate reader. The instrument was set up to conduct measurements using an orbital averaging mode, where a series of measurements takes place on an orbit of definable diameter within the well in order to provide an average measurement value.

Data analysis was done with Microsoft Excel. The fold increase in caspase 3/7 activity was calculated for each treatment group by dividing the mean luminescence value of the group by that of the untreated control. The number of wells per treatment group was 4-6 wells. In most cases, the “0 min UV” and “9 min UV” categories were analyzed separately (i.e. all values are relative to the untreated control for the respective category). The error on the calculated values represents the standard deviation between independent experiments or the standard deviation between sample wells (for single experiments).

5.9 - Necrosis Inhibitor Experiment

HeLa cells were seeded at a density of 2500 cells per well and cultured for 48 hours in complete medium. The necrosis inhibitor Nec-1s was diluted to 100 µM in serum-free medium, along with the caspase inhibitor Z-DEVD-fmk (≤ 2% v/v DMSO) and 50 µL was added to the cells 1 hour before the treatment solutions (50 µL of 2X concentrated treatment solutions to yield a final concentration of 20 µM of exogenous C2 Cer, free Bhc-coumarin or caged ceramide **9b**, in serum-free medium). Treatment solutions were prepared as described above for other WST-1 viability assays and the final amount of organic solvent did not exceed 2% (v/v). The assay was carried out after 24 hours (2 hours of incubation before 6 minutes of UV irradiation + 22 subsequent hours of treatment). UV irradiation (350 nm) was performed as described earlier.

5.10 - Carboxy-H_2DCFDA Reactive Oxygen Species (ROS) Detection

HeLa cells were seeded at a density of 2500 cells per well and cultured for 48 hours in complete medium before being labelled with carboxy-H_2DCFDA (10 µM) in HBSS buffer for 45 minutes in the dark, at 37 ^{o}C. The cells were then washed once with buffer before being treated with the coumarins **17** and **18** (20 µM), with the caged ceramide **9b** (20 µM) or with the control compound TBHP (100 µM) in HBSS buffer. In some cases, the cells were pre-treated for one hour with either ascorbic acid (200 µM), Trolox (100 µM) or alpha-tocopherol (100 µM) in HBSS buffer (≤ 1% v/v ethanol). After 2 hours of incubation, the samples were irradiated with UV light (350 nm) for 6 minutes in a Rayonet photochemical reactor equipped with four lamps (same set up as described previously) and immediately subjected to fluorescence measurements using a FLUOstar Omega microplate reader. A filter set with 485 nm excitation detecting emission at 520 nm was used. The instrument was set up in well scanning mode, where different points are measured within a well (in a matrix style) in order to provide an average measurement value.

Data analysis was performed using Microsoft Excel. The fold increase in ROS was determined for each treatment group by dividing the mean fluorescence value for the group by that of the untreated control. The number of wells per treatment group was 6-12 wells. The “0 min UV” and “6 min UV” categories were analyzed separately (i.e. all values are relative to the untreated control for the respective category). The error on the calculated values represents the standard deviation between independent experiments or the standard deviation between sample wells (for single experiments).

5.11 - References

(1) Kim, Y. A.; Ramirez, D. M. C.; Costain, W. J.; Johnston, L. J.; Bittman, R. *Chemical Communications* **2011**, *47*, 9236.

(2) Jones Ii, G.; Jackson, W. R.; Halpern, A. M. *Chemical Physics Letters* **1980**, *72*, 391.

(3) Pal, H.; Nad, S.; Kumbhakar, M. *The Journal of Chemical Physics* **2003**, *119*, 443.

Chapter 6: Concluding Remarks and Future Directions

6.1 – Concluding Remarks

This thesis describes a study of the biological effects of ceramide in cells using coumarinyl-caged ceramides. The findings from this work have shown that photocaging is a useful approach for delivering long- and very long-chain natural ceramides to cells in a minimally invasive manner. The presence of the coumarinyl caging moiety in the caged ceramides increases the aqueous solubility and membrane permeability of the lipid, which allows for it to be internalized by the cells. The caging group is then removed by the means of UV irradiation and the bioactive form of the molecule is released with spatial and temporal control. Coumarinyl-caged ceramides were prepared by our collaborators in the Bittman group and used for assessing the biological effects of specific ceramides *in vitro*. HeLa cells were chosen for these experiments based on their wide use in other studies involving ceramide. As shown in chapter 2, the caged ceramides are readily taken up by the cells when a short incubation with the compounds (~2 hrs) is performed. Photocleavage of the compounds can then be achieved with exposure to UV irradiation (~6 min) in order to generate ceramide photochemically in the cells.

The results from viability assays, which are presented in chapter 3, revealed that the photochemical generation of ceramide, particularly C16 Cer, by irradiating the Bhc-caged C16 Cer (**9b**) in HeLa cells causes a marked decrease in viability that can be detected after 24 hours of treatment. This effect was not observed in the absence of UV irradiation, which is indicative of the spatial and temporal control of

ceramide release that is offered by the caged compound. Since the biological activity of ceramide is known to be dependent on N-acyl chain length[1], a series of pegylated Btcmoc-caged ceramides incorporating different ceramide molecules was prepared for the purpose of this study. When these compounds were tested in the cells, the extent of the decrease in viability detected with the different Btcmoc-caged ceramides, with the longer UV irradiation time, was equivalent to that which was observed with the free Btcmoc. Since we can't exclude that these effects occur as a result of UV irradiation of the free coumarin in the cells, it is not possible to draw any conclusions here regarding the N-acyl chain length dependence of the biological activity of ceramide. In addition, the Btcmoc-caged ceramides were shown to require longer UV exposure times than the caged ceramide **9b** in order to significantly affect the viability of HeLa cells, which suggests that the pegylated photocages were not an improvement over the Bhc-caged compound.

When different experiments were conducted in order to elucidate the mechanism of cell death that takes place with the caged ceramide **9b**, it was observed that a decrease in the mitochondrial membrane potential ($\Delta\psi_m$) occurs in the cells that are treated with the compound and UV-irradiated, as shown in chapter 4. Caspase activation was also probed in the cells treated with the caged ceramide **9b**, as well as with other caged ceramides and no caspase 3/7 activity was detected, which implies that cell death occurs in a caspase-independent manner in this system. In addition, it was determined that the mode of cell death does not involve RIP1 kinase signalling, but possibly involves some intracellular ROS generation, which is consistent with the mitochondria having a role in this pathway. These

findings have shown that caged ceramides cause a caspase-independent form of programmed cell death implicating the mitochondria, also known as the “intrinsic pathway”.

6.2 – Future Directions

These studies using coumarinyl-caged ceramides have proven useful in identifying some of the challenges involved with utilizing photocages for studying the biological effects of ceramide in cells. In light of this, certain points should be considered for future design of these photocages. It was determined that the presence of the mTEG moiety on the coumarin, which was thought to increase the biocompatibility of the compounds, inadvertently reduced the ability of the caged ceramides to cause decreases in cell viability with UV exposure. This could be due to the less efficient photochemistry exhibited by these compounds (qualitatively speaking), which was demonstrated early in this work, or due to substantial differences in cellular uptake or subcellular localization. Since we determined that ROS generation occurs in HeLa cells treated with the Bhc-caged C16 Cer (**9b**), it would be interesting to assess, in future work, whether treatment with the Btcmoc-caged ceramides (**21**-**24**) causes ROS to be generated in the cells. This would, perhaps, indicate whether ceramide that is generated photochemically in the cells using these pegylated compounds has a significant effect on viability.

In order to design coumarinyl-caged ceramides that are highly effective in delivering ceramide to cells, it would be useful not only to characterize the photophysical and photochemical properties of the compounds prior to conducting

experiments *in vitro*, but also to measure their aqueous solubility. This could be assessed by determining the octanol:water partition coefficients for the compounds. In addition, it would be important to precisely determine the subcellular localization of the coumarinyl-caged ceramides prior to investigating the mechanisms of cell death that result from the photochemical generation of ceramide in cells. This could be achieved by performing fluorescence imaging experiments and looking at possible co-localization of the caged ceramides with different dyes that are known to label specific components in the cell.

The work presented in this thesis illustrates the complexity of cell signalling pathways implicating lipid second messengers such as ceramide. The results that were obtained suggest that the mitochondria are involved in cell death induced by coumarinyl-caged ceramides. In future work, it would be interesting to further investigate the role of the mitochondria during this process. Since it is well known that long- and very long-chain ceramides are confined to the subcellular location in which they are generated, the localization of caged ceramides upon their uptake into cells is crucial in eliciting a particular biological response.[2,3] It would, therefore, be important to demonstrate that the caged ceramides reach the mitochondria after being taken up by the cells, where the photo-release of ceramide causes distinct biological effects.

In order to investigate potential localization of coumarinyl-caged ceramides, it would be useful to prepare a photo-stable version of these compounds that could be visualized in the cells by fluorescence microscopy. These probes would also allow for assessing uptake in a quantitative manner in the cells, which would also be

useful. A possibility for such a probe would be a coumarinyl-caged ceramide in which the carbonate linker is replaced with a carbamate linker. Furthermore, preparing caged ceramides that allow for targeted delivery of long- and very long-chain ceramides to the mitochondria could provide insight into the role of this organelle in cell death induced by caged ceramides. This could be achieved by including a positive charge on the lipid headgroup portion of the compound, for example. Cationic ceramide analogues have been shown, in other studies, to cause biological effects at the level of the mitochondria.[4,5] Coumarinyl-caged ceramides bearing a positive charge would have the added benefit of provoking temporally controlled ceramide-induced effects in cells due to the requirement for uncaging of the lipid. Such work would allow for further elucidation of the mechanism of cell death caused by the bioactive sphingolipid ceramide when it is generated photochemically *in vitro*.

6.3 – Claims to Original Research

1. Spectral characteristics and fluorescence quantum yield values were measured for coumarinyl-caged ceramides (particularly Btcmoc- and Tcmoc-caged) in buffered aqueous solution. Photo-cleavage of these coumarin-based photocages was also demonstrated. In addition, uptake of the Bhc- and Btcmoc-caged compounds in HeLa cells was shown.

2. Bhc-caged C16 ceramide was shown to cause morphological effects, as well as reduced viability in HeLa cells, with UV irradiation. It was demonstrated that cell

death occurs in a caspase- and RIP1 kinase-independent manner, but involves mitochondrial depolarization and ROS generation.

3. Btcmoc-caged ceramides were shown to cause decreased viability in HeLa cells, with UV irradiation. However, longer UV irradiation times were required in order to achieve these effects and the extent of the effects was not different than that caused by the free Btcmoc-coumarin.

6.4 - References

(1) Grösch, S.; Schiffmann, S.; Geisslinger, G. *Progress in Lipid Research* **2012**, *51*, 50.
(2) Hannun, Y. A.; Luberto, C. *Trends in Cell Biology* **2000**, *10*, 73.
(3) Venkataraman, K.; Futerman, A. H. *Trends in Cell Biology* **2000**, *10*, 408.
(4) Beckham, T. H.; Lu, P.; Jones, E. E.; Marrison, T.; Lewis, C. S.; Cheng, J. C.; Ramshesh, V. K.; Beeson, G.; Beeson, C. C.; Drake, R. R.; Bielawska, A.; Bielawski, J.; Szulc, Z. M.; Ogretmen, B.; Norris, J. S.; Liu, X. *Journal of Pharmacology and Experimental Therapeutics* **2013**, *344*, 167.
(5) Dahm, F.; Bielawska, A.; Nocito, A.; Georgiev, P.; Szulc, Z. M.; Bielawski, J.; Jochum, W.; Dindo, D.; Hannun, Y. A.; Clavien, P. A. *Br J Cancer* **2007**, *98*, 98.